UCL Université catholique de Louvain

École polytechnique de Louvain (EPL)

Functional soft nanotubes for drug delivery applications

Dissertation presented by
Roselien VERCAUTEREN

for obtaining the Master's degree in
Chemical and Materials Engineering

Supervisors
Alain JONAS, Sophie DEMOUSTIER

Readers
Diana GUADALUPE RAMIREZ WONG, Jean-François GOHY

Academic year 2016-2017

Abstract

This work aimed to build polyelectrolyte nanotubes bearing in mind future drug delivery applications. Such structures are obtained by combining Layer-by-Layer assembly, a material deposition technique, with template synthesis, using a nanoporous polycarbonate membrane as template. Two different systems were studied: one comprised of synthetic polyelectrolytes, namely poly(allylamine hydrochloride) (PAH) and poly(sodium 4-styrenesulfonate) (PSS), and one comprised of semi-natural polyelectrolytes, namely chitosan (CHI) and hyaluronan (HA). These two systems were chosen for the purpose of building core-shell structures. In the present work, the effect of several assembling conditions was studied for both systems in order to gain a better understanding of their respective properties.

Firstly, PAH/PSS multilayers were built with varying ionic strength and pH. Even the lowest salt concentration chosen for the PE solutions resulted in thicker layers compared to zero ionic strength. However, a negligible influence was found for small concentration increases. For pH, only a small variation was investigated and it was found to cause no effect on the thickness or on the morphology of the nanotubes. The stability of the nanotubes after a prolonged contact with water was also explored. It was noted that, although there is a slight loss in rigidity at first, the PAH/PSS nanotubes remain stable when stored in water for longer periods of time.

The same investigations were then performed on CHI/HA multilayers. Ionic strength was observed to cause opposing effects for flat and nanoporous substrates. It led to thicker layers for nanotubes, but the effect was more complex for flat films: for low ionic strength there was an increase in layer thickness, yet for higher values, there was a loss of thickness, suggesting that the critical salt concentration was reached. Variations in the assembling pH are in line with the ionisation curves found in the literature, creating thinner layers at pH 5 and thicker ones at pH 4 and 6. In terms of stability in water, CHI/HA nanotubes were found to lose a great deal of rigidity upon contact with water, even more for tubes assembled at pH 6. For prolonged storage in aqueous solution, further losses of rigidity and changes in morphology were observed only in the first 24 hours. Finally, the cross-linking of the multilayers was investigated in order to increase the nanotubes rigidity in water, but no effect was noticed for the chosen concentrations of EDC and sulfo-NHS.

Although some assembling parameters require further explorations before entirely understanding the studied systems properties, this work still paves the way for further investigations involving core-shell nanotubes comprised of the two systems described above.

Acknowledgement

I would like to thank Prof. Sophie Demoustier-Champagne and Prof. Alain Jonas for the opportunity to work on this subject, as well as for their supportive supervision during these few months.

My sincere thanks to Diana as well, who has guided me throughout this project and with whom I was able to have many fruitful discussions. Without her guidance, I would not have been able to achieve all the objectives we set for this thesis. She always encouraged me to methodologically plan my experiments and to analyse the results more thoroughly. I am thankful for her patience and support, as well as for her sunny disposition even after long days of work.

I would like to thank the BSMA team for their welcome and competence. A special thank you to Colette Douchamps and Delphine Magning for their assistance with SEM analysis, Etienne Ferain for the porometry measurements of all my samples, and Sabine Bebelmann for her help with the FTIR measurements. Also many thanks to Bruno Aor who helped me with the ellipsometry analysis.

I am very grateful to my parents, my brother and sisters for their encouragements during the completion of this thesis. Many thanks to my flatmates Elisabeth, Fanny and Naomi, and especially to Robin, for their daily support and encouragement.

List of abbreviations

AAO	Anodised aluminum oxide
CHI	Chitosan
EDC	1-Ethyl-3-(3-dimethylaminopropyl)carbodiimide
FTIR	Fourier transform infrared
HA	Hyaluronan
LbL	Layer-by-Layer
L_p	Persistence length
PAA	Poly(acrylic acid)
PAH	Poly(allylamine hydrochloride)
PC	Polycarbonate
PE	Polyelectrolyte
PEI	Polyethylenimine
PEM	Polyelectrolyte multilayer
PET	Polyethylene terephthalate
PSS	Poly(sodium 4-styrenesulfonate)
$< R_{EE}^2 >^{1/2}$	Root-mean-square end-to-end distance
SEM	Scanning Electron Microscopy
STEM	Scanning Transmission Electron Microscopy
sulfo-NHS	N-hydroxy sulfosuccinimide sodium salt

Contents

Introduction **1**

1 State of the art **3**
1.1 Layer-by-layer assembly: the basics . . . 4
1.1.1 Polyelectrolyte adsorption in detail . . . 6
1.1.2 Multilayer growth: linear versus exponential . . . 7
1.2 Effect of the assembling conditions . . . 10
1.2.1 pH . . . 10
1.2.2 Ionic strength . . . 12
1.2.3 Temperature . . . 14
1.2.4 Molecular weight of PE . . . 15
1.3 Properties of assembled multilayers . . . 15
1.3.1 Water content . . . 16
1.3.2 Cross-linking . . . 16
1.4 Membrane-templating . . . 18
1.4.1 Nanoporous planar templates . . . 18
1.4.2 Membrane-templated Lbl assembly . . . 19
1.5 LbL for drug delivery applications . . . 22
1.5.1 Drug delivery systems . . . 22
1.5.2 LbL nanotubes for drug delivery . . . 24

2 Materials and methods **27**
2.1 Materials . . . 28
2.1.1 Polyelectrolytes . . . 28
2.1.2 Cross-linkers . . . 28
2.1.3 Substrates . . . 28
2.2 Assembly of multilayer films on flat substrates . . . 29
2.3 Characterisation of the flat multilayer films . . . 29
2.3.1 Ellipsometry . . . 29
2.3.2 Fourier Transform Infrared (FTIR) Spectroscopy . . . 30
2.4 Assembly of multilayer nanotubes . . . 30
2.5 Collection of the nanotubes . . . 31
2.6 Characterisation of the nanotubes . . . 32
2.6.1 Porometry . . . 32
2.6.2 Scanning electron microscopy (SEM) and Scanning transmission electron microscopy (STEM) . . . 32

3 Results and discussion **35**
3.1 PAH/PSS multilayers . . . 36
3.1.1 Growth . . . 36
3.1.2 Effect of the dipping time . . . 37

3.1.3 Effect of the ionic strength . . . 39
3.1.4 Effect of pH . . . 47
3.1.5 Effect of storage in water . . . 48
3.2 CHI/HA multilayers . . . 49
3.2.1 Growth . . . 50
3.2.2 Effect of pH . . . 51
3.2.3 Effect of the ionic strength . . . 54
3.2.4 Cross-linking . . . 57
3.2.5 Effect of storage in water . . . 60
3.3 Summarising table . . . 62

Conclusion **63**

Appendices **65**

A Drug delivery **67**
A.1 Drug loading . . . 67
A.2 Drug release . . . 67

B Summary of multilayers thickness and rigidity index values **69**

Introduction

Nature has always been a great source of inspiration for mankind. Chemistry and Materials Science are used to remodel nature for mankind's benefits. In the living world, functional entities take all shapes and sizes. Thanks to the fast-growing field of nanotechnology, these entities can be mimicked or even redesigned to serve specific applications. There are nowadays numerous available techniques that enable the assembly of molecules into functional designs of varying forms and dimensions. These techniques can be divided into top-down and bottom-up approaches. Top-down approaches have been proven to be efficient, but cannot meet the challenge of downsizing features to even smaller scales. For example, when using traditional photolithography, the dimensional limit is 1 micrometre. Bottom-up approaches have therefore emerged. One such technique is Layer-by-layer (LbL) assembly, which saw the light of day in the early 1990s thanks to the pioneering work of Decher and Hong [1]. LbL is highlighted in a little less than a decade of its origin as "electrostatic self-assembly" (ESA) due to the work Bertrand *et al.* [2]. Their group reviewed, among other aspects, the possible building blocks and substrates that are suitable for this technique, but also discussed possible applications [2]. In their work, they describe LbL assembly as a self-assembly adsorption strategy, in which complementary molecules are sequentially adsorbed on a surface. The only requirement is that there exist some sort of interactions (electrostatic, hydrogen bonding, etc.) between each of the constituents. As illustrated in Figure 1, the number of scientific publications related to LbL assembly has considerably grown over the past decade, manifesting the booming interest in this strategy. The main advantages of this technique are its simpleness, efficiency, robustness and flexibility. It allows the fabrication of highly ordered multilayered nanostructures, with tailored size, shape, composition, properties and functionalities. LbL is extremely versatile and therefore a powerful tool to address many applications such as tissue engineering, biosensors, bioelectronics, energy or even information storage [3, 4, 5].

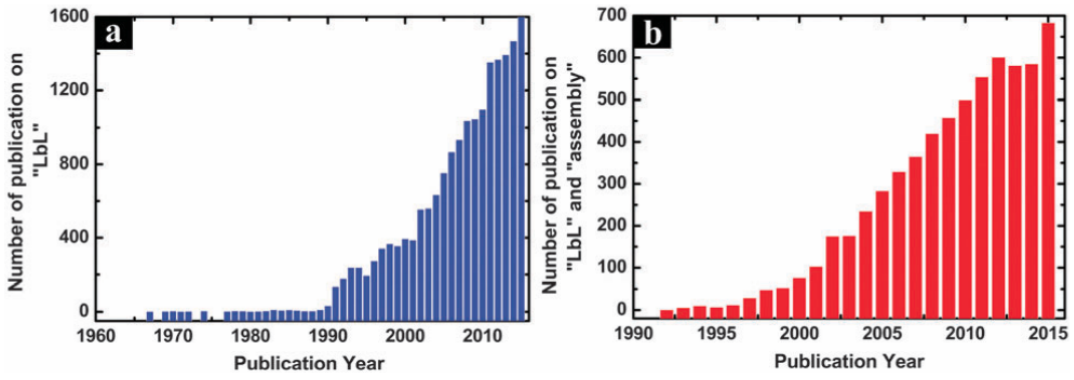

Figure 1: Illustration of the growing interest in LbL assembly, based on the number of yearly publications with keywords of (a) "layer- by-layer" since 1967 and (b) "layer-by-layer" and "assembly" since 1992 [4].

Since bio-molecules can be used as building blocks for the multilayered structures, LbL assembly is especially appealing for biomedical applications. One such application is drug delivery. Research about LbL drug delivery systems is rapidly growing, as the limitations of "free" drugs are numerous: instability in a physiological environment, undesired effects on healthy organs due to the drug distribution throughout the whole body, risks of immune responses and rapid clearance. These limitations can be addressed by using nanocarriers prepared with LbL assembly. Such structures can be biocompatible and biodegradable, and allow the targeted stimuli-responsive delivery of therapeutics throughout the body. Among all possible nanostructures, nanotubes are of particular interest for drug delivery applications as they have a larger surface to volume ratio. They indeed present large inner and outer surface areas that enable a larger drug loading on the inside and a higher functionalisation on the outside. Their particular shape is useful to isolate the cargo from the surrounding environment. Finally, they have been found to exhibit a longer circulation time in vivo and a much faster incorporation in the cells [6, 7].

LbL nanotubes are fabricated by combining the LbL method with templating. Many factors can affect the morphology of the nanostructures during their assembly, like for example pH and ionic strength. Some of these factors have been extensively studied for flat films, but their effect when the assembly takes place in confined geometries has not yet been thoroughly investigated. The objective of this thesis is therefore to investigate how the assembling conditions, such as dipping time, pH and ionic strength, will influence the nanotube properties. We chose to focus the present study on two different systems: one comprised of two synthetic polyelectrolytes, poly(allylamine hydrochloride) (PAH) and poly(sodium 4-styrenesulfonate) (PSS), and the second one comprised of two semi-natural polyelectrolytes, chitosan (CHI) and hyaluronan (HA). These two systems were chosen in the view of building core-shell nanotubes, which combine the properties of both polyelectrolyte pairs.

This report is divided into three chapters. The first chapter gathers all the information obtained about LbL assembly in the literature. Besides the general concepts behind this method, the effects of several parameters on the polyelectrolyte multilayers assembly are presented for flat films. The impact of templating on the multilayers is also overviewed, as well as the use of LbL structures for drug delivery applications. The second chapter of this report features the materials and methods used for the build-up and characterisation of both polyelectrolyte films and polyelectrolyte nanotubes. The third chapter presents all the results gathered in the scope of this thesis, as well as the discussions they entailed. The chapter is divided into two parts: a first part focuses on the PAH/PSS system and the second section describes the CHI/HA system. Finally, we will end this report by summarising the main conclusions of the performed research and by presenting some future perspectives for LbL nanotubes.

Chapter 1

State of the art

Contents

1.1 Layer-by-layer assembly: the basics 4
1.1.1 Polyelectrolyte adsorption in detail 6
1.1.2 Multilayer growth: linear versus exponential 7
1.2 Effect of the assembling conditions 10
1.2.1 pH 10
1.2.2 Ionic strength 12
1.2.3 Temperature 14
1.2.4 Molecular weight of PE 15
1.3 Properties of assembled multilayers 15
1.3.1 Water content 16
1.3.2 Cross-linking 16
1.4 Membrane-templating 18
1.4.1 Nanoporous planar templates 18
1.4.2 Membrane-templated Lbl assembly 19
1.5 LbL for drug delivery applications 22
1.5.1 Drug delivery systems 22
1.5.2 LbL nanotubes for drug delivery 24

Overview

This chapter offers an overview about LbL principles and applications. A first section provides information about the basics of Layer-by-Layer (LbL) assembly: How is it done ? With which materials? What are the resulting structures? This section also provides details about the physics behind LbL assembly. The effect of assembling conditions on the build up of flat films will be the focus of the second section of this chapter. It is also important to note that the properties of the LbL assembled structures can vary, namely with water content or by using cross-linking for example. This subject will be explored in the third section. The fourth section describes how LbL nanotubes are built using a nanoporous template. The last section focuses on the use of LbL assembly for drug delivery applications.

1.1 Layer-by-layer assembly: the basics

Layer-by-layer (LbL) assembly is a strategy involving the sequential adsorption of compatible species on a surface. It is an inexpensive and reproducible technique that enables the fabrication of nanostructured polymeric multilayer films, with customised shape, size and properties. This technique can use a wide range of inexpensive materials and be performed in entirely aqueous solutions. It does not require extreme conditions (such as high temperature and excessive pH) or exposure to harmful solvents, rendering it an environmentally friendly fabrication process [3, 5].

The basic principle of LbL thus involves the alternated deposition of complementary molecules on a surface for the build-up of multilayered structure. Depending on their nature, the complementary molecules will interact in a specific way and form a multilayered film. A washing step is needed after each deposition in order to remove the excess of molecules that are loosely attached and thus to avoid the contamination of the next adsorption step. The adsorption-washing cycle can be repeated until the number of desired layers is achieved [3, 4].

Building blocks and substrates

A wide range of materials can be used as LbL building blocks, going from charged molecules to nano-objects. These building blocks can be polymers, peptides, clays, dyes, metal oxides or even nanoparticles and carbon nanotubes. Bio-molecules like polysaccharides, nucleic acids, proteins, enzymes and viruses can also be incorporated into a layer [3, 4, 8, 9].

The multilayers can be deposited on any type of substrate (planar or cylindrical structures, porous or colloidal particles) of almost any surface chemistry. The dimensions and form of the substrate do not limit the deposition. It is thus possible to build nanostructures of all shapes and sizes.

Interactions dominating LbL assembly

LbL assembly does not rely on only one sort of specific multilayer interactions. Indeed, electrostatic interactions, hydrogen bonds, hydrophobic interactions, host-guest interactions, etc. can hold the layers together [3, 4].

Electrostatic interactions are, however, the predominant driving force of LbL assembly and are by far the most studied one. This type of inter-chain pairing will also be the interaction of interest for this thesis. In this scenario, the layers are built by the alternate deposition of oppositely charged polyelectrolytes (PEs) on a charged surface. This means that at each deposition step, the surface charge is inverted [3].

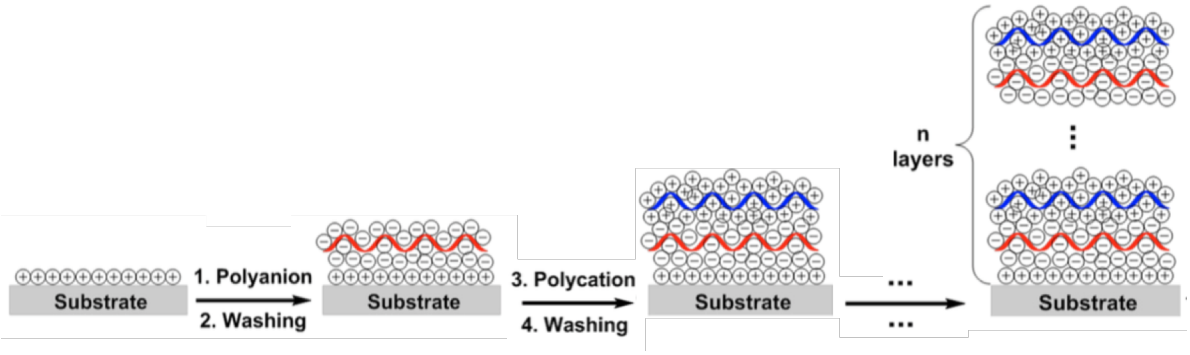

Figure 1.1: Schematic representation of the assembly of a multilayer via electrostatic interactions [3].

Through this type of interaction, it is possible to control the composition, the structure and the thickness of each layer. It is well suited for the fabrication of homogeneous ultrathin layers. Whatever the interactions holding the layers together, various parameters can influence the structure of the LbL assembled films: pH, temperature, ionic strength, solvent and properties of the PE, such as charge density and molecular weight [3, 4]. The effect of these parameters when electrostatic interactions are the main driving force of the assembly will be detailed in Section 1.2.

Resulting nanostructures

Layer-by-layer assembly can be used for the coating of a substrate. By adsorbing certain materials on a support, the surface properties of the substrate can be modified. In other words, LbL assembly can easily be used to functionalise a surface as uniform and stable coatings can be formed through this technique. LbL coatings are often used on metal or semiconducting nanoparticles for biomedical applications.

LbL is also used for the coating of implantable devices such as prosthetics and stents in order to improve their integration and their biorecognition. The coating also influences the adhesion of proteins and cells and thus the efficiency of the device [4, 5].

Layer-by-layer assembly can also be coupled with templating. This means that templates are filled with LbL deposited materials; after a drying step, the template is removed, yielding free-standing structures. The resulting structures are dependent on the template morphology. They are listed in Figure 1.2: nanotubes, nano-particles, multilayer films, nanorods and capsules [4, 10].

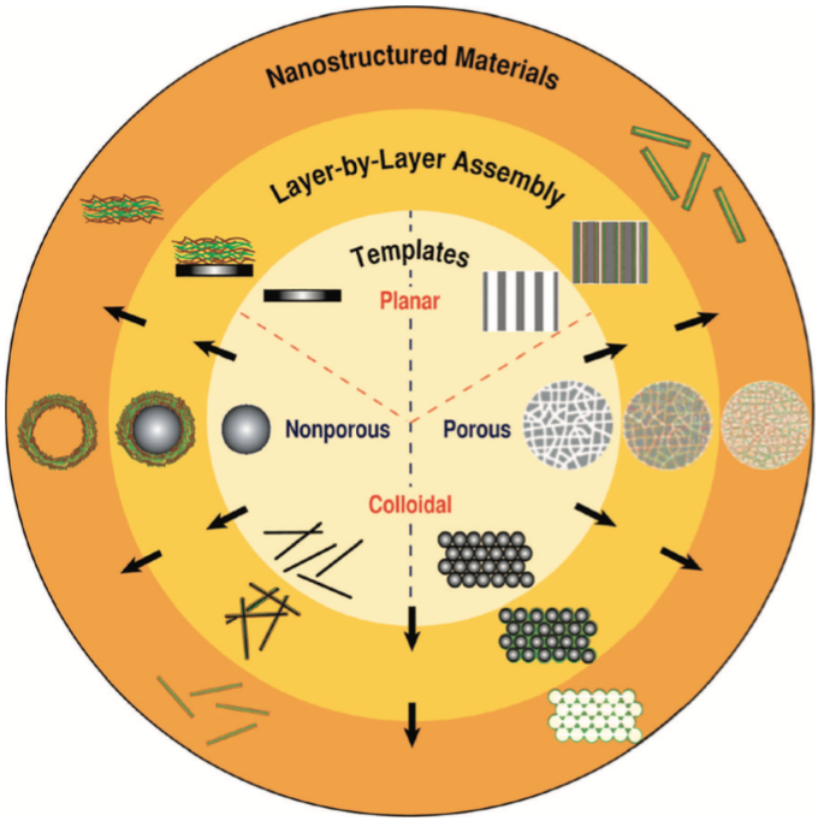

Figure 1.2: Illustration of various nanostructures that can be achieved through LbL assembly on templates [10].

LbL assembly processes

Several fabrication processes exist to build LbL assembled multilayers, namely dipping, spin-coating and spraying (see Figure 1.3). The dipping method is the most commonly used one, but it has the disadvantage of being time-consuming and requiring a large amount of material for each deposition step. Spin-coating and spraying are promising alternatives that significantly reduce the deposition time while remaining low cost, therefore more suitable for industrial applications [3, 4, 11].

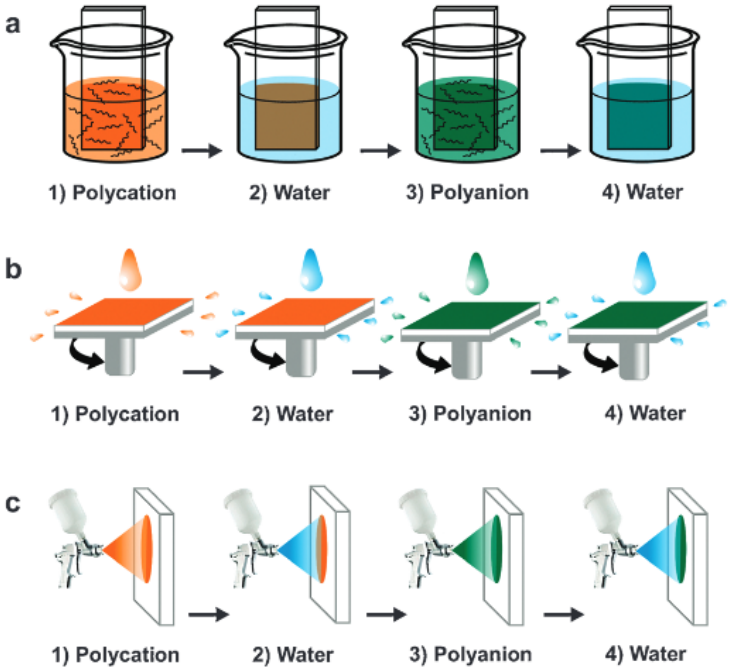

Figure 1.3: Schematic representation of Layer-by-Layer assembly process through the (a) dipping, (b) spin-coating and (c) spraying method for electrostatic interactions [11].

1.1.1 Polyelectrolyte adsorption in detail

Electrostatic LbL assembly consists of the sequential adsorption of a polycation and a polyanion (1 and 3 in Figure 1.4) with intermediate rinsing steps (2 and 4 in Figure 1.4). These steps are repeated until the desired number of layers is attained. The adsorption step consists of dipping a substrate with a charged surface in a solution containing a polyelectrolyte and some additional salts for a specific amount of time. During this immersion, the polyelectrolyte chains interact with the oppositely charged surface. An important requirement of this technique is the charge inversion of the surface. This means that in order for the surface to adsorb a sufficient amount of oppositely charged polyions and inverse its charge, there must be an excess of charge with respect to the previous layer, often called charge overcompensation.

Ion-exchange model

The adsorption of the PE chains on the oppositely charged substrate can be qualitatively explained by the ion exchange model. This model states that there is a competition between the PE chains and the counterions for the pairing with the charged sites on the surface (either the initial substrate or the previously deposited layer). The repulsion between charged PE segments

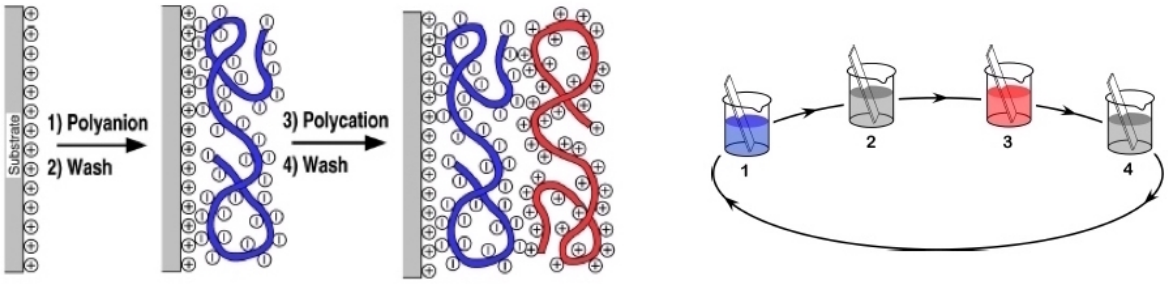

Figure 1.4: Schematic illustration of the Lbl assembly techniques [12].

prevents the accumulation of chains on the surface, while surface-PE interactions encourage adsorption. From an energetic point of view, this means that the system gains entropy upon counterion liberation and loses entropy upon PE adsorption. However, the entropy gain prevails, promoting PE adsorption. In terms of enthalpy, the change is quite small, as counterion-PE interactions are replaced by surface-PE and ionic interactions, and can, therefore, be neglected. This means the PE adsorption is driven mainly by an entropic change [13].

The ion-exchange model is often used to explain the effect of the charge density of PE chains or of ionic strength on the assembled layers. The model is, however, not perfect. For example, it fails to explain the irreversible nature of the adsorption phenomenon. Another shortcoming of the ion-exchange model is the inability to explain the charge overcompensation found upon layer adsorption [13].

Kinetics of polyelectrolyte adsorption

The adsorption phenomenon of polyelectrolytes on flat surface occurs in two steps: (1) a rapid first step consisting of the hefty accumulation of PE chains on the surface, and (2) a second step with reduced kinetics due to the reconformation of the deposited layer. The first step takes just a few minutes while the second step may take hours or even days. Since the reconformation is slower than the adsorption, the chains that are not fully anchored to the surface (i.e. only part of their charged groups interact with the surface or the underlying layer) do not have the time to rearrange and attach to neighbouring sites before those are occupied by other chains. This creates the aforementioned charge inversion [13].

Charge overcompensation is required for a successful layer-by-layer assembly. The resulting topmost layer contains not only chain segments that are anchored to the previous layer, but also tails and loops that create the necessary additional charges. Tails and loops thus determine the amount of material adsorbed for the next layer. This also means the portion of absorbed material depends on the underlying layer. This notion is very important when considering the first adsorption step, when the PEs interact with the template. The template surface will have a different effect on the loops and tails formation than the outer layer of PE multilayers. Hence, the first few layers will not have the same growth rate as the subsequent layers [13].

1.1.2 Multilayer growth: linear versus exponential

The multilayer growth regime depends on the nature of the assembling materials. Since electrostatic interactions were chosen as the driving force of the LbL assembly in the particular case of this thesis, only polyelectrolytes will be considered here. Polyelectrolytes are composed of ionisable monomers that become charged upon dissociation in a solution. There are thus polycations, which carry positive charges, and polyanions, which carry negative charges.

It is important to note that polyelectrolytes can either be synthetic or natural. Examples of natural PEs are proteins, polypeptides and polysaccharides. This distinction is important because those two categories of polyelectrolytes are likely to have different growth regimes: synthetic PE multilayers tend to have a linear growth while natural multilayers tend to grow exponentially [3]. Indeed, synthetic polyelectrolytes are often designed as strong polyelectrolytes, like poly(styrenesulfonate) (PSS) for example. Natural PEs, on the other hand, are weak polyelectrolytes. The distinction between strong and weak PE is based on how easily the ionisable groups on the PE chains become charged.

A strong polyelectrolyte is fully ionised over a large range of pH, resulting in numerous interactions between chains. Therefore, a linear growth regime is mainly dominated by electrostatic interactions and as a result each PE layer only interpenetrates with its adjacent layers [14].

For a weak PE, the degree of ionisation strongly depends on pH. Fewer interactions are therefore created, inducing the swelling of the system. The exponential growth can be explained by the diffusion of single polyelectrolyte chains into and from the layers during each adsorption step, thus increasing the already adsorbed amount and the total layer thickness [14, 15]. Lavalle *et al.* proposed a model to describe how this chain diffusion occurs. The validity of this model, which is described in Figure 1.5, was demonstrated on PLL/HA multilayers [16]. To explain this theory, one must imagine a multilayer composed of a polycation A and polyanion B, with i multilayers. According to the model, there are chains inside the layers that are not involved in interactions. Indeed, some chains diffuse within the multilayers during the dipping steps and become mobile chains inside the layers (Figure 1.5, B). When the multilayered film $(A/B)_i$ is put in contact with polycation A, the mobile chains of polyanion B diffuse out of the multilayers and form polycation/polyanion complexes at the outer layer of the film (Figure 1.5, D). These complexes are weakly bonded to the film. Only after all the free chains of material B have diffused "out" of the layers do the chains of material A diffuse "in" the film until overcompensation is reached (Figure 1.5, E and F). [17]. The "in" and "out" diffusion, therefore, explains the exponential growth of the multilayers.

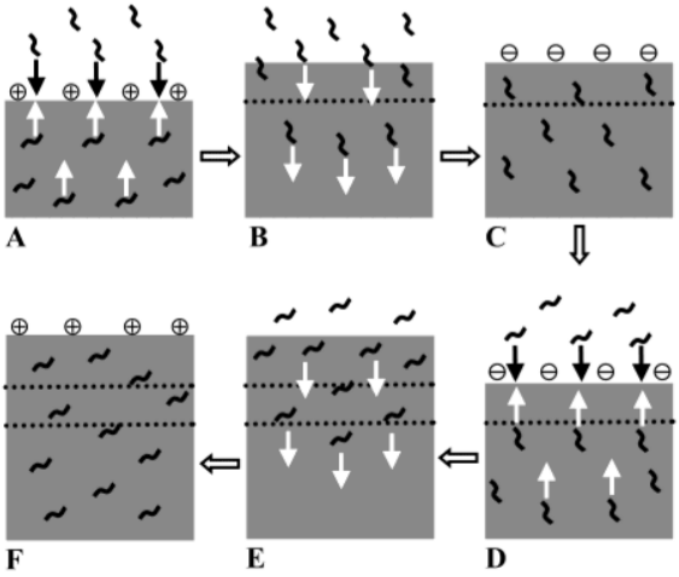

Figure 1.5: Model for exponential growth: A) "out" diffusion of polycations, B) "in" diffusion of polyanions, C) negative charge overcompensation, D) "out" diffusion of polyanions, E) "in" diffusion of polycations and F) positive charge inversion [17].

Case of study

In the particular case of this thesis, the complementary species that were used for the LbL assembly were poly(allylamine hydrochloride) (PAH) and poly(sodium 4-styrenesulfonate) (PSS) or chitosan (CHI) and hyaluronan (HA). PAH and PSS are both synthetic polyelectrolytes. They form one of the most studied systems for LbL assembly. CHI and HA are polysaccharides. Those biomolecules are both biocompatible and non-toxic, and therefore often used for biomedical applications. CHI/HA multilayers have potential uses in tissue engineering strategies or for drug delivery [14].

These systems show different growth regimes on flat substrates: the assembly of PAH/PSS multilayers follows a linear growth [18], while the build of CHI/HA multilayers follows an exponential growth [19], as can be seen in Figures 1.6 and 1.7, respectively.

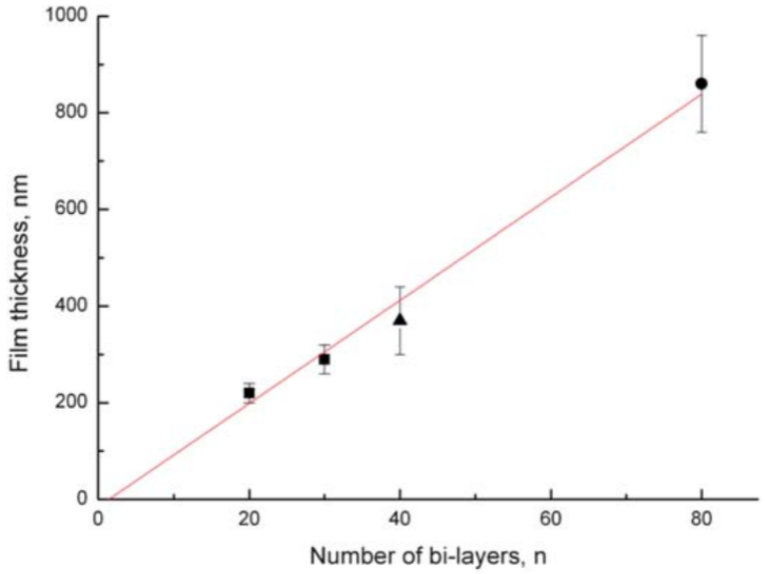

Figure 1.6: Film thickness as a function of the number of PAH/PSS layers [18].

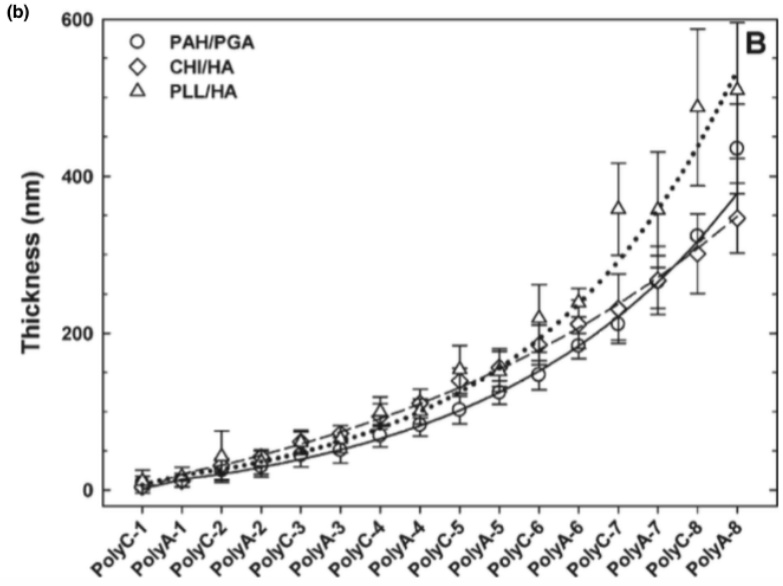

Figure 1.7: Film thickness as a function of the deposited CHI/HA layers [19].

1.2 Effect of the assembling conditions

Nanostructures assembled through electrostatic LbL assembly can be influenced by experimental parameters, namely pH, temperature and ionic strength, as well as by the properties of the PE (molecular weight, charge density, etc.). The effect of these parameters also depends on the nature of the assembling species. The case of study presented in the previous section will be used in order to illustrate how changes in the assembling conditions affect linear and exponential growth systems in a different manner.

1.2.1 pH

The effect of pH depends not only on the nature of the polyelectrolytes (synthetic or natural) but also on their properties (weak or strong). Indeed, the high degree of ionisation of strong PEs over a large range of pH lowers the need to finely control the assembling conditions. It, however, restricts the ability to tune layer morphology and thickness. For a weak polyelectrolyte, the degree of ionisation is strongly dependent on pH. A weak polyanion will only be negatively charged when the surrounding pH is considerably higher than its pKa. Likewise, a polycation will only become positively charged below its pKa.

Changes in pH during the LbL assembly thus mostly affect the growth and stability of weak polyelectrolytes. Indeed, for such PEs, a small variation of pH can induce changes in the structure, composition and thickness of the layers. The effect of pH on the thickness of PAH and PAA layers, both weak PEs, is illustrated in Figure 1.8. Layer thickness is depending on the PEs charge, and the more the complementary PE chains are charged, the more they attract each other, creating thinner layers due to a closer arrangement of the chains. For example, both PAH and PAA are fully charged PE in region III of Figure 1.8 and, therefore, the thinnest layers are built for this range of pH. On the other hand, in region II, PAA chains are not yet fully ionised. In this case, chains cannot take up a flat conformation upon adsorption on the previous layer but form dense loops, thus creating thicker layers.

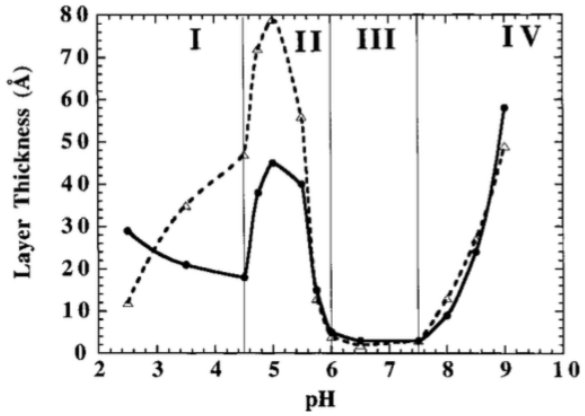

Figure 1.8: Average thickness contributed by a PAA (solid line) and PAH (dashed line) adsorbed layer as a function of solution pH [20].

Linear growth system

The layer thickness in Figure 1.8 was computed for PAA/PAH multilayers. One must, however, take into account that the effect will be slightly different for PAH/PSS multilayers, especially since PSS is a strong PE. Bieker *et al.* observed that the degree of interaction between PAH and PSS decreases when increasing pH. In basic conditions, the NH_3^+ groups on the PAH chains

are depronotised, lowering the electrostatic repulsion between the chain segments and creating a more coiled chain conformation [18]. In terms of layer thickness, this is translated into a thickness gain upon increasing the pH of the PE solutions. This increase is moderate when increasing pH for 4 to 7, but gets even bigger when going to extreme basic conditions, as depicted in Figure 1.9

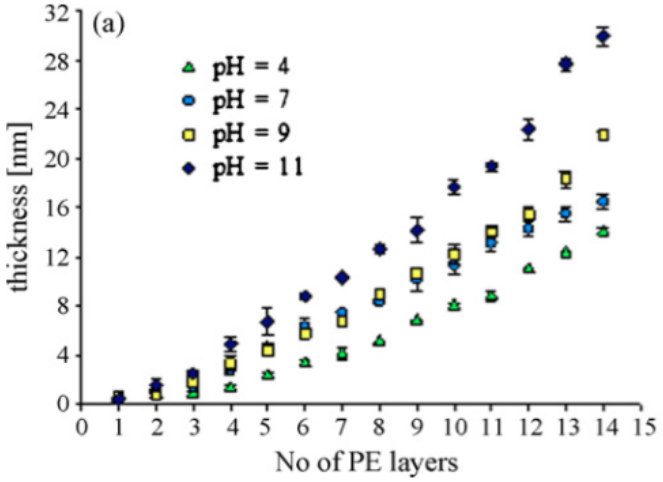

Figure 1.9: Film thickness as a function of PAH/PSS layers deposited on a silicon substrate for different pH values [18].

Exponential growth system

CHI and HA are both weak bio-polyelectrolytes, meaning their ionisation degree varies with pH. The pK_a of CHI and HA are ca. 6.5 and 2.9, respectively. These values can slightly vary according to the molecular weight of the polysaccharides. For chitosan, molecular weight and therefore pKa are depending on the degree of deacetylation (DDA). Indeed, CHI is obtained by partial deacetylation of chitin. This reaction is however never fully completed, hence the need to define a DAA. A pKa value of circa 6.5 is valid for chitosan with a DDA of 80% [21]. As a consequence of the pKa values described above, there is only a narrow pH window in which both materials can be used together [21]. From the ionisation curves represented in Figure 1.10, it can be deduced that CHI is fully ionised for pH lower than 4, while HA is fully ionised for pH higher than 5.5.

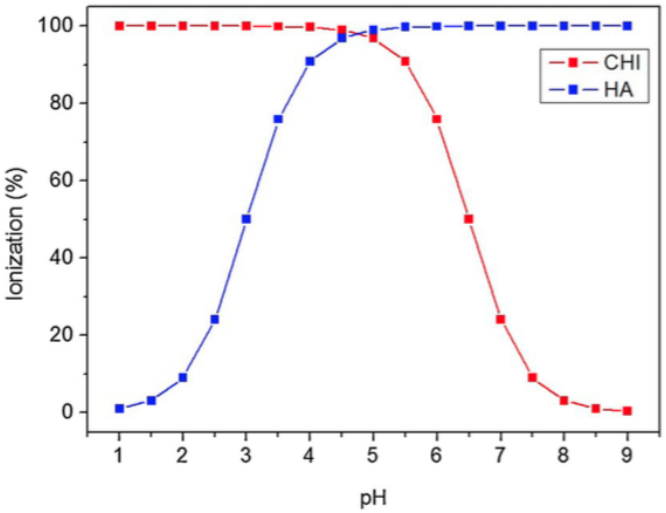

Figure 1.10: Ionisation curves of CHI and HA versus pH [22].

When the polysaccharide electrolyte chains are only partially charged, they do not fully interact with the oppositely charged surface or polyelectrolyte and one needs to add more of them to reach charge inversion; hence the thickness should increase. As illustrated in Figure 1.11, experimental results for CHI/HA multilayers assembled on PEI functionalised Si substrates show an increase of the film thickness for pH 3.0 compared to pH 4.5 (using the same ionic strength), as HA is then only partially ionised while CHI is fully ionised [22]. This can also be explained by Figure 1.12: a lower charge density results in loopy chains and thus thicker layers.

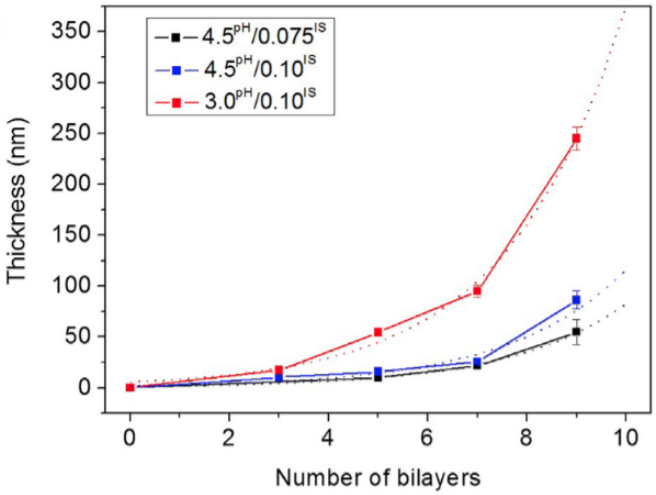

Figure 1.11: Thickness profile for CHI/HA multilayers assembled on PEI functionalised Si substrates, at different pH/NaCl concentrations [22].

1.2.2 Ionic strength

Ionic strength enables a certain control over the layer thickness, permeability and stability. Both salt type and concentration are important factors to take into account during LbL assembly. For example, the increase of salt concentration will modify the number of available charges on the PE chains and therefore affect the PE layer conformation. Low salt concentrations cause PE chains to fully extend, while for high salt concentrations, the chains form loops due to the reorganisation of the charges in the chains (see Figure 1.12). An increase in ionic strength thus leads to the swelling of the layers. One must, however, keep in mind that very high salt concentrations can lead to the complete desorption of the PE chains due to reduced electrostatic interactions [3, 4].

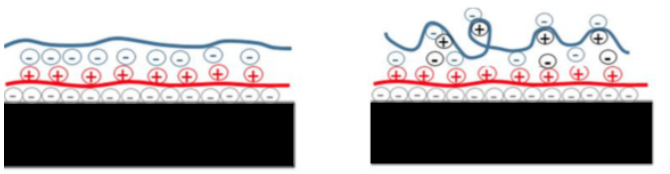

Figure 1.12: Schematic representation of a thinner layer with planar chain conformation and higher charge density on the left and a thicker layer with loopy chain conformation and lower charge density on the right [23].

Linear growth system

Köhler *et al.* gathered data from different publications concerning the effect of ionic strength on PAH/PSS films and outlined a dependence based on those results (see Figure 1.13). When the salt concentration exceeds 0.5 M, a linear correlation is found between ionic strength and bilayers thickness. For lower concentrations, the bilayer thickness is correlated to the square root of the ionic strength [24].

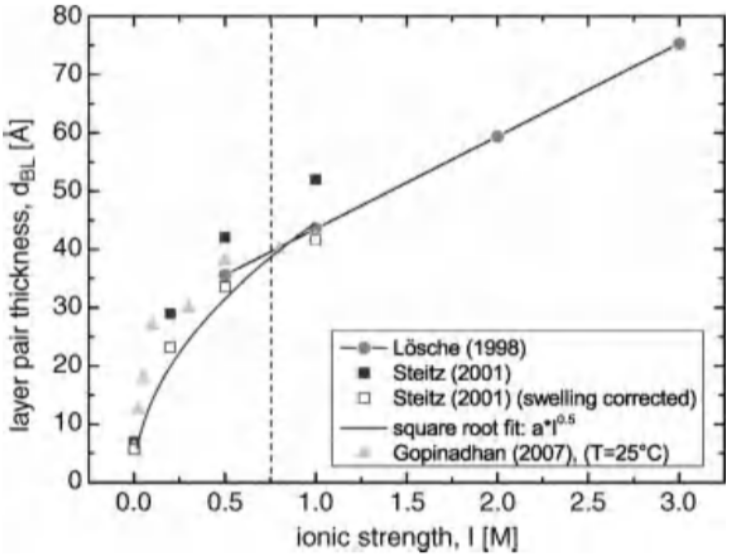

Figure 1.13: Thickness of PAH/PSS bilayers as a function of the ionic strength of the dipping solution [24].

The ion type also has an impact on the PEM structure. The use of different monovalent cations has no obvious effect on the film thickness, but has an effect on the amount of absorbed water. Indeed, smaller ions tend to keep their water of hydration, unlike bigger ions around which the water of hydration can be removed with ease. When studying the impact of the anions, it was observed that the addition of larger anions resulted in the formation of thicker and rougher layers. The impact was found to be qualitatively the same as increasing ionic strength. The addition of multivalent salts was also studied. It was noted that incorporating a multivalent salt to the polyelectrolyte solutions leads to a considerable increase in thickness. This effect is translated by the fact that multivalent ions interact more efficiently with the polyelectrolyte chains than monovalent ones [24]. Multivalent ions may also induce the physical cross-linking of the multilayers when they interact with two complementary PE chains.

Exponential growth system

The standard ionic strength used when assembling CHI/HA multilayers lays between 0.1 and 0.2 M, which corresponds to the physiological ionic strength [25]. Typically, 0.15M of NaCl is added to the polysaccharide solutions [14, 19, 22, 26, 27]. For lower levels of ionic strength, the thickness of the polysaccharide multilayers is decreased [14, 22]. This is illustrated in Figure 1.11, where a slight thickness decrease is visible for nine CHI/HA bilayers when lowering the NaCl concentration from 0.1 M to 0.075 M during the assembly of the multilayers [22].

Lower salt concentrations also result in a different layer build up: instead of an exponential growth, the growth becomes progressively linear when reaching 10^{-4} M of NaCl. This is depicted in Figure 1.14, in which $-\Delta(f/\nu)$ is proportional to the deposited amount of polymer [14].

Furthermore, ionic strength has an effect on the surface coverage of the film. At very low salt concentrations (e.g. 10^{-4} M) , the polysaccharides deposit in islets and a homogeneous coverage is only reached after numerous layers (20 bilayers in the case of 0.01 M of NaCl for example). At higher salt concentrations (e.g. 0.15 M) , the islets give way to a continuous film after only several deposition steps [14].

Unlike the PAH/PSS system, multivalent salts like calcium chloride may cause the negatively charged HA to ionically cross-link and are therefore not added to the polysaccharides solutions. Ca^{2+} ions weakly bind HA chain together, leading therefore to the formation of HA aggregates in solution [28]. The adsorption of aggregates instead of single chains may affect the stability of the multilayers. Indeed, under biological conditions, the Ca^{2+} ions may be replaced by monovalent cations such as sodium, therefore slowly de-cross-linking or even causing the desorption of the layers [29].

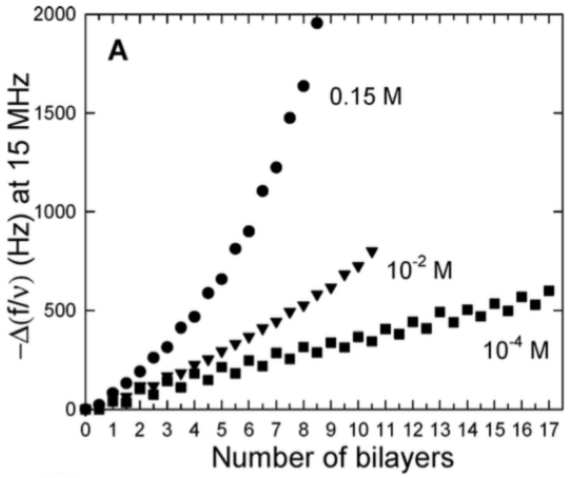

Figure 1.14: Quartz crystal microbalance of CHI/HA multilayered films on glass slides for different salt concentrations. The parameter $-\Delta(f/\nu)$ is proportional to the deposited amount of polymer [14].

1.2.3 Temperature

Temperature also affects the stability, thickness and internal structure of the assembled multilayers. It has been observed that multilayers assembled at high temperature are thicker than layers assembled at ambient conditions. The high temperature induces the swelling of the films and the increase of interpenetration of the layers. It, however, results in increased internal roughness. The effect of temperature is related to the change of the polyelectrolytes structure in solution upon heating: they take on a more coiled conformation and remain that way inside the multilayers [3, 4, 21].

Linear growth system

In the case of PAH/PSS, the temperature effect is dependent on the ionic strength: below the threshold of 0.05 M of salt concentration, temperature has no effect. Electrostatic interactions are too strong and affect the PE chains conformation. However, when increasing the ionic strength above this threshold, the effect of temperature emerges and becomes more prominent with increasing screening [24].

1.2.4 Molecular weight of PE

Variations in molecular weight (M_w) may induce a change in growth regime during the LbL assembly of PE multilayers. Indeed, both polycation and polyanion exhibit a specific threshold molecular weight below or above which the growth regime changes, and therefore the thickness of the multilayers as well [30].

Linear growth system

The effect of molecular weight of PAH/PSS is not yet fully understood and was only investigated recently. Molecular weight can affect the layers growth regime, the internal roughness or can play a role in the PE swelling behaviour [4]. When using low M_w synthetic PEs, chains are able to diffuse inside the layers, leading to thicker and exponentially growing layers [3]. For PAH/PSS this effect is, however, rather small [31].

Exponential growth system

The effect of molecular weight was more thoroughly studied in the case of CHI and HA. For a given number of bilayers, the higher the molecular weight, the thicker the layers. Furthermore, as depicted in Figure 1.15, the exponential growth is also dependent on the molecular weight: the transition from a linear to an exponential regime occurs earlier for lower M_w [32].

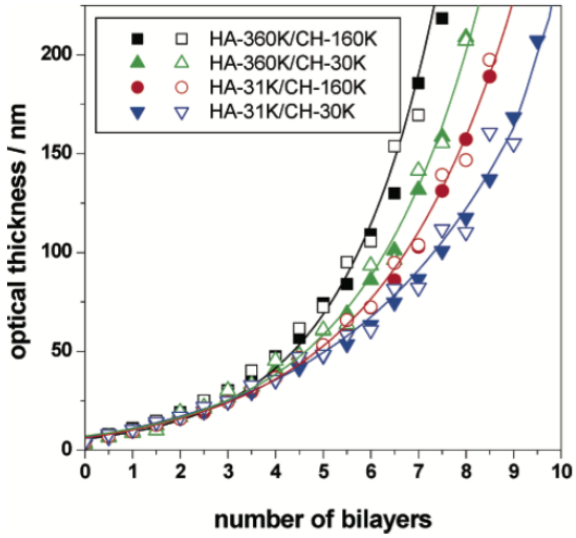

Figure 1.15: Effect of molecular weight on the exponential growth and thickness of CHI/HA multilayers [32].

1.3 Properties of assembled multilayers

The parameters of the surrounding medium may also affect the multilayers structure post-LbL-assembly. For example, changing the ionic strength may induce a swelling of the layers [21]. Likewise, varying the pH after the assembly gives rise to swelling and deswelling transitions for PAH/PSS multilayers assembled at pH lower than 8.5 [33]. The effect of those two parameters has also been studied for CHI/HA multilayers [34]. Two other but still very important factors will be detailed in this section: the effect of water content and the effect of cross-linking.

1.3.1 Water content

An important property in polyelectrolyte multilayers is water content. Water is not only used as solvent during the LbL assembly, it is also an active part of the assembled layers. Water can lead to the swelling or shrinkage of the multilayers, depending on the surrounding conditions like the adjacent humidity. The presence of water can also induce chain mobility.

It has been observed that PAH and PSS are respectively surrounded by one and four water molecules [24]. This may, however, vary with the preparation conditions, such as pH and ionic strength. For example, the water uptake of the multilayer films is known to increase with the salt concentration of the PE solutions during the layers assembly. The water content of "wet" multilayers, meaning just after the adsorption, is in the range of 40 to 55 %. Upon drying, the multilayers shrink and have a 30 to 35 % water content. It was also discovered that there is a lower water uptake in the core of the film than in the outer film zone [21].

When using polysaccharides, and especially when using HA, the water uptake is much higher. For CHI/HA systems, it can range from 80 to 95 %, depending on the number of layers and the preparation conditions. As HA-based films are already highly hydrated, they do not tend to swell further when put in aqueous solution [19, 24].

1.3.2 Cross-linking

Biopolymers are soft and sensitive materials. Therefore, multilayers built from biopolymers are much affected by external conditions like pH and ionic strength, as the electrostatic interactions holding them together become unstable. However, for some applications, the stability and the preservation of the structure of the multilayers is crucial. One possible way to ensure this is to use of chemical cross-linking. [35].

The structural integrity and the overall stability of the PE multilayers can be ensured by adding covalent interactions to the electrostatic ones. Cross-linking enables a fine control over the structure through the control of the amount of cross-linker in contact with the material [35, 36].

In our case of study, CHI/HA possesses carboxylic acid groups and primary amines and can be cross-linked by 1-ethyl-3-(3-dimethylaminopropyl)carbodiimide hydrochloride (shortened EDC) and N-hydroxy sulfosuccinimide sodium salt (sulfo- NHS) [35, 37]. The reaction induced by these cross-linkers is depicted in Figure 1.16. In the first step of this reaction, EDC interacts with carboxyl groups in order to form amine-reactive intermediates. There are three possible reactions for these activated forms in the second step of the cross-linking: (i) they encounter primary amines and form amine bonds; (ii) they hydrolyse back into their inactivated carboxyl form; (iii) they form another active intermediate when in the presence of sulfo-NHS, this intermediate being more stable and storable. The addition of sulfo-NHS therefore increases the efficiency of the reaction, as the sulfo-NHS reactive intermediates can interact with primary amines later on in the reaction [37].

The standard protocol for this method of cross-linking was developed by Richert *et al.* and involves 400 mM EDC and 100 mM sulfo-NHS, prepared in a 0.15 M NaCl solution at pH 5.5. The multilayers must remain in contact with the cross-linkers for 12 hours at 4°C and must be rinsed abundantly with a 0.15 M NaCl solution afterwards [35].

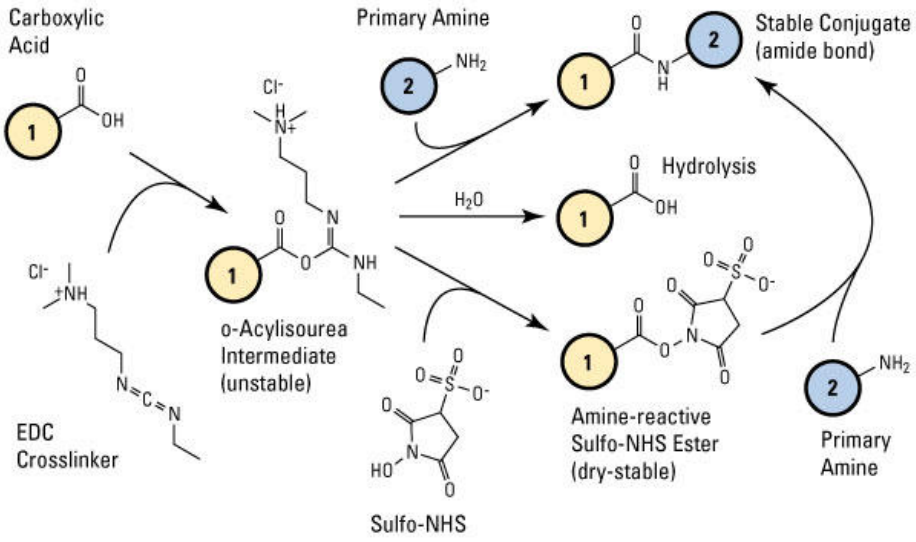

Figure 1.16: Cross-linking reaction scheme for carboxyl-to-amine linking using EDC and sulfo-NHS [37].

Boudou *et al.* studied the evolution of the cross-linking reaction for different EDC concentrations and for different systems, including CHI/HA. All the cross-linking reactions followed the same trends: an initial increase, followed by a plateau for higher EDC concentration. In the case of CHI/HA (◊ on the Figure 1.17), the limit of cross-linking was already reached for less than 50 mg/mL of EDC (which is equal to ca. 260 mM) [19, 36].

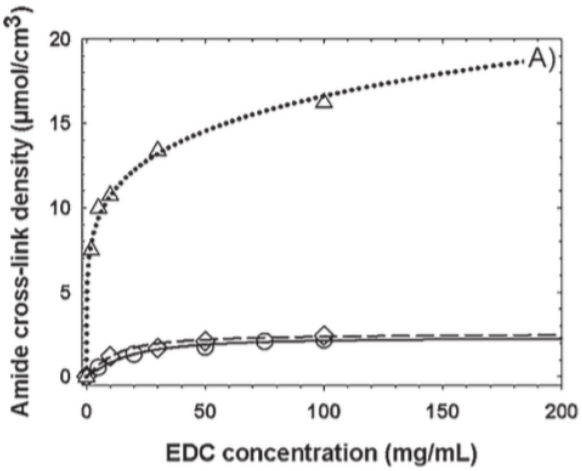

Figure 1.17: Molar density of covalent amide bonds created during the cross-linking reaction for (PAH/PGA) (o), (CHI/HA) (◊) and (PLL/HA) (△) films [19].

Likewise, Picart *et al.* investigated the cross-linking kinetics for CHI and HA multilayers at different EDC concentrations, namely 25, 200 and 750 mM. To do so, they performed FTIR measurements on $(CHI/HA)_9$ films assembled on glass slides, cross-linked with different EDC concentrations. They then substracted the obtained spectra from the initial spectrum of the multilayers, before cross-linking. As cross-linking involves the creation of amide bonds, there should be an increase of the amide I and II bands in the absorbance spectrum, which are respectively situated in the 1630±1700 cm^{-1} region and in the 1440±1500 cm^{-1} region. There should also be a decrease in the carboxylic COO^- peak at 1412 cm^{-1} and in the saccharide

peaks in the 950±1200 cm^{-1} region, which characterise the skeletal vibrations of the PEs. Two particular peaks in this region indicate C-O stretching and are situated at 1082 and 1032 cm^{-1}. In Figure 1.18, one can see that these changes are strongly observed for a EDC concentration of 200 mM, while there are almost no changes for 25 mM [27]. Picart *et al.* offered no explanation as to why the peaks are slightly lower when using 750 mM of EDC, but they do however declare that kinetics were similar for 200 and 750 mM. It could thus be suggested that even at 200 mM EDC concentration, one can observe new covalent bonds.

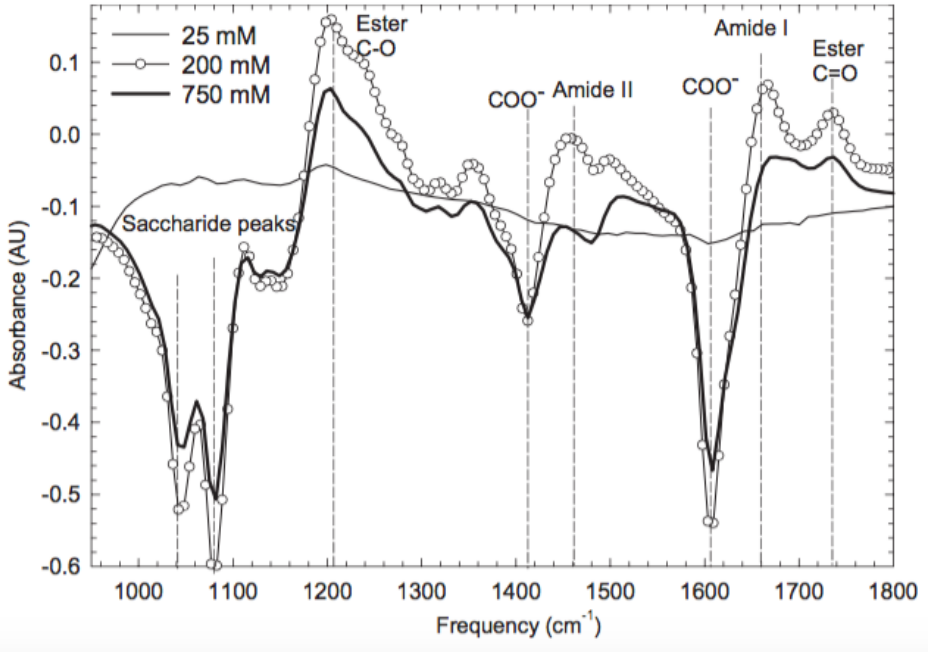

Figure 1.18: Resulting substraction of the spectra before and after cross-linking for three EDC concentration: 25 mM (thin black line), 200 mM (circles), and 750 mM (thick black line) [27].

1.4 Membrane-templating

Membrane-templating is a common method used to assemble LbL nanotubes. Tubular structures are prepared inside nanoporous substrates such as an anodic aluminium oxide (AAO) template or a track etched polycarbonate (PC) membrane. After the assembly, the template is dissolved, releasing the nanotubes. In this section, the fabrication of the templates will be quickly overviewed before explaining how layer are built within the pores and how the assembly is different than on flat substrates.

1.4.1 Nanoporous planar templates

AAO templates are created by subjecting a polished alumina film to a two-step anodisation, as depicted in Figure 1.19: a first anodisation results in rather disordered pores that, however, rearrange themselves deeper inside the templates; the top aluminium oxide layer is etched away, leaving only an ordered landscape at the surface of the film; the second anodisation step results in the formation of parallel pores, initiated from the previously obtained landscape [38].

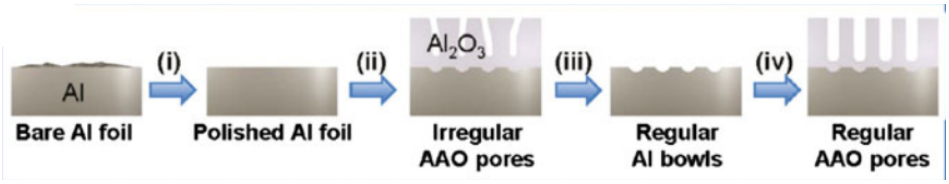

Figure 1.19: Schematic representation of the synthesis of a AAO template: (i) polishing, (ii) first anodisation, (iii) AAO wet etching and (iv) second anodisation [38].

The porous film morphology (pore size, pore density and thickness) will be determined by the used anodisation conditions, namely the utilised acid electrolyte, the anodisation voltage, the anodisation time and the temperature. However, for AAO templates, the pore size is dependent on the pore density: the higher the pore density, the smaller the pore size, and vice versa [6, 38].

PC templates are fabricated by track-etching. This consists of bombarding the film with energetic heavy ions, accelerated in a cyclotron. This results in damaged chemical bonds and the formation of linear damage tracks. These tracks are the revealed by a specific chemical wet etching, creating parallel nanopores in the template [39, 40].

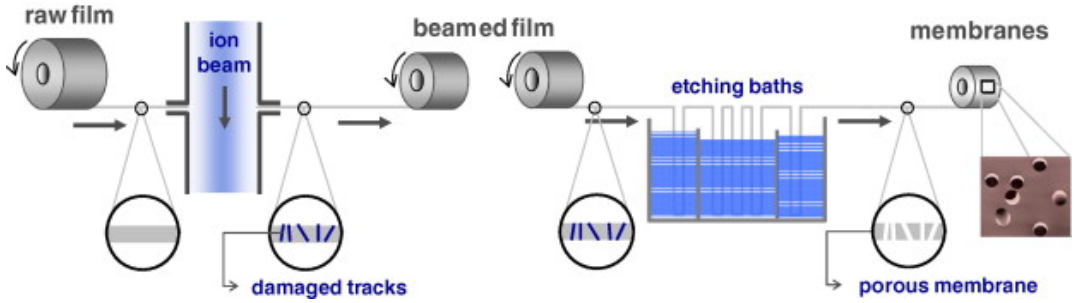

Figure 1.20: Schematic representation of the track-etching process of a PC template [40].

In an AAO template, the pores are arranged in regular arrays, while they are randomly distributed in a PC template. However, the latter is preferred for the LbL assembly of nanotubes as the complete removal of the AAO template requires extreme pH values (pH $\leq$ 4.5 or pH $\geq$ 8.5) that may affect or damage the multilayers [6].

1.4.2 Membrane-templated Lbl assembly

The principles behind polyelectrolyte adsorption detailed in section 1.1.1 remain true, whether it is for flat substrates or for nanoporous templates. The standard dipping procedure still holds as well. Nanotubes are thus assembled by successively dipping a nanoporous template in solution containing oppositely charged polyelectrolytes. The resulting structure is a number of concentric layers held together by electrostatic interactions, as depicted in Figure 1.21.

The main difference with flat films is that the polyelectrolyte chains need to diffuse through the pores before interacting with the inner pore walls. This diffusion step can affect not only the growth inside the pores, but is also an additional parameter that needs to be taken into account when varying the assembling conditions. The embedded nanotubes are released by dissolving the template, which in the case of a PC template is achieved with an organic solvent. The nanotubes, therefore, remain in an organic suspension. This suspension can either be filtered, or the tubes can be deposited on flat substrates for further analyses [6, 7, 41].

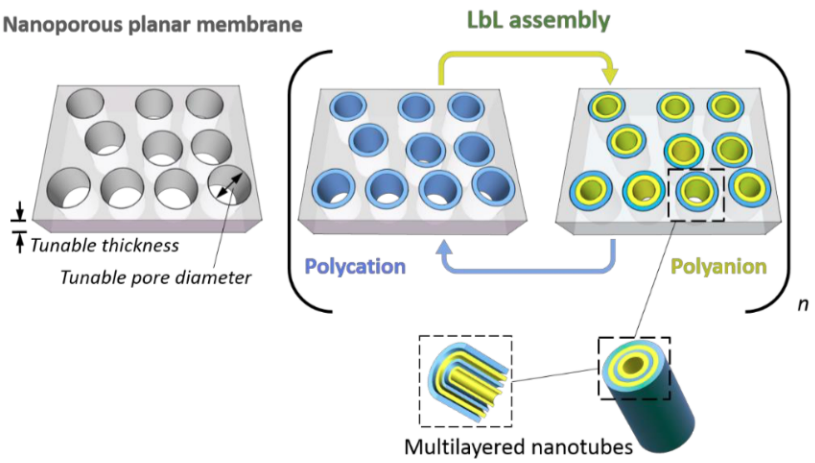

Figure 1.21: Schematic representation of the Lbl assembly in a nanoporous template [6].

Effect of geometrical confinement on LbL multilayer growth

It has been observed that when Lbl assembly is carried out within nanopores, the thickness of the deposited layer at each cycle is much larger than on flat surfaces, up to 100 times larger in some cases [42]. This increase does not depend on the molar mass of the polyelectrolytes, nor on the ionic strength. It was, however, observed that the assembled layer thickness depends strongly on the pore size, especially for small pores. Furthermore, the pores can be filled up to their maximum in only one deposition cycle, suggesting that upon further deposition steps the newly adsorbed chains entangle with the first deposited layer in the confined space of the pore. Upon drying, the entangled web of chain settles at the pore walls, creating nanotubes [42].

The growth mechanism within a nanopore is thus entirely different than on a flat substrate. In the case of PAH/PSS multilayers, it was found that there are two growth regimes when assembled in a nanoporous template, as depicted in Figure 1.22.

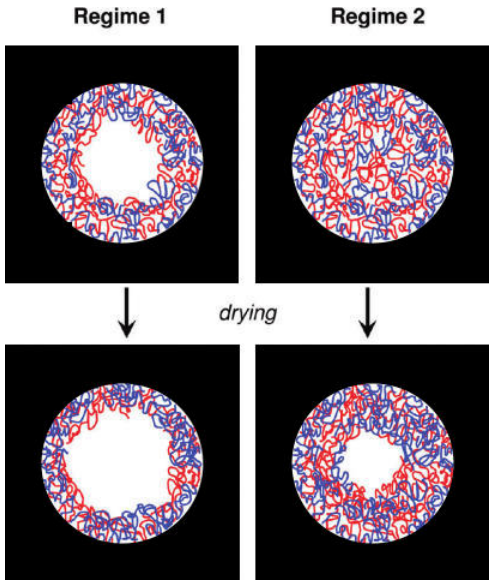

Figure 1.22: Schematic representation of the two growth regimes for LbL assembly in nanoporous substrates [43].

The first regime is linear and comparable to the growth mechanism on flat substrates. The growth is not limited by the diffusion of PE chains into the pores. The second regime is characterised by decreased kinetics. The transition to this regime occurs when the pore is almost entirely filled by the wet and swollen multilayers. At this stage, an interconnected web between PE chains appears, increasing with the number of deposited layers and resulting in the formation of dense gel-like layers. PE diffusion in the nanopores is thus growth-limiting in this second regime. Even though the pore is entirely filled in solution, the PE layers are known to shrink upon drying, enabling the formation of nanotubes instead of nanowires [43]. For LbL nanotubes comprised of natural polyelectrolytes, two different growth regimes were also observed: a first fast-growing regime followed by a slower growth. This transition was also attributed to reduced diffusion of PE chain into the pores. [44].

Effect of geometrical confinement on LbL assembly conditions

Geometrical confinement does not only affect the growth of multilayers, but also has an impact on the assembly conditions. It has been observed that the geometry of the template particularly influences two factors: dipping time and the effect of ionic strength.

Dipping time

When using nanoporous templates, one must take into account the time needed for the chains to diffuse through the pores. Therefore, the commonly used dipping time for PAH/PSS is 30 minutes [7, 45], which is longer than for flat substrates. Indeed, for flat films, it has been observed that both PAH and PSS adsorbed in less than 10 min [13].

Studies about reducing this dipping time were performed for flat films. When the deposition time ranges from 1 to 5 minutes, it was noticed that surface is mostly covered by random islands while for deposition times of over 10 minutes, the adsorbed layer was homogeneous [13]. For confined geometries such as nanoporous templates, similar studies seem yet to be performed.

Ionic strength

When working with nanoporous templates, ionic strength may also participate in the infiltration of the polyelectrolyte chains inside the pores [46]. This is especially important when the pore diameter is extremely small, for example lower than 100 nm. In such conditions, the addition of a multivalent salt like $CaCl_2$ is crucial as it leads to the shrinking of the PE chains due to reduced electrostatic interactions. The PE chains are then small enough to migrate into and adsorb onto the nanopores. A monovalent salt has the same effect on the chains structure but also decreases the net charge of the chains. However, a multivalent salt yields oppositely charged monomers, enhancing the electrostatic attractions between unbound chains and calcium-bound chains. The inter-chain repulsion is thus reduced, resulting in a higher surface coverage inside the pores [47].

In nanopores, the excessive addition of salt also results in the neutralisation of the PE chains, or even its charge inversion. Both prevent PE adsorption and the latter may even result in the precipitation of the PE chains in the dipping solution. Furthermore, above a certain critical concentration of salt, the creation of opposite charges on the chains can create clusters of chains. Those clusters can then clog the pores by depositing at the top surface of the porous template. It is, therefore, necessary to determine the critical salt concentration. It the case of 15 PAH/PSS bilayers assembled in AAO templates with sub-100-nm pore size, the threshold was 5 mM of $CaCl_2$ [47] (See Figure 1.23).

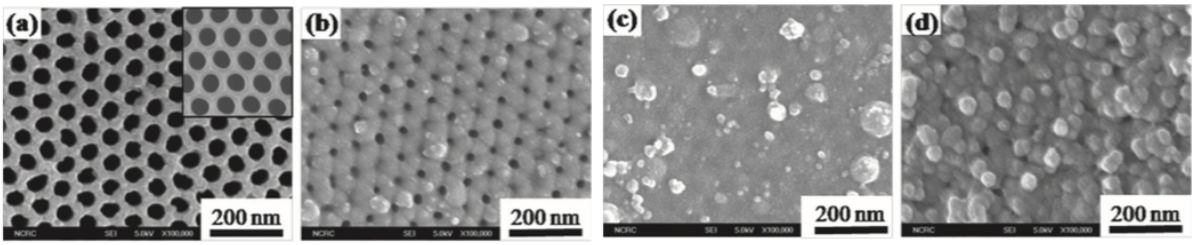

Figure 1.23: $(PAH/PSS)_{15}$ multilayers assembled on nanoporous AAO-membrane templates as a function of $CaCl_2$ concentration: (a) 1, (b) 5, (c) 50, (d) 100 mM. The inset is (a) shows the AAO membrane before the LbL assembly [47].

1.5 LbL for drug delivery applications

Layer-by-layer assembly provides the tools and possibility to fabricate systems that can achieve localised and stimuli-responsive drug delivery. Within the last decade, much progress has been made in the development of LbL-based delivery films or capsules. The interest in nanotubes for delivery applications remains low, although slowly growing over the past few years [6, 41, 48].

1.5.1 Drug delivery systems

Nanocarrier-based drug delivery platforms are considered suitable alternatives to traditional vehicles since 1) they enable the accumulation of drugs at specific sites of interest, therefore limiting the undesired side effects to healthy organs; 2) they limit the required doses as they only reach specific targeted sites; and 3) they prolong the circulating half time of the drugs.

Despite all these potential advantages, drug delivery systems still have to overcome one challenge: face a series of biological barriers that prevent the drug to properly achieve its therapeutic effect. Some strategies have, however, been developed to overcome these obstacles, including various surface functionalisation schemes like PEGylation [49].

Layer-by-layer assembly is a suitable method to construct such nanocarrier as it is possible to finely engineer their size and shape. Other assets are the ability to tune the composition, stability and surface functionalisation thanks to the wide range of material available for this technique [50]. More importantly, we can use biopolymers as assembling materials in LbL nanocarriers which are quite interesting for biomedical applications. Indeed, LbL assembly can be performed in aqueous solution and does not require any organic solvent, which is a notable advantage when using bio-molecules such. Among biom-olecules, proteins are suitable for delivery applications because of their low or even non-existent toxicity and efficient removal from the body. Protein-based delivery vehicles are able to evade the immune system and overcome internal barriers in order to reach the site of action [41, 50].

Drug loading

One requirement for drug delivery systems is the ability to correctly incorporate toxic and fragile therapeutics compounds and shield them from the body. This can be achieved by three methods: 1) incorporation of the drug into the layers, 2) the preloading of the template with the drug, and 3) trapping of the cargo inside the delivery vehicles. Theses are all depicted in Figure 1.24. Layer-by-layer assembly allows the build up of any of these systems. [41, 48, 50, 51]. .

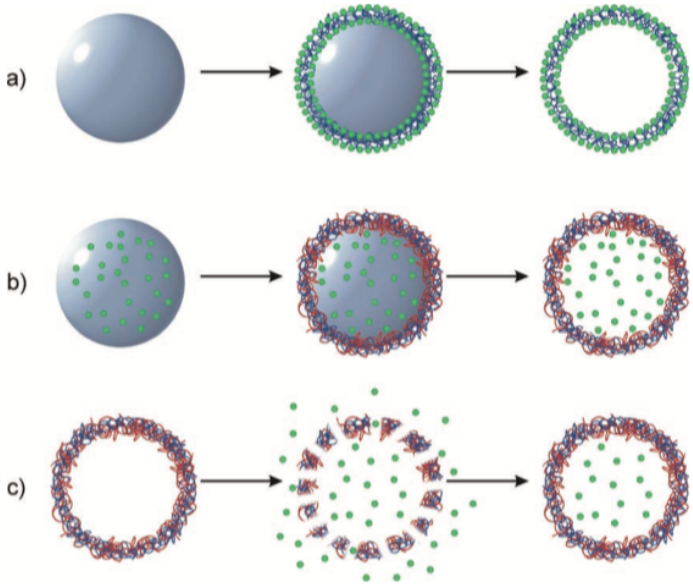

Figure 1.24: Methods for drug encapsulation within LbL capsules. a) Incorporation of the cargo in the capsule walls b) Preloading the template with the drug before LbL assembly c) Postloading the drug delivery system by changing the wall permeability [50].

Drug delivery and cellular internalisation

There are several paths to introduce the drug into the body, depending on the therapeutic and the disease. In the case of drug delivering nanotubes, the treatment is most commonly introduced into the body through injection. However, one must note that LbL assembly is also suitable to prepare implants, enabling a controlled or prolonged release of therapeutics from the implant [50].

The delivery of the therapeutic may be directed by adding targeting agents on the delivery vehicle. Depending on the surface functionalisation of the drug carrier, specific cells or tissues can be targeted. The benefits of localised delivery are the minimisation of the side effect by restricting the access to healthy tissue, and the increase of the local concentration of the drug, thus enabling a lower dosage of therapeutics without affecting the efficiency [50]. Once the nano-carrier has reached the targeted organ or tissue, barriers at the cellular level need to be crossed. All these barriers are depicted in Figure 1.25.

The first barrier is the lipid bilayer membrane. Depending on the size and shape of the carrier, several internalisation schemes are possible: either the carrier is small enough to directly cross the cellular membrane, or they have to rely on endocytosis or phagocytosis. Endocytosis consists of the cells membrane engulfing the outside material, thus forming a so-called endosome. Phagocytosis is one of the many mechanisms of endocytosis, but is triggered by the presence of specific materials (such as synthetic particles, bacteria or viruses) [50].

Once internalised by the cell, the nano-carrier is contained in an endosomal vesicle, which can merge with lysosomes. These vesicles have a notably lower pH (4.5-5) and contain enzymes that can degrade foreign materials. Some drug vehicles thus degrade or take advantage of the change in pH to release their cargo; the specifics of the drug release will be discussed later on. Some delivery vehicles can also escape the vesicles. Several strategies for endosome or lysosome release exists, one example being the incorporation of membrane disrupting peptides into the carriers multilayers [50].

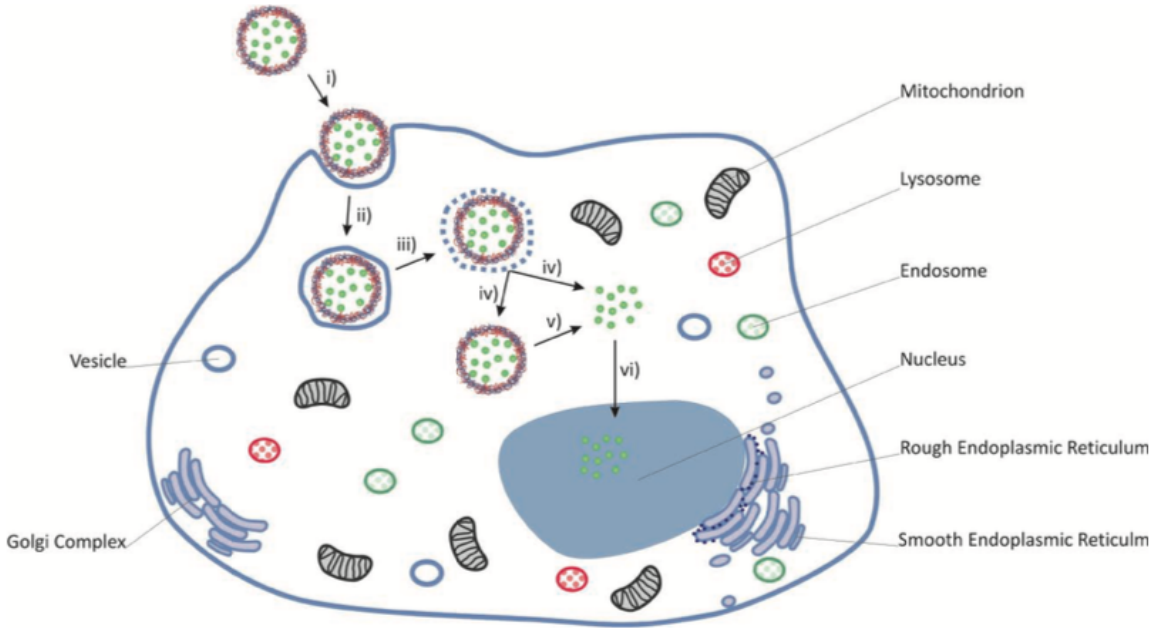

Figure 1.25: Drug delivery path: i) nano-carrier internalisation by endocytosis; ii) endosomal or lysosomal vesicle; iii) rupture of the vesicle; iv) release of the nano-carrier in the cytosol; v) drug release from the nano-carrier; vi) further transport into the nucleus or other organelles [50].

Drug release

Once the carrier has reached its target and has been incorporated into the cells, the drug release can either be "passive", meaning it occurs through drug diffusion, or it can be stimuli-responsive. There are three types of stimuli: biological, physical (light, electric or magnetic field, temperature) or chemical (pH, ionic strength). The release of the drug might also require the degradation of the carrier. A quick review of some available release routes is presented in Appendix A [50, 51, 52].

1.5.2 LbL nanotubes for drug delivery

Although most of the nanostructures assembled by LbL for biomedical applications are capsules and films [50], there are some papers that cover the use of LbL nanotubes for drug delivery applications [41, 53].

The use of hollow nanotubes for drug delivery applications presents some significant advantages: i) it enables the tailoring of the nano-carrier shape and size; ii) the nanotubes present larger inner and outer surface areas enabling, respectively, a larger drug loading and a higher functionalisation (for targeting for example); iii) they have a longer circulation time in vivo and are much faster incorporated in cells [6, 7, 41]. By using LbL assembly to build up nanotubes, it is also possible to incorporate multiple functions into to inner and outer surfaces, thanks to the inclusion of various components [41].

For drug delivery applications, the nanotube dispersion in aqueous media is required, which is not as forthcoming as it may seem. Indeed, nanotubes tend to aggregates, irreversibly sticking to each other or on the surface, rendering the re-dispersion of the nanotubes after filtration impossible. Saghazadeh *et al.* have however developed a universal method to transfer membrane-templated nanotubes to aqueous media without damage [7]. This technique will be discussed in Section 2.5.

Once dispersed in an aqueous media, drug loading can occur. As nanotubes have two open ends, large quantities of drug molecules can be loaded in the inner cavities, as illustrated in Figure 1.26. The only obvious requirement is that the inserted particles are smaller than the inner diameter of the LbL nanotubes. Molecular capture can by achieved by exploiting the binding abilities of certain proteins, which can be used as building block for the tubes. The release of the cargo can be induced by changes in pH or by replacement reaction [41].

Figure 1.26: Schematic representation of nanoparticle loading in hollow nanotubes of 200 nm inner diameter [41].

It has been observed that synthetic nanotubes are more likely to undergo cellular internalisation than biopolymer-based ones due to their superior rigidity [6]. Core-shell nanotubes are therefore of particular interest, as they can combine both synthetic and natural polyelectrolytes. Rubner *et al.* fabricated such structures using (PAH/PSS) as synthetic PEs and (CHI/HA) as natural PEs [54]. Depending on the position of each system, the properties of the multilayers will change. It is therefore important to understand the properties of each individual system before making core-shell structures. In this work, we will thus investigate the morphology and the properties of (PAH/PSS) and (CHI/HA) films and nanotubes.

Chapter 2

Materials and methods

Contents

2.1 Materials 28
2.1.1 Polyelectrolytes 28
2.1.2 Cross-linkers 28
2.1.3 Substrates 28
2.2 Assembly of multilayer films on flat substrates 29
2.3 Characterisation of the flat multilayer films 29
2.3.1 Ellipsometry 29
2.3.2 Fourier Transform Infrared (FTIR) Spectroscopy 30
2.4 Assembly of multilayer nanotubes 30
2.5 Collection of the nanotubes 31
2.6 Characterisation of the nanotubes 32
2.6.1 Porometry 32
2.6.2 Scanning electron microscopy (SEM) and Scanning transmission electron microscopy (STEM) 32

Overview

This chapter gathers the all experimental information related to this thesis. It presents all the materials and methods that were used to build and characterise both flat polyelectrolyte films and polyelectrolyte nanotubes.

2.1 Materials

2.1.1 Polyelectrolytes

Poly(sodium 4-styrenesulfonate) (PSS, M_w = 70 kDa) was purchased from Acros organics. Poly(allylamine hydrochloride) (PAH, M_w = 120 to 200 kDa) was purchased from Alfa aesar. Their respective chemical structures are represented in Figure 2.1.

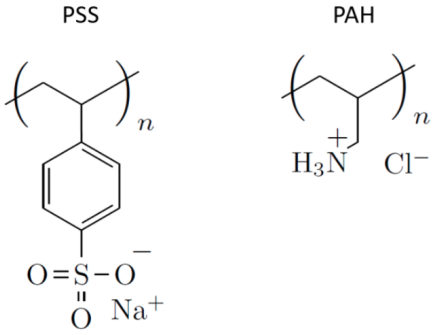

Figure 2.1: Chemical structure of PSS and PAH polyelectrolytes.

Hyaluronan, in the form of research graded dried sodium hyaluronate (M_w=151 kDa - 300 kDa), was acquired from Lifecore Biomedical. Chitosan chloride (M_w = ca. 269kg/mol and 86% DAA) was provided by NovaMatrix. The product is called "Protasan UP CL 213". The chemical structure of these two natural polyelectrolytes is presented in Figure 2.2.

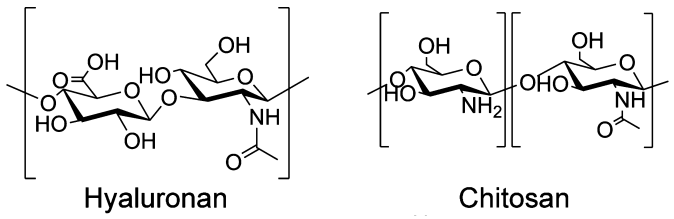

Figure 2.2: Chemical structure of CHI and HA polyelectrolytes [55].

2.1.2 Cross-linkers

1-ethyl-3-(3-dimethylamino-propyl)carbodiimide hydrochloride (EDC) (M_w = 191.7 Da) and N-Hydroxysulfosuccinimide sodium salt (Sulfo NHS) (M_w = 217.13 Da) were purchased from Sigma-Aldrich. Both materials are characterised by a purity of ≥98%. EDC and Sulfo NHS were stored at -20℃ and 4℃ respectively before use.

2.1.3 Substrates

Silicon wafers were purchased from Topsil. They are n-doped with Phosphorus, with a diameter of 100 mm and a thickness of 500-550 µm. They are characterised by a [100] orientation and a resistivity ranging from 3 to 9 Ohm·cm. The top surface is polished while the back surface is alkaline etched.

Sheets of track-etched PC membranes were provided by It4ip (Louvain-la-Neuve, Belgium, `http://www.it4ip.be`). Theses membranes had a pore diameter of 300 nm, a thickness of 25

µm and on average a pore density of $1{\cdot}10^8$ pores·cm^2. The sheets were cut into circles of two different diameters, namely 12.5 and 26 mm.

It4ip also provided the hydrophilic poly(ethylene terephthalate) (PET) used for the microscopy observations (see Section 2.6.2) . These membranes have a pore size of 200 nm, thickness of 23 µm and pore density of ca. $5{\cdot}10^8$ pores·cm^2. They were covered with a 200-nm gold coating using a Cressington 208HR Sputter Coater.

2.2 Assembly of multilayer films on flat substrates

Silicon wafer was cut into 1 cm^2 squares thanks to a diamond pen. Next, the pieces were cleaned with a mix of acetone, ethanol and methanol before being plasma etched for 10 min in an Emitech K1050X with a 100 W power supply.

For synthetic polyelectrolytes, the solutions were freshly prepared before each use, with a concentration of 1 mg/ml. Milli-Q water was used as solvent in all the experiments, to which salt was added in varying concentrations. In the case of PAH/PSS, both monovalent salt (NaCl) and divalent salt ($CaCl_2$) were used simultaneously in concentrations ranging respectively from 0 to 0.5 M and from 0 to 35 mM. The polyelectrolyte solutions were each stirred for 30 minutes, after which their pH was adjusted thanks to a pH-meter. The pH was fixed at 5.5 for PAH/PSS solutions.

For natural polyelectrolytes, the solutions were prepared the eve of their use, with a concentration of 1 mg/ml. The polysaccharide solutions were prepared in aqueous solutions with NaCl concentrations ranging from 0 to 0.5 M. They were left to stir overnight, before undergoing a pH check before their usage. The pH was fixed at 4, 5 or 6.

The build-up of n bilayers occurred in the same manner for both PAH/PSS and CHI/HA multilayers: first the Si squares were dipped for 5 minutes in the polycation solution, then rinsed twice for 2 minutes, after which they were dipped in the polyanion solution for 5 minutes and rinsed again twice for 2 minutes. This cycle was repeated n times, and finally, the samples were immersed in Milli-Q water for 5 minutes before being dried with an air gun. The rinsing solution contained the same salt concentration and was adjusted at the same pH as the polyelectrolyte solutions.

For some CHI/HA multilayers, an additional cross-linking reaction was performed. Each sample was placed in a cell well box with 24 plates and covered with 400 µL of an aqueous solution containing 30 mM EDC and 50 mM Sulfo NHS. The cross-linking solution was freshly prepared: EDC and Sulfo NHS were diluted separately in solutions containing 0.15 M of NaCl, pH 5.5. Each solution was stirred for 30 min and then stored at 4 ℃ until their usage. Once the multilayer assembly was completed, the EDC and sulfo NHS were mixed together and distributed among the samples. The samples were left at 4 ℃ for 24 hours before undergoing a 3-step rinsing (twice for 5 minutes and once for 10 minutes under stirring) and a drying stage.

2.3 Characterisation of the flat multilayer films

2.3.1 Ellipsometry

Ellipsometry enables the measurement of the mulitlayers thickness when these are assembled on flat substrates.

The ellipsometer used in the scope of this thesis was a HORIBA Jobin Yvon single-wavelength ellipsometer. The laser operates in the visible spectral region, with a wavelength of 632.8 nm. The incidence angle varies but is close to 70.5° for all samples. The ellipsometer collects Ψ and Δ values during each measurement. Indeed, the measured signal reflects the change of polarisation when the incident radiation interacts with the measured material. This change is quantified by the amplitude ratio, Ψ, and the phase shift, Δ. Both quantities depend not only on the materials refractive index, but also on the thickness [56].

A macro developed on the Igor Pro software was used to transform Ψ and Δ data into values of film thickness. For this purpose, the measured multilayers were assimilated to a single layer of homogeneous refractive index. The indices of refraction were fixed at 3.882 and 1.525 for the Si substrate and the PE film respectively. For each sample, five measurements were performed on five different spots along the films. The thickness of a clean Si wafer was also measured as reference, which was substracted from all other measurements in order to remove the height of the substrate.

2.3.2 Fourier Transform Infrared (FTIR) Spectroscopy

Fourier transform infrared (FTIR) spectroscopy was performed in order to follow the cross-linking reaction of CHI/HA films.

A Nexus 870 spectrometer from Thermo Scientific was used in transmission mode to measure the spectral fingerprint of CHI/HA film assembled on Si wafers, before and after cross-linking. The samples were simply placed in the path of the incident beam. The resolution was fixed at 4 cm^{-1}, and 16 scans were taken in a row over a wavelength region ranging from 4000 to 400 cm^{-1}. The background was measured before each sample and substracted from the spectra.

The spectra were then analysed using the Omnic software. A baseline correction was performed, fixing the baseline at 3100, 2700, 2100, 1800, 1550 and 900 cm^{-1}, as well as at the edges of the considered wavelength region.

2.4 Assembly of multilayer nanotubes

The polyelectrolyte solutions were prepared in a similar manner than described in Section 2.2, at the same concentration.

PAH/PSS multilayers in nanopores were built by alternatively dipping the PC template in a PAH and PSS solutions for 10 minutes each. For the build-up of CHI/HA multilayers, the adsorption steps lasted 30 minutes each. Between deposition steps, the templates were rinsed twice for 2 minutes in a Milli-Q water solution containing the same amount of salt and adjusted at the same pH as the dipping solution. The rinsing steps served to remove the unadsorbed materials. This cycle was repeated until the number of desired layers were reached, which was 6 in our particular case. Once the build up is finisher, the template is rinced one last time for 5 minutes in milli-Q water.

As each dipping step induces the formation of a membrane on top and at the bottom of the template, a decrusting step needed to be performed in order to prevent the pores from clogging. This is depicted in Figure 2.3. For PAH/PSS nanotubes, the PC membranes were decrusted with cotton swabs every three bilayers. As natural polyelectrolytes tend to clog the nanopores more quickly, the templates were scrubbed every two bilayers for the build-up of CHI/HA nanotubes.

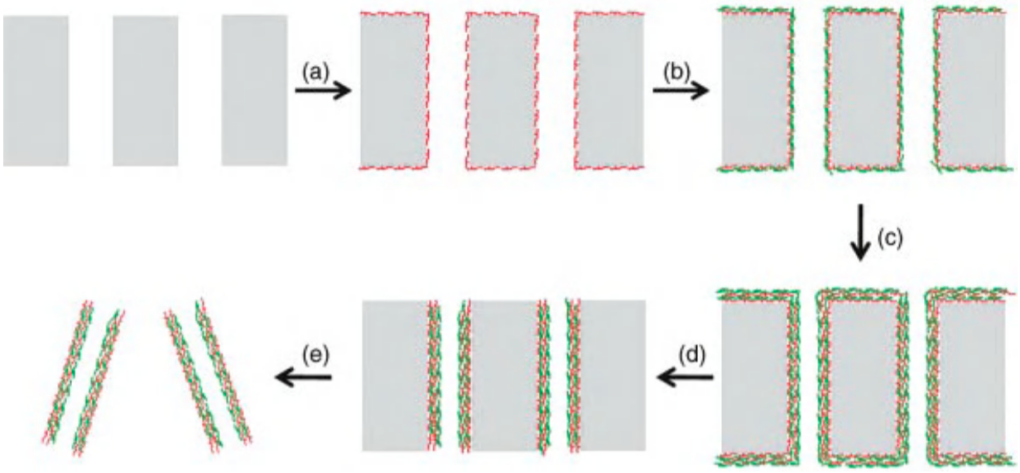

Figure 2.3: Scheme of one cycle of the assembly of polyelectrolytes multilayers inside nanopores [57].

The cross-linking of CHI/HA nanotubes was performed according to the same scheme described in Section 2.2, using the LbL-functionalised membranes and before PC dissolution.

2.5 Collection of the nanotubes

We used the LbL-nanotube collection method described by Saghazadeh *et al.* [7]. In this method, which is depicted in Figure 2.4, the PC template is dissolved in dichloromethane (CH_2Cl_2). The nanotubes dispersed in CH_2Cl_2 are then filtered on a PET filter coated with an adjuvant, in this case, dextran. More precisely, dextran dispersed in CH_2Cl_2 is first filtered over a PET filter. The dextran forms a fine porous pellet on top of the filter. Then, the tubes suspension in CH_2Cl_2 is also mixed with dextran and filtered. This also forms a porous pellet, in which nanotubes are trapped within the dextran. To make sure that all PC is dissolved from the pellet, additional CH_2Cl_2 is passed through the filter. This process creates a powder, that can be collected and immersed in water. The dextran will dissolve, leaving the nanotubes in suspension [6, 7].

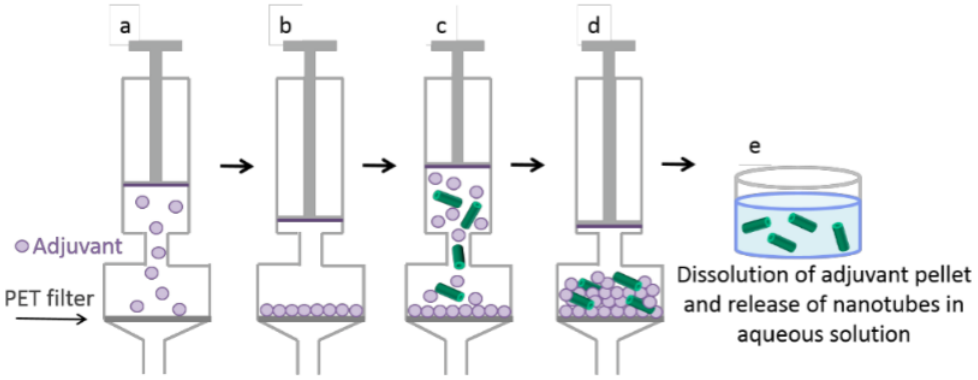

Figure 2.4: Schematic illustration of the nanotubes collection (a) filtration of adjuvant dispersed in CH_2CL_2 through PET filter; (b) formation of the adjuvant pellet on the PET filter; (c) filtration of adjuvant dispersed in the suspension of nanotubes in CH_2CL_2; (d) formation of a powder inside which the nanotubes are trapped; (e) addition of water to dissolve the adjuvant and release the nanotubes [6].

The aqueous solution containing the dispersed nanotubes was filtered through a gold-coated PET filter for the SEM characterisation of the tubes morphology.

2.6 Characterisation of the nanotubes

2.6.1 Porometry

Gas-flow porometry is a technique used to measure the mean diameter of the pores inside the nanoporous templates. It was therefore utilised to measure the pore diameter LbL-modified PC membranes. Porometry measurements were performed by It4ip.

All sample were air-dried before the measurements. They were then fixed on a holder, with an effective area of 0.137 cm^2. They were analysed at ambient temperature by delivering a nitrogen gas flow upstream from the sample. The gas was pressurised at 0.7 bar. The air flow (ml/min) downstream of the sample is measured with a flowmeter. By using relationships based on the Knudsen diffusion and the viscous or Hagen-Poiseuille flow, it is possible to calculate the average pore diameter.

The following expressions relate respectively the Knudsen diffusion flux and the viscous flux (mol/m^2·s)

$$J_{diff} = \frac{4}{3}\frac{d}{l}\frac{(P_{up} - P_{down})}{\sqrt{2\pi MRT}} \quad \text{and} \quad J_{visc} = \frac{d^2}{l}\frac{(P_{up}^2 - P_{down}^2)}{\sqrt{64\mu RT}}$$

in which d is the pore diameter (m), l is the membrane thickness(m), P_{up} and P_{down} are the pressures (Pa) upstream and downstream from the PC membrane respectively, M is the gas molar weight (kg/mol), μ is the dynamic viscosity of the gas (kg/m s), R is the ideal gas constant (J/K·mol), and T is the gas temperature (K) [43].

The sum of these two equations enables the expression of the total volume flow rate Φ (m^3/s):

$$\Phi = (SP)\frac{RT}{P_{atm}}(J_{diff} + J_{visc})$$

with S the effective section area of the PC membrane (m^2), P_{atm} the atmospheric pressure (Pa) and P the transparency of the membrane, which can be expressed in terms of the pore density N (m^{-2}) and the pore diameter

$$P = N\frac{\pi d^2}{4}$$

Finally, the dried wall thickness of the nanotubes in the pores was calculated by substracting the measured pore diameter from the initial pore diameter and dividing this difference by 2.

2.6.2 Scanning electron microscopy (SEM) and Scanning transmission electron microscopy (STEM)

Microscopy observations of the nanotubes morphology were obtained in two different manners, as depicted in Figure 2.5: first using STEM for nanotubes dispersed in CH_2Cl_2 and deposited on a TEM grid, then using SEM for nanotubes dispersed in H_2O deposited on a gold-coated porous PET membrane.

Samples were observed with a JEOL 7600F SEM, which has a transmission detector included. Nanotubes dispersed in CH_2Cl_2 were observed at 30 kV in the STEM mode, using a transmission detector. The gold-coated PET filters were imaged in SEM mode at 5 or 15 kV, depending on the samples.

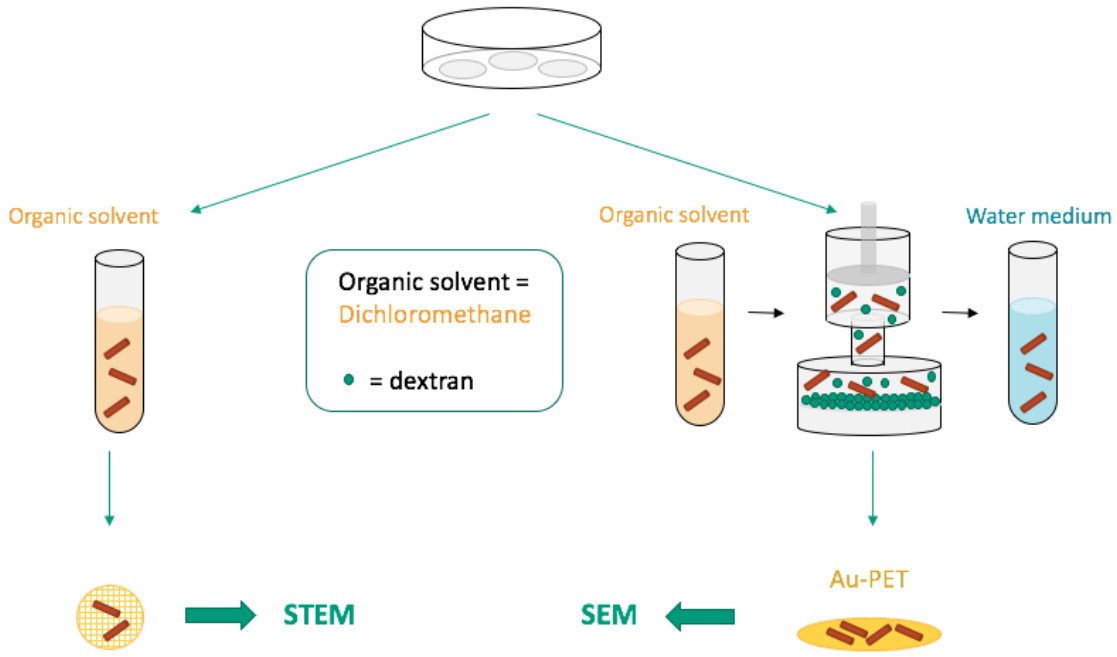

Figure 2.5: Schematic illustration of how the tubes are prepared before microscopy observations

As LbL nanotubes are known to bend and to twist once dispersed in water, a rigidity index was defined in order to quantify the effect of the aqueous solution. This rigidity index involves the root-mean-square end-to-end distance $< R_{EE}^2 >^{1/2}$ of the nanotubes as well as the average contour length L [7]. Theses values were measured using the ImageJ program.

Indeed, nanotubes in water can be assimilated to wormlike objects, with persistence length L_p and contour length L. When L_p is much smaller than L, the end-to-end distance is $< R_{EE}^2 >= 2L \cdot L_p$. However, when L_p is larger than L, $< R_{EE}^2 >= L^2$. This means $< R_{EE}^2 > /L^2$ ranges from 1 when the tubes are very rigid and to $2L_p/L$ for softer tubes with shorter persistence lengths. This index thus reflects the bending rigidity of the nanotubes relatively to their length [7]. Measurements of R_{EE}^2 and L^2 were performed on 25 nanotubes for each system.

Chapter 3

Results and discussion

Contents

3.1 PAH/PSS multilayers 36
3.1.1 Growth 36
3.1.2 Effect of the dipping time 37
3.1.3 Effect of the ionic strength 39
3.1.4 Effect of pH 47
3.1.5 Effect of storage in water 48
3.2 CHI/HA multilayers 49
3.2.1 Growth 50
3.2.2 Effect of pH 51
3.2.3 Effect of the ionic strength 54
3.2.4 Cross-linking 57
3.2.5 Effect of storage in water 60
3.3 Summarising table 62

Overview

This chapter is divided into two sections. The first section outlines the results and discussions related to the assembly and characterisation of PAH/PSS nanotubes with varying processing conditions. The second section presents how these assembling conditions affect nanotubes assembled from natural polyelectrolytes, namely CHI and HA. Both systems were studied separately in order to understand their specific properties. These investigations were performed for the perspective of building core-shell structures comprised of the two analysed systems. The main results are summarised in a table at the end of this chapter, and values for multilayers thickness and rigidity index are gathered in Appendix B.

3.1 PAH/PSS multilayers

The objective of this study is to understand how it is possible to impact the properties of synthetic polyelectrolyte multilayers, such as their rigidity, by selecting specific conditions during the assembly.

The investigated system is PAH/PSS. PAH is a weak polycation with a pKa value of 8.7 when diluted in solution. When the pH of the surrounding environment is in the range of this value, PAH is only half ionised, becoming fully charge for lower pH values. PSS is a strong polyanion, meaning that it remains fully ionised over a large pH range.

3.1.1 Growth

The first aspect that was studied during this thesis was the growth of PAH/PSS multilayers on flat Silicon substrates. In order to do so, samples with increasing numbers of PAH/PSS bilayers were prepared using a solution containing 0.1 M NaCl and 5 mM $CaCl_2$, with the pH fixed at 5.5. The results, presented in Figure 3.1, show a linear growth. This is expected since we work with synthetic PEs, a weak and a strong one.

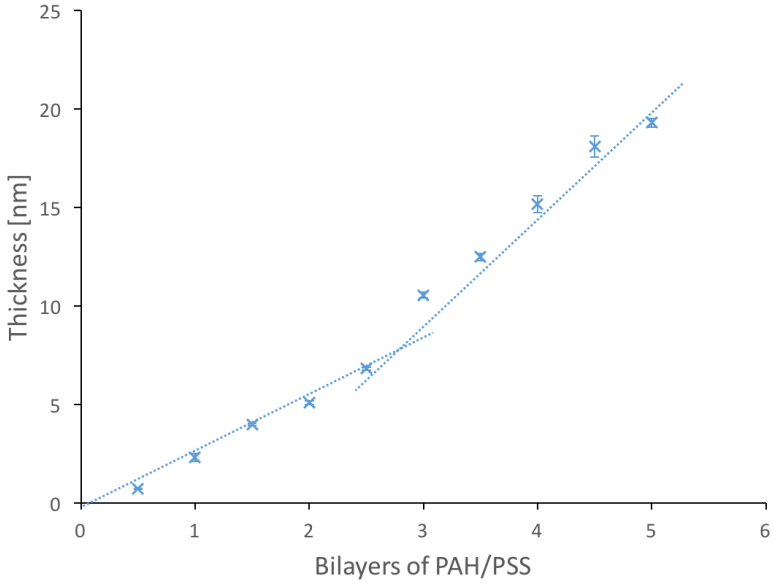

Figure 3.1: Evolution of the film thickness for PAH/PSS multilayers assembled on flat silicon wafers in 0.1 M NaCl and 5 mM $CaCl_2$ at pH 5.5

The final thickness for 5 bilayers is 19.3±0.2 nm, with ca. 4 nm per bilayer. In the literature, the thickness gain after each adsorbed bilayers ranges from 1 to 10 nm, depending on the selected processing parameters and the substrate [13]. Tronin *et al.* assembled PAH/PSS multilayers on Si substrates with added salts $MnCl_2$ and NaBr at pH 2 and measured a thickness gain of 6.1 ± 0.7 nm per bilayer [58]. Kolainska *et al.* also used silicon as substrate, but used different assembling conditions. They added 0.15 M NaCl, with a pH ranging from 5 to 6 and used 0.5 g/L of polyelectrolyte for the dipping solution. They measured an average thickness of 0.5 nm per layer [59]. Elzbieciak *et al.* fabricated PAH/PSS films on Si substrates in a solution of 0.15 M ionic strength, with 0.5 g/L PE concentration. They fixed the pH at 4, 7, 9 and 11 and measured, for 6 bilayers, a final thickness of ca. 4, 7, 6 and 9 nm respectively [18]. The measurements represented in Figure 3.1 are situated in the expected range. The variations compared to other observed values in the literature can be explained by the difference in processing conditions.

The presence of two zones can also be highlighted in Figure 3.1: a first zone close and thus affected by the substrate and a second zone which is the real "bulk" film. The transition from one zone to the next occurs after 3 bilayers. A third zone could also be expected, which is affected by the upper air interface, but it is not visible in our case. In accordance to what can be found in the literature on this subject [41,60], the first zone is characterised by thinner layers. The first layer of PAH adsorbed on the Si-SiO_2 wafer surface adopts a flat conformation but there are many voids. These voids only start to be filled after the third layer, as the second layer is PSS and thus only adheres on the PAH chains. It takes a few layers for the film to uniformly cover the substrates [41,60].

3.1.2 Effect of the dipping time

Typically, when building nanotubes, each dipping step is fixed at 30 minutes. This duration allows the tubes to diffuse inside the pores and to adsorb on the pore walls. However, as many experiments needed to be performed in the scope of this thesis, it was crucial to gain time. Therefore, we studied the possibility to decrease the dipping time when working on nanoporous templates. In order to see how the dipping time affects the tubes, PAH/PSS nanotubes were built in a PC membrane with 300 nm sized pores. The dipping solutions contained 0.1 M NaCl and 5 mM of $CaCl_2$, with a pH fixed at 5.5. Three different dipping times were tested out in parallel: 10 minutes, 20 minutes and 30 minutes.

Porometry measurements provided the evolution of the inner pore diameter for these nanotubes assembled with these different dipping times. The results were translated into wall thicknesses, which are depicted in Figure 3.2. In parallel, we used STEM to determine the average inner and outer diameters for each sample, based on the measurement of 25 nanotubes. Typically obtained images are gathered in Figure 3.3.

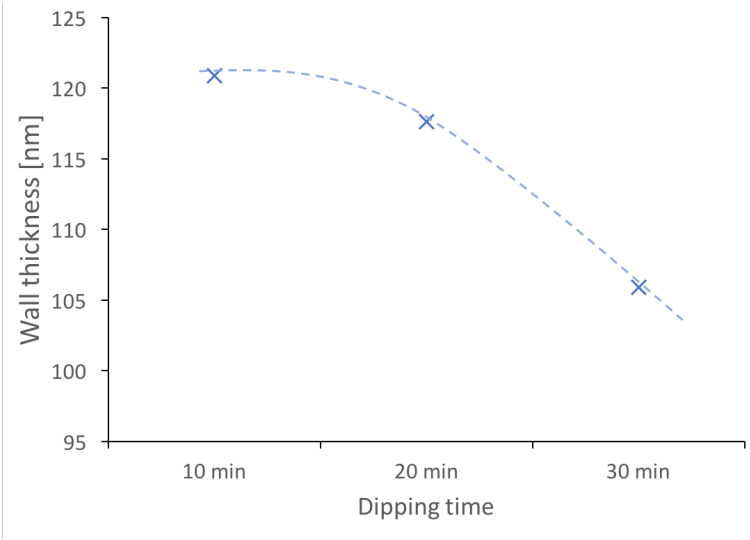

Figure 3.2: Evolution of the $(PAH/PSS)_6$ final wall thickness for increasing dipping times (based on one measurement per sample, see Table B.1 for indicative error values).

Porometry measurements suggest that the wall thickness is similar for 10 and 20 minutes dipping. For 30 minutes of dipping, there is, however, a decrease. One will thus have the impression that thinner layers are built with longer deposition steps. This is quite surprising, as one would expect the opposite effect. A possible explanation for this would be a bad decrust on the 30-minutes samples. This explanation may prove to be correct as no significant difference was observed in the STEM measurements for the average inner and outer diameters of the nanotubes for all the studied samples.

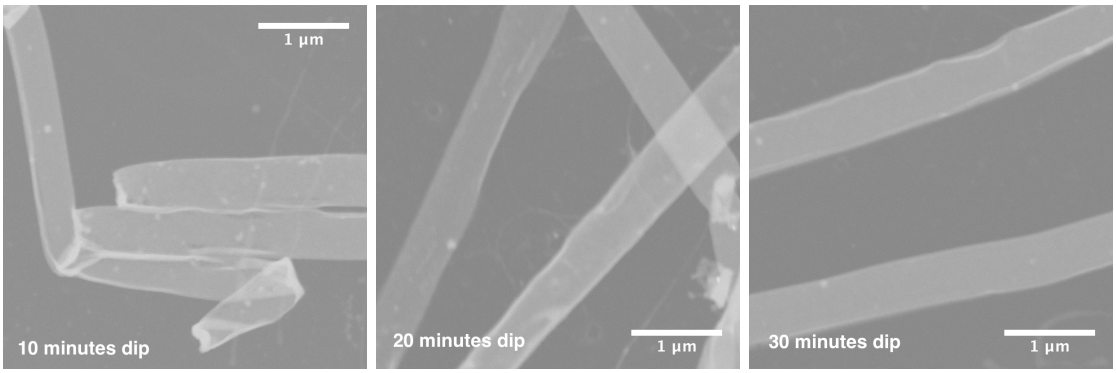

Figure 3.3: STEM images of $(PAH/PSS)_6$ nanotubes assembled with increasing dipping time dispersed in CH_2Cl_2 (left to right: 10 minutes, 20 minutes and 30 minutes).

To ascertain if a decrease of dipping time does not affect the tubes morphology, the multilayered nanotubes were released from the templates and dispersed in both CH_2Cl_2 and water. Scanning electron microscopy measurements were then performed. Some of the obtained images are gathered in Figures 3.4 and 3.5. There are no visible effects of the decreased dipping times on the tubes morphology.

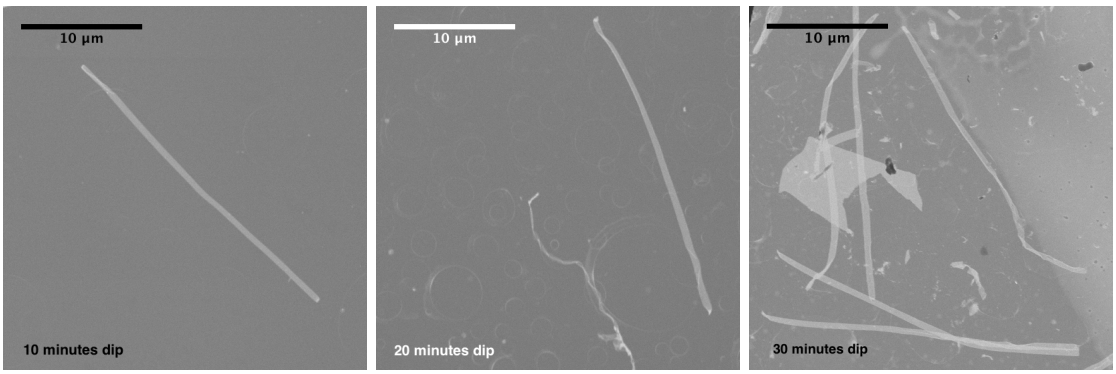

Figure 3.4: STEM images of $(PAH/PSS)_6$ nanotubes assembled with increasing dipping time dispersed in CH_2Cl_2 (left to right: 10 minutes, 20 minutes and 30 minutes).

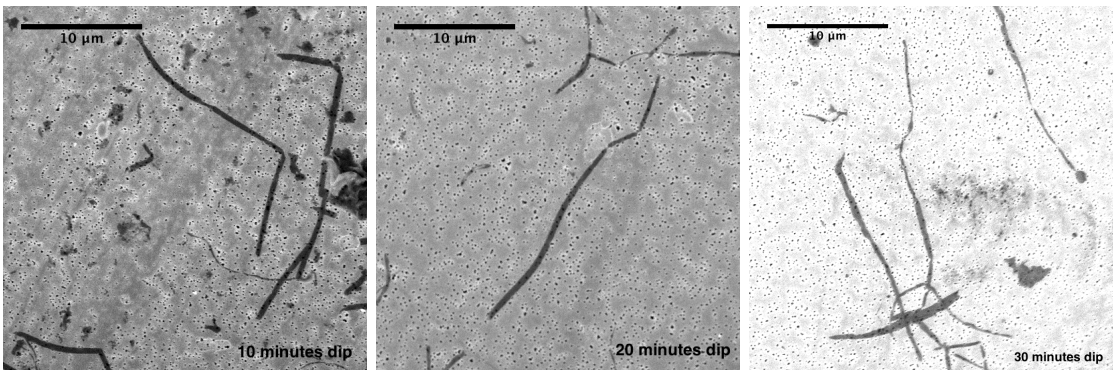

Figure 3.5: SEM images of $(PAH/PSS)_6$ nanotubes assembled with increasing dipping time dispersed in H_2O (left to right: 10 minutes, 20 minutes and 30 minutes).

Next, the rigidity index was analysed both in CH_2Cl_2 and in water. These results are gathered in Figure 3.6. Like for porometry results, there is no significant difference in rigidity for tubes assembled with 10 minutes dipping compared to tubes assembled with 20 minutes dipping: the rigidity indices are similar, both in CH_2Cl_2 and in water. The rigidity index for nanotubes with

30 minutes dipping step was higher when dispersed in CH_2Cl_2, but comparable to the other samples when dispersed in water.

As the dispersion in water is the aspect of interest in view of drug delivery applications, and because of the lack of effect of decreased dipping times on this factor, the dipping time for further experiments was set at 10 minutes.

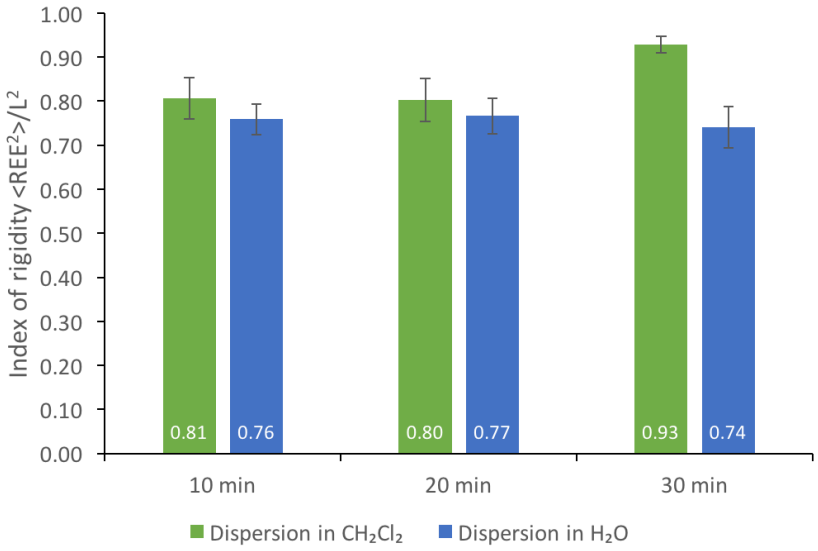

Figure 3.6: Evolution of the rigidity index for $(PAH/PSS)_6$ nanotubes assembled with increasing dipping times, dispersed in CH_2CL_2 and in H_2O (based on the measurements of 25 nanotubes).

3.1.3 Effect of the ionic strength

An important parameter in the assembly of LbL nanotubes is the concentration of added salts. Most studies use varying concentration of NaCl, going from 0.1 M to sometimes as high as 3 M [21, 61]. For biomedical applications, the typical ionic strength is 0.15 M. Multivalent salts are sometimes also added in order to further increase the film thickness [21], one such salt is $CaCl_2$.

In this section, the effect of increasing concentration of both NaCl and $CaCl_2$ will be analysed, first on flat substrates, then in nanoporous substrates. The pH value was fixed at 5.5 in both cases.

On flat Si wafers

PAH/PSS films with 6 bilayers were assembled on Si wafer at pH 5.5 with different salt concentrations. The standard protocol of our group contains 0.1 M NaCl and 5 mM $CaCl_2$. First, the concentration in $CaCl_2$ was increased to 15 mM while keeping the concentration in NaCl fixed at 0.1 M. For another sample, no $CaCl_2$ was added at all. The ellipsometry measurements of the multilayers thickness are presented in Figure 3.7, and compared to a sample assembled in simple Milli-Q water.

What can be highlighted from these results is that there is a significant thickness gain when adding NaCl compared to zero salt addition during the assembly. The addition of salt does not affect the growth regime, as it remains linear. There is also a slight increase in the films thickness when adding $CaCl_2$ on top of the 0.1 M NaCl to the dipping solution, but increasing the concentration further has no significant effect.

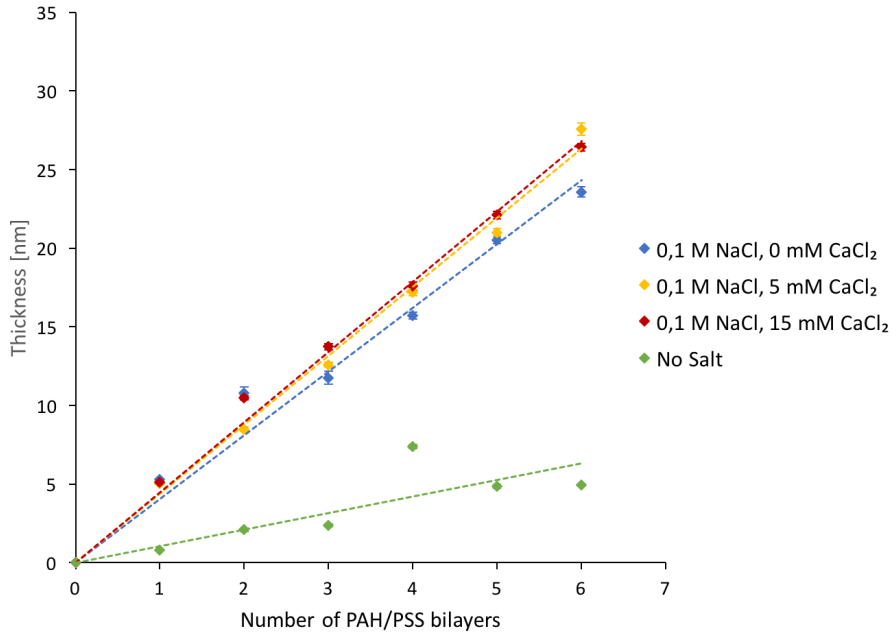

Figure 3.7: Evolution of the film thickness for PAH/PSS multilayers on Si substrates built in increasing concentrations of $CaCl_2$ at fixed 0.1 M NaCl concentration.

Next, the concentration of NaCl was increased from 0 M to 0.5 M while keeping the content in $CaCl_2$ fixed at 15 mM. Samples with intermediate salt concentrations (0.1 M and 0.2 M) were also assembled in the same conditions. The thicknesses of the resulting films are gathered in Figure 3.8. Once again, there is a notable thickness increase when adding salt to the dipping solution. The linear growth is not affected either. However, for NaCl concentrations of 0, 0.1 or 0.2 M, there is no effect on the film thickness. It is only when adding 0.5 M of NaCl to the PE solutions that one can observe a gain in film thickness. Nevertheless, this increase remains quite small, only adding 5 nm to the final thickness after the adsorption of 6 PAH/PSS bilayers.

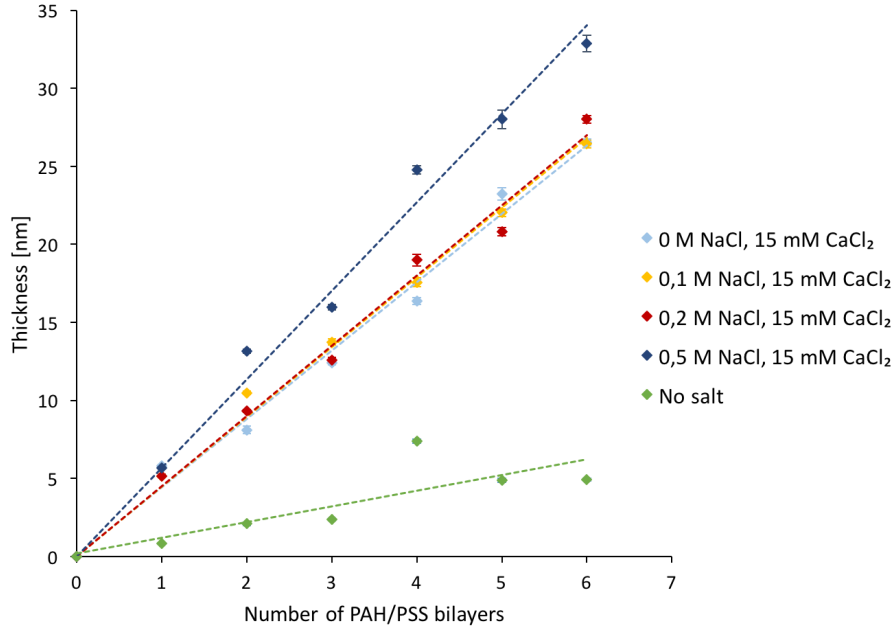

Figure 3.8: Evolution of the film thickness for PAH/PSS multilayers on Si substrates built in increasing concentrations of NaCl at fixed 15 mM $CaCl_2$ concentration.

The data presented above can be translated into average thickness per bilayer by taking the slopes of the growth curves. This is presented in Figure 3.9. From theses graphs, one can observe that adding $CaCl_2$ in increasing concentrations to the PE solutions has little to no effect on the thickness per bilayer. For NaCl, there is only a slight effect when increasing the concentration above 0.2 M.

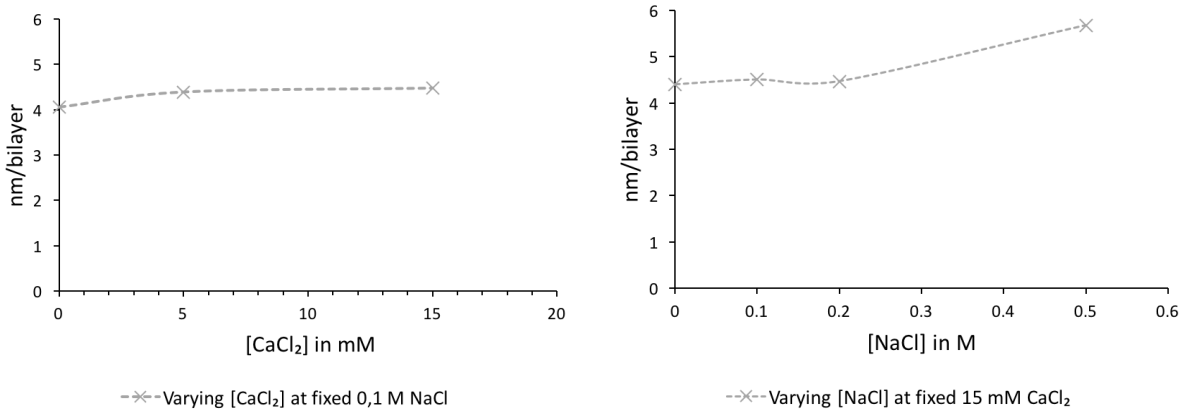

Figure 3.9: Thickness per bilayer for $(PAH/PSS)_6$ multilayers Si substrates, built in increasing $CaCl_2$ (left) and NaCl concentrations (right).

The measured thickness per bilayer for films that were assembled without the addition of any salt is ca. 1 nm/bilayer. Layers, therefore, grow four times thicker when adding salt to the polyelectrolyte solutions, be it only 15 mM of $CaCl_2$ or 0.1 M of NaCl. This also points out that when using a multivalent salt, the effect is the same as for monovalent salt while using much smaller quantities.

As both a monovalent and a divalent salt are used, it is possible to calculate the ionic strength as $I = \frac{1}{2}\sum_{i=1}^{n} c_i z_i^2$ in which c_i is the molar concentration of ion i (for both anions and cations) and z_i is the charge number of that ion. Figure 3.10 plots the thickness per bilayer in terms of ionic strength for the sake of clarity. This graph indicates that by slightly increasing the ionic strength (from 0 to 0.045 M), there is a considerable gain of thickness per bilayers. However, one must go to an ionic strength of ca. 0.5 M in order to note a further increase in layer thickness.

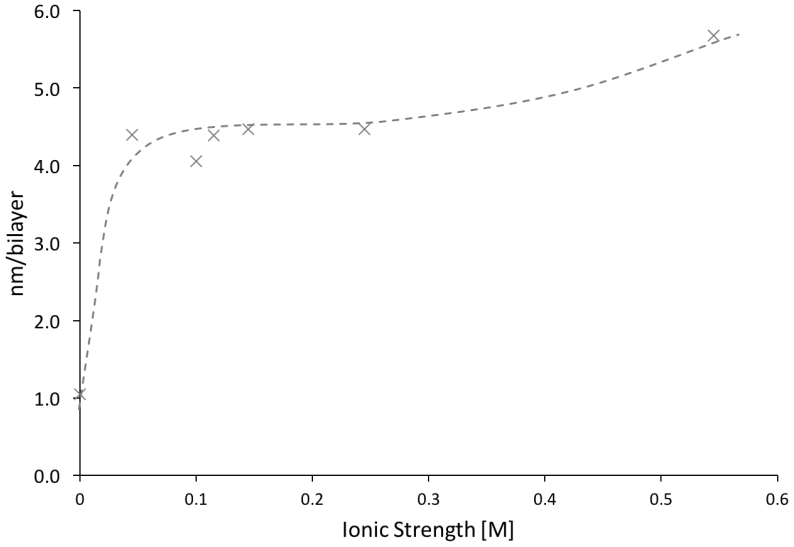

Figure 3.10: Evolution of the film thickness for PAH/PSS multilayers on Si substrates with increasing ionic strength.

In conclusion, adding salt to the PE solutions during LbL assembly causes the films to gain in thickness. However, using higher concentrations than the standard 5 mM of $CaCl_2$ and 0.1 M of NaCl does not have a pronounced effect, except when considerably increasing the salt concentration (like adding 0.5 M of NaCl for example).

In a nanoporous template

In a similar manner $(PAH/PSS)_6$ multilayers were built in a nanoporous PC membrane. The salt concentration of the PE solution varied, but the pH was fixed at 5.5 for all samples. The substrates were dipped in each polyelectrolyte solution for 10 minutes.

To analyse and compare salt concentration effect, we first altered the $CaCl_2$ content of the PE solutions, ranging from 0 mM to 35 mM, with 5 mM, 15 mM and 25 mM as intermediate concentrations. The NaCl content was fixed at 0.1 M for all these samples. Higher concentrations of $CaCl_2$ were not tested as they tend to induce the clogging of the nanopores [47].

Porometry measurements were performed on each sample in order to compute the wall thickness of the PAH/PSS nanotubes. To be sure that the measurements were not affected by remaining crust on top or at the bottom of the PC membrane, each sample was decrusted before the analysis and left to dry. The resulting evolution is presented in Figure 3.11. From this graph, one can see that the addition of a multivalent salt helps to adsorb thicker layers of PAH/PSS. There is indeed a thickness gain of about ca. 15 nm. However, increasing the concentration of $CaCl_2$ above 5 mM has no noticeable effect, as the wall thickness reaches a plateau.

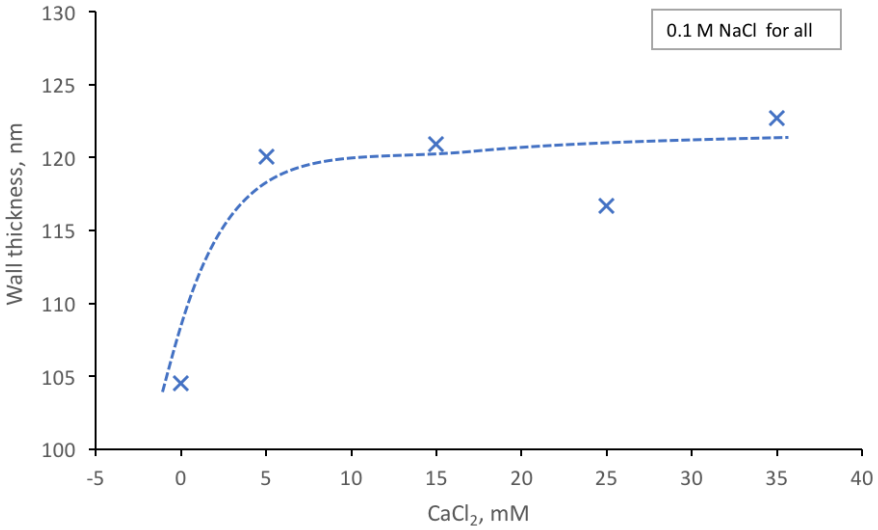

Figure 3.11: Evolution of the wall thickness for $(PAH/PSS)_6$ nanotubes for increasing concentrations of $CaCl_2$ at fixed 0.1 M NaCl concentration (1 measurement per sample, see Table B.1 for guide value for the error bars).

To observe the effect on their morphology, the nanotubes were released from the PC membranes and dispersed in both CH_2Cl_2 and H_2O. These solutions were then filtered through respectively a TEM grid and a gold-coated PET filter in order to be observed by STEM and SEM. Some of the resulting images are gathered in Figures 3.12 and 3.13. No observations can be made from the images of CH_2Cl_2-dispersed tubes. However, from the snapshots of water-dispersed nanotubes, one will have the impression that the addition of $CaCl_2$ to the PE solutions renders the nanotubes more rigid.

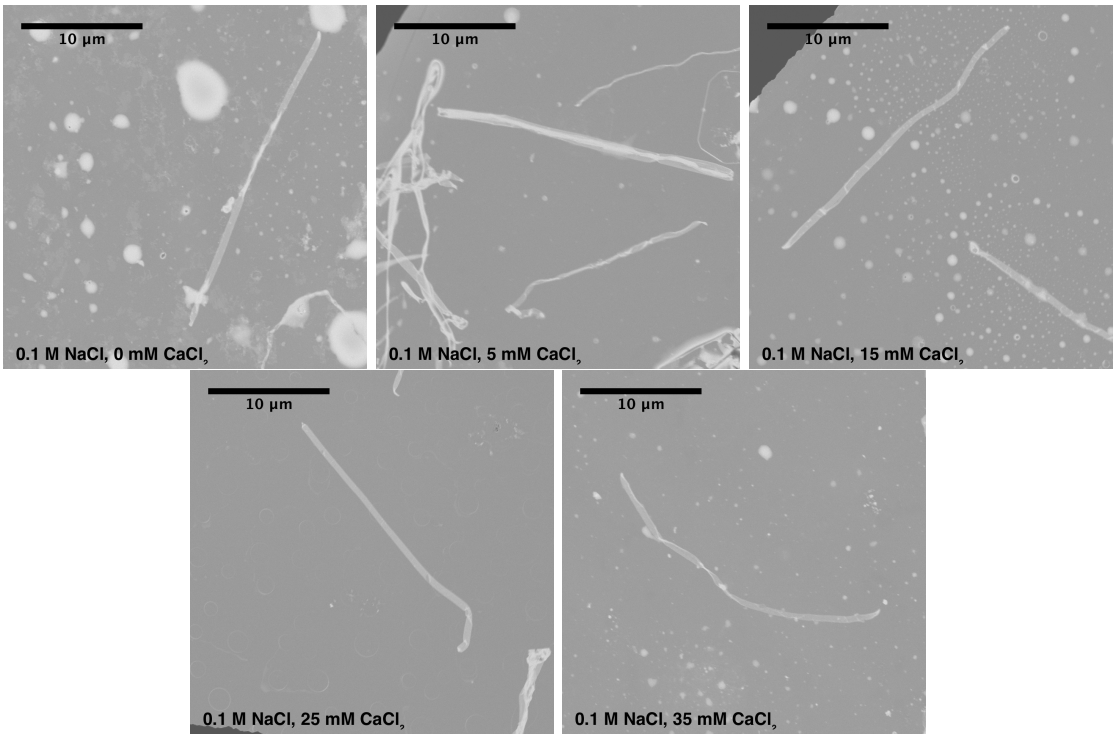

Figure 3.12: STEM images of $(PAH/PSS)_6$ nanotubes assembled in 0.1 M of NaCl and increasing concentration of $CaCl_2$, dispersed in CH_2Cl_2. From left to right: 0 mM, 5 mM, 15 mM and below, 25 mM and 35 mM.

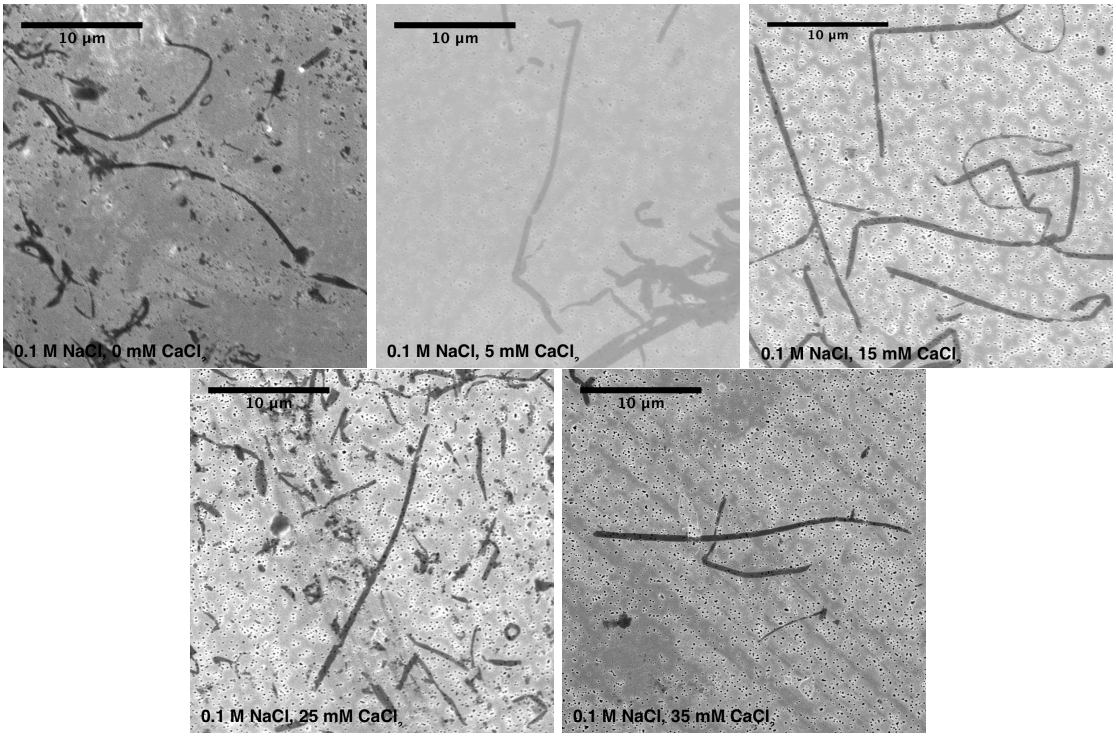

Figure 3.13: SEM images of $(PAH/PSS)_6$ nanotubes assembled in 0.1 M of NaCl and increasing concentration of $CaCl_2$, dispersed in H_2O. From left to right: 0 mM, 5 mM, 15 mM and 25 mM and 35 mM on the second row.

To verify this assumption, the rigidity index was computed for each of these samples. The results are depicted in Figure 3.14. From these measurements, one can say that although average rigidity is slightly improved at 15 mM $CaCl_2$, the effect remains very small. Despite the fact that adding 5 mM of $CaCl_2$ increases the film thickness compared to 0 M $CaCl_2$, there is no impact of the $CaCl_2$ concentration on the rigidity of the $(PAH/PSS)_6$ tubes.

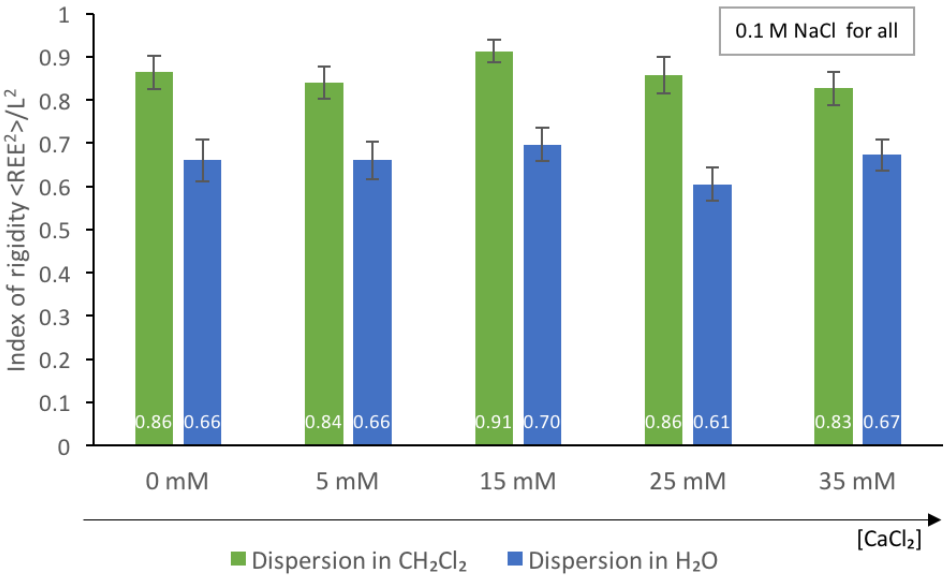

Figure 3.14: Evolution of the rigidity index for $(PAH/PSS)_6$ nanotubes assembled in increasing concentrations of $CaCl_2$ at fixed 0.1 M NaCl concentration, dispersed in CH_2CL_2 and in H_2O (based on the measurements of 25 nanotubes).

Next, the effect of varying concentration of NaCl was studied. The $CaCl_2$ content was fixed at 15 mM, as this value slightly improved the rigidity of the tubes. The concentration of NaCl was increased from 0 to 0.5 M, by step of 0.1 M.

The average inner pore diameter was measured using porometry and enabled the determination of the wall thickness of the tubes. The results are represented in Figure 3.15.

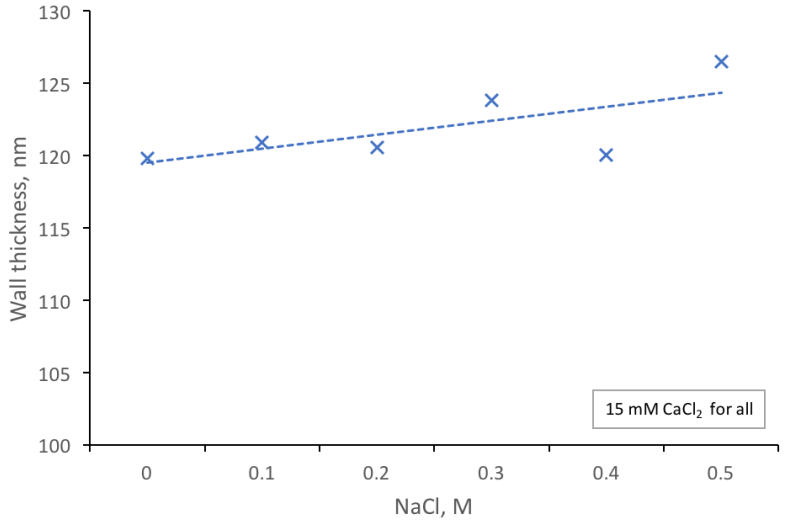

Figure 3.15: Evolution of the wall thickness for $(PAH/PSS)_6$ nanotubes built in increasing concentrations of NaCl at fixed 15 mM $CaCl_2$ concentration (1 measurement per sample, see Table B.1 for indicative error values).

The observed trend seems to be a slight increase, but as the total increase is less than 5 nm, this is negligible. It could, however, be suggested that the increase of the layers thickness was hindered by the fact that, when wet, the multilayers completely fill up the pores. Indeed, with an average inner diameter of ca. 60 nm when dry, one expects that the wet layers would take up the entirety of the available space in the nanopores. This suggestion also holds for the measurements presented in Figure 3.11.

The nanotubes were also released from the PC template and imaged after both CH_2Cl_2 and H_2O dispersion. From the images of the nanotubes after PC dissolution, one can observe that the addition of NaCl seems to render the tubes less soft and therefore straighter. While they still bend, they do not have the slightly wavy morphology they have when no NaCl is added to the polyelectrolyte solutions during the LbL assembly.

For tubes collected from water dispersion, one can see that the filtration of the aqueous solution through the PET filter causes some damage to the tubes. The presence of broken pieces of nanotubes is visible for most samples. This was also the case for the samples in Figure 3.13. Other observations on the tubes morphology with respect to the NaCl concentration cannot be made based on theses images alone.

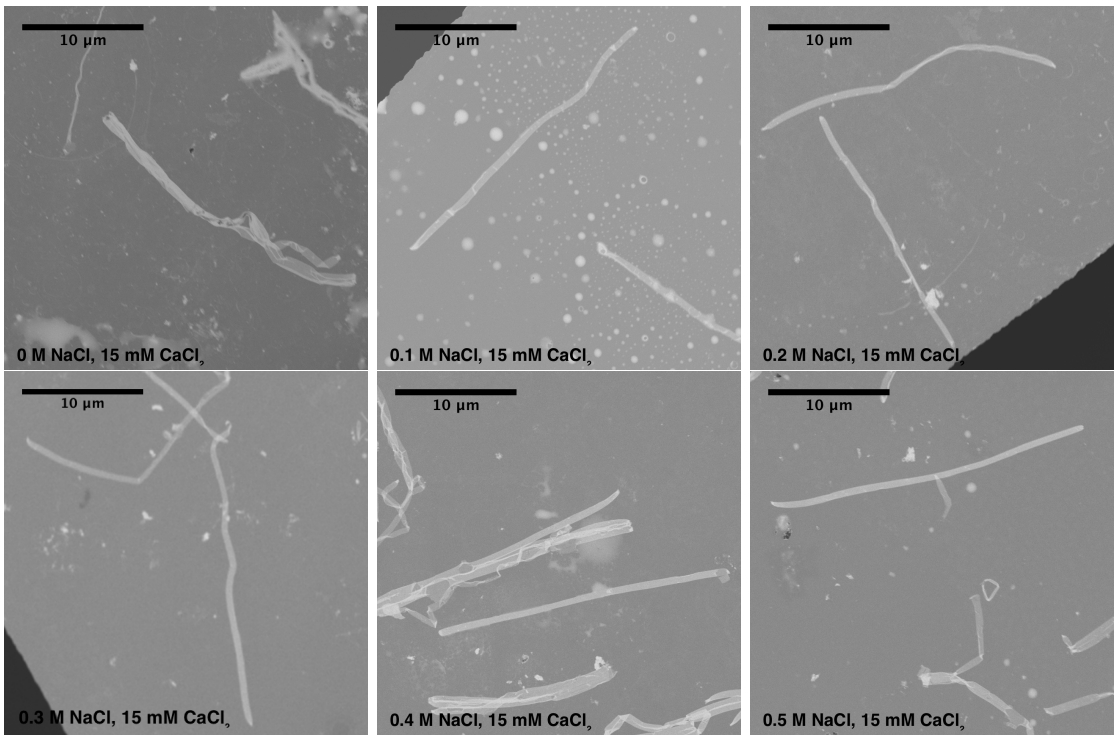

Figure 3.16: STEM images of $(PAH/PSS)_6$ nanotubes assembled in 15 mM of $CaCl_2$ and increasing concentration of NaCl, dispersed in CH_2Cl_2. From left to right: 0 M, 0.1 M and 0.2 M; on the second row: 0.3 M, 0.4 M and 0.5 M.

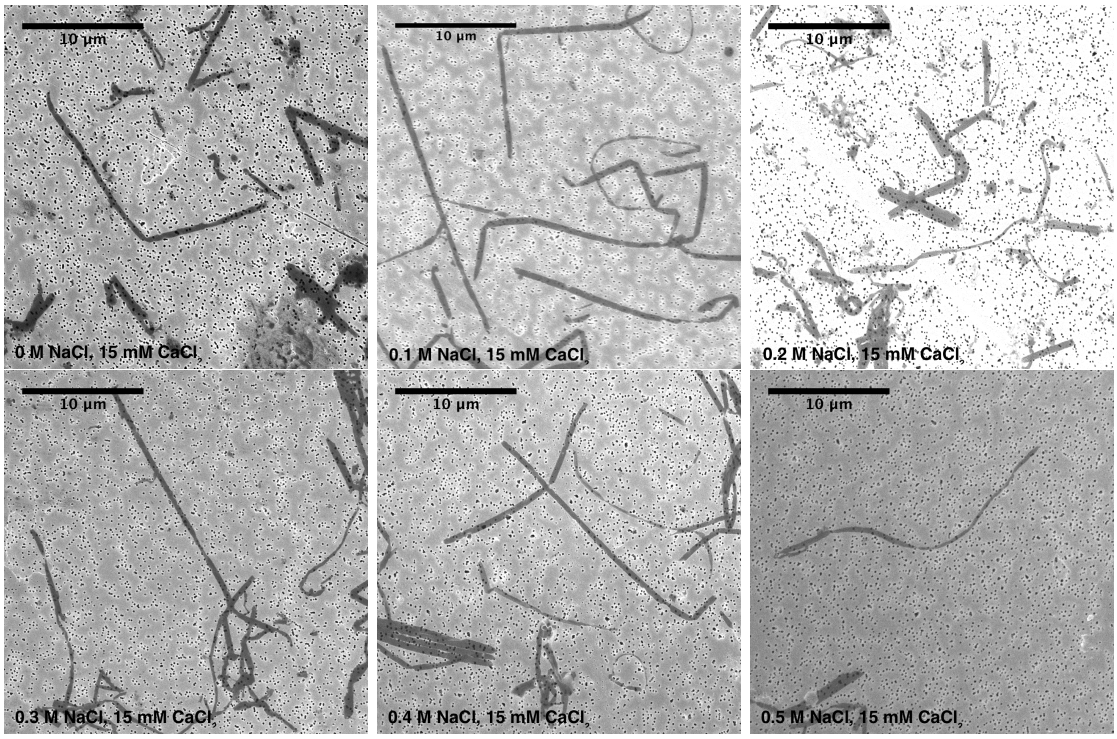

Figure 3.17: SEM images of $(PAH/PSS)_6$ nanotubes assembled in 15 mM of $CaCl_2$ and increasing concentration of NaCl, dispersed in H_2O. From left to right: 0 M, 0.1 M and 0.2 M; on the second row: 0.3 M, 0.4 M and 0.5 M.

In order to quantify the effect of increasing NaCl concentrations on the tubes morphology, the rigidity index was determined for each sample, both for CH_2Cl_2 and H_2O dispersed tubes. The resulting data is gathered in Figure 3.18.

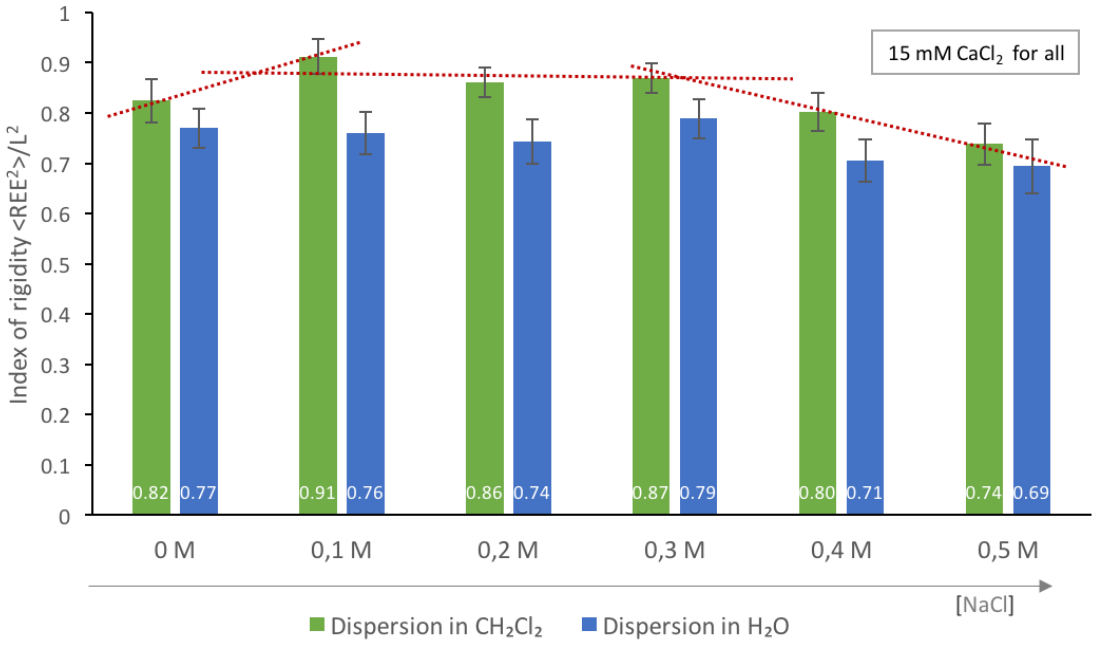

Figure 3.18: Evolution of the rigidity index for $(PAH/PSS)_6$ nanotubes assembled in increasing concentrations of NaCl at fixed 15 mM $CaCl_2$ concentration, dispersed in CH_2Cl_2 and in H_2O (based on the measurements of 25 nanotubes).

No significant trend can be identified on this graph. There is a slight increase in the rigidity upon the addition NaCl, but for concentration ranging from 0.1 to 0.3 M, the rigidity index hardly varies, for both media. Only after reaching 0.4 M is there a slight decrease in rigidity upon increasing ionic strength. This could mean that chains start to desorb at these concentrations, or that they do not properly diffuse through the pores because the pores are clogged by polymer deposition on the top surface of the membrane [47]. These assumptions, however, need to be verified.

In conclusion, we can say that increasing the concentration of $CaCl_2$ above 5 mM has no significant effect on the multilayers thickness. This observation can be made for both flat films and nanotubes. One must, however, note that for nanotubes, the rigidity is slightly improved at 15 mM of $CaCl_2$. Increasing the content in NaCl has no significant effect of the swelling of the layers. There is a slight increase at first, but the addition of NaCl will render the tubes less rigid for 0.4 M or more.

3.1.4 Effect of pH

Another important parameter in the assembly of LbL multilayers is the pH of the PE solutions. For films assembled on flat substrates, the effect of pH on the thickness has already been studied [15], but that is not the case for multilayers assembled in nanoporous templates.

For this purpose, 6 bilayers of PAH/PSS were assembled in nanoporous PC membranes in the presence of 0.1 M of NaCl and 5 mM of $CaCl_2$ at two different values of pH: 5.5 and 6.5. These values were chosen because, according to Shiratori *et al.*, they respectively create the thickest and thinnest layers of PAH [20]. Therefore, one would expect thicker layers for nanotubes assembled at pH 5.5 than for those built at pH 6.5.

Porometry measurements report that the wall thickness for films assembled at pH 5.5 and pH 6.5 are ca. 121 nm and 126 nm, respectively. This increase is nonetheless insignificant and one can thus say that a slight variation in pH does not induce the swelling of the layers. But again, the lack of effect of pH could be explained by the fact that pores are saturated with 6 bilayers when the multilayers are still wet, therefore hindering the growth of thicker layers.

Next, the effect of pH on the morphology of the tubes was studied. To this end, the PC membranes were dissolved in CH_2Cl_2. Some of the tubes were filtered and transferred to an aqueous medium. The nanotubes were then observed with STEM and SEM. Examples of the obtained images can be found in Figures 3.19 and 3.20. For these snapshots, there is no noticeable difference between the tubes assembled at different pH and it is therefore not possible to make assumptions on the effect of pH on the tubes morphology, whatever the surrounding medium.

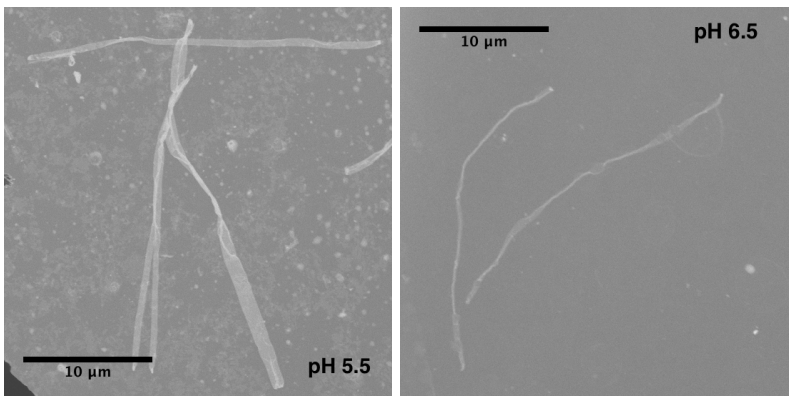

Figure 3.19: STEM images of $(PAH/PSS)_6$ nanotubes assembled in 5mM $CaCl_2$ and 0.1 M NaCl at pH 5.5 (left) and at pH 6.5 (right), dispersed in CH_2Cl_2.

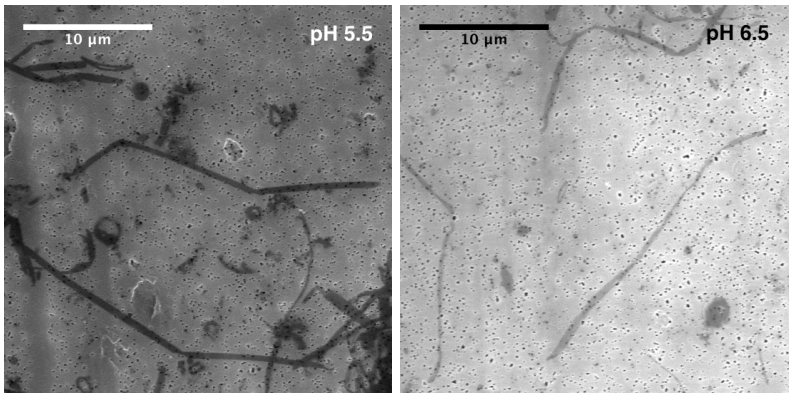

Figure 3.20: SEM images of $(PAH/PSS)_6$ nanotubes assembled in 5mM $CaCl_2$ and 0.1 M NaCl at pH 5.5 (left) and at pH 6.5 (right), dispersed in water.

Therefore, the rigidity index was computed for each sample. The resulting data is presented in Figure 3.21. From this graph, one can deduce that pH does not affect the morphology of the tubes.

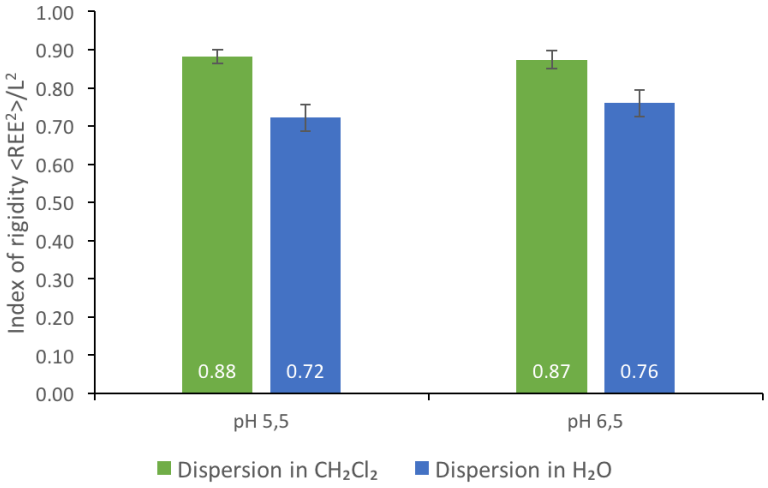

Figure 3.21: Evolution of the rigidity index for $(PAH/PSS)_6$ nanotubes assembled for different pH value, at fixed 5 mM $CaCl_2$ and 0.1 M NaCl concentrations, dispersed in CH_2Cl_2 and in H_2O (based on the measurements of 25 nanotubes).

This experiment indicates that increasing the pH from 5.5 to 6.5 has no effect on the tubes, be it on their thickness or on their morphology. For further conclusions about the effect of pH, a wider range of values should be tested out.

3.1.5 Effect of storage in water

In view of drug delivery applications, it is important to know how the tubes behave when dispersed in water for long periods of time. For this purpose, 6 bilayered PAH/PSS nanotubes were assembled at pH 5.5 in the presence of 0.1 M NaCl and 5 mM $CaCl_2$. Once air dried, the PC membrane was dissolved with CH_2Cl_2 and the nanotubes were dispersed in Milli-Q water after a dextran-assisted filtration. The solution was left to stir and a few droplets were placed on a gold-coated PET template after 6, 24, 48 and 72 hours of storage in water. These samples were then imaged with SEM, and some of the obtained images are presented in Figure 3.22.

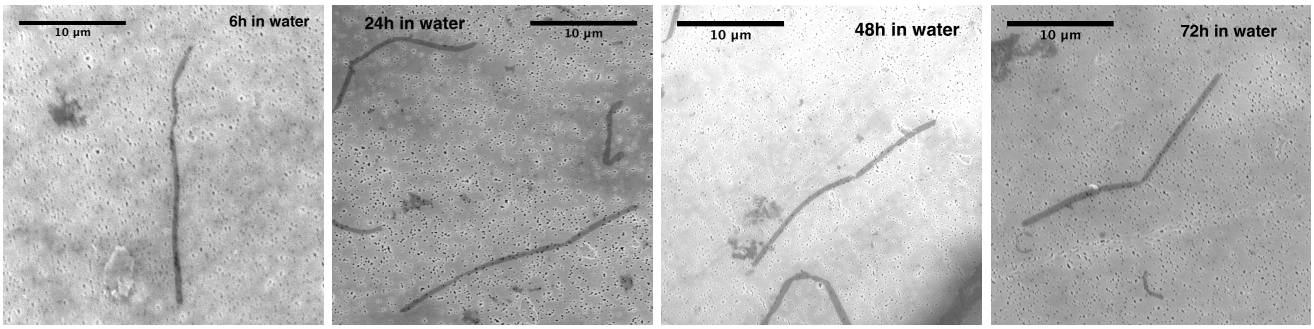

Figure 3.22: SEM images of $(PAH/PSS)_6$ nanotubes assembled in 5mM $CaCl_2$ and 0.1 M NaCl at pH 5.5, dispersed in water for (from left to right) 6h, 24h, 48h and 72h.

As no visible effect was observed on the SEM images, the rigidity index was computed for each sample. The results are gathered in Figure 3.23.

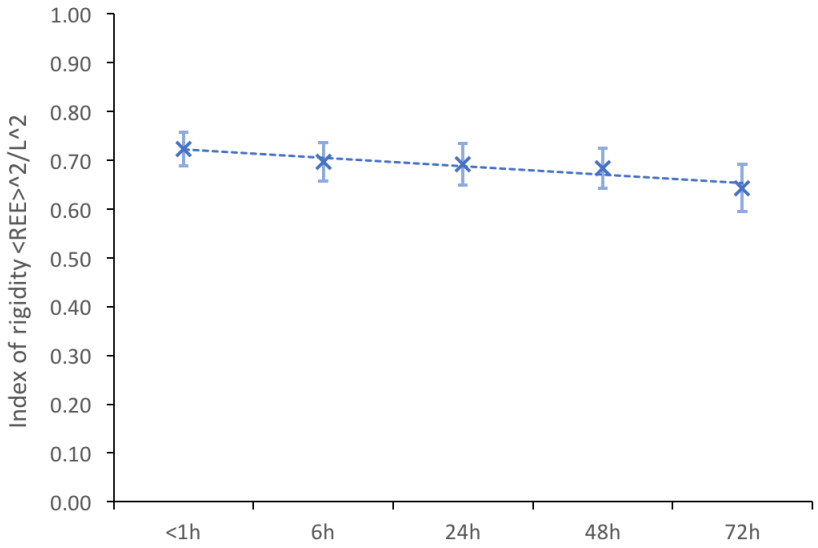

Figure 3.23: Evolution of the rigidity index for $(PAH/PSS)_6$ nanotubes assembled at fixed 15 mM $CaCl_2$ and 0.1 M NaCl concentrations, dispersed in H_2O for increasing times (based on the measurements of 25 nanotubes for each sample).

From the graph above, one can note that, although there is a faint decrease in the rigidity index with time, the morphology remains overall stable. This means the nanotubes remain integer when dispersed in water for longer periods of time. PAH/PSS could thus be used as the rigid component of core-shell structures.

3.2 CHI/HA multilayers

The second part of this chapter will be related to LbL films based on semi-natural polyelectrolytes, namely chitosan and hyaluronan.

Hyaluronan (HA) is a linear polysaccharide composed of alternating N-acetyl-b-D-glucosamine and b-D-glucuronic acid residues. It is a weak polyelectrolyte, with a pKa value of ~ 3. The molecular weight of HA depends on its origin: HA can either be extracted from natural sources -like from a rooster comb for example- or from microbial production, the latter method enabling a better control over the molecular weight [62].

Chitosan (CHI) is a natural polyelectrolyte that takes the form of a linear random copolymer of N-acetyl-b-D-glucosamine (M_w = 221 Da) and b-D-glucosamine (M_w = 179 Da) . It is obtained by partial deacetylation of chitin, which is the main component of shell fish. As this deacetylation is never fully completed, the chitosan can vary in degree of deacetylation (DAA), which is defined as the average molar fraction of glucosamine units per chain. As a results of theses varying DAA, properties like molecular weight and pKa also vary from sample to sample [57]. For example, the pKa value can range from 6.0 to 6.5 [55] for chitosan of 80% DAA.

The focus of this section will be on the effect of the processing conditions, with the purpose of understanding the properties CHI/HA nanotubes assembled using a specific set of conditions.

3.2.1 Growth

Like for PAH/PSS multilayers, the first aspect that was investigated was the growth of CHI/HA films on flat Si substrates. To this end, films with increasing numbers of layers were built in the presence of 0.15 M NaCl at pH 5. The thickness of the resulting films is measured using ellipsometry. The results are depicted in Figure 3.24. CHI and HA multilayers, as most films built using weak and natural polyelectrolytes, are characterised by an exponential growth.

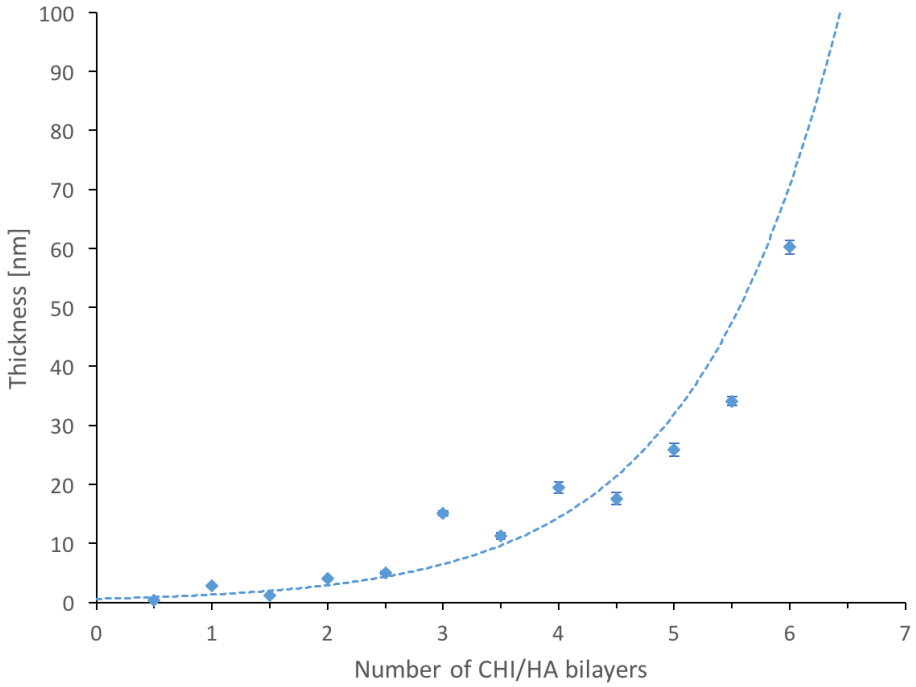

Figure 3.24: Evolution of the film thickness for CHI/HA multilayers assembled on Si substrates at fixed 0.15 M NaCl and pH 5.

The final thickness for 6 bilayers is 60.2±1.2 nm. In the literature, several indicative values can be found. For example, Hernandez *et al.* assembled CHI/HA multilayers in 0.17 M NaCl at pH 3 on PEI functionalised Si substrate and measured a final thickness for 6 bilayers of ca. 75 nm [26]. Boudou *et al.* used a sodium acetate-NaCl buffer (0.01 M, 0.15 M NaCl, pH 4.6) to build their CHI/HA films. The thickness for 6 bilayers was measured at ca. 180 nm [19]. However, these measurements were performed on wet films, whereas in our case, ellipsometry was performed on dry films. A typical LbL assembly will double its thickness when immersed in water. Therefore, although our assembling conditions are slightly different, our results are of the same order of magnitude as the ones found in the literature.

3.2.2 Effect of pH

The first parameter that was studied for the CHI/HA system was pH. CHI and HA are both weak polyelectrolytes and literature describes them as strongly affected by variations in pH. LbL assembly can only take place in a restricted range of pH. Three pH values were tested out in the scope of this thesis: 4, 5 and 6. These values are between the pKa values of CHI and HA, although pH 6 is very close to the pKa of CHI. Lower values were not tried out in the view of the selected application for this thesis, namely drug delivery. Indeed, acidic pH needs to be avoided when considering proteins or enzymes as cargo for the drug delivery system as this may cause the denaturation of the load. pH needs to remain as close as possible to the physiological pH.

On flat Si wafers

The effect of pH was first studied on flat films. CHI/HA multilayers were assembled in 0.15 M NaCl at pH 4, 5 and 6, with total numbers of six bilayers. The final thickness of the films was measured using an ellipsometer. The resulting measurements are gathered in Table 3.1.

Table 3.1: Final dry thickness for $(CHI/HA)_6$ multilayers assembled on Si substrates with increasing pH at fixed 0.15 M NaCl concentration.

pH	NaCl [M]	Final thickness [nm]
4	0.15	55.9±1.4
5	0.15	46.4±7.7
6	0.15	60.2±4.3

Based on the ionisation curves of CHI and HA (see Figure 1.10), one expects thinner films for pH 5 and thicker ones for pH 4 and 6. This is indeed the case. The effect is only small, but the variations on the ionisation curve for these pH values are also small, so this is not surprising. Ellipsometry measurements also suggest that the films are fairly rough, with rather large variations in the final thickness. This was also observed by Hernandez *et al.* [22].

Lundin *et al.* fabricated multilayers of CHI and Heparin (HEP) on silica substrates at different salt concentrations and pH. They observed that the first layer of CHI is much thicker when assembled at pH 5.8 than when assembled at pH 4.2. This can be explained by the fact that the silica substrate is more charged at pH 5.8, while CHI is lowly charged and therefore many more CHI chains are adsorbed onto the surface [63].

In a nanoporous template

In order to see if the effect of pH is the same for LbL assembly in confined geometries, CHI/HA nanotubes were built using a PC template. They were fabricated with an ionic strength of 0.15 M and different pH values, namely 4, 5 and 6. Once air-dried, porometry measurements were performed for every sample. Three measurements were carried out for each set of conditions, and the obtained results are gathered in Figure 3.25.

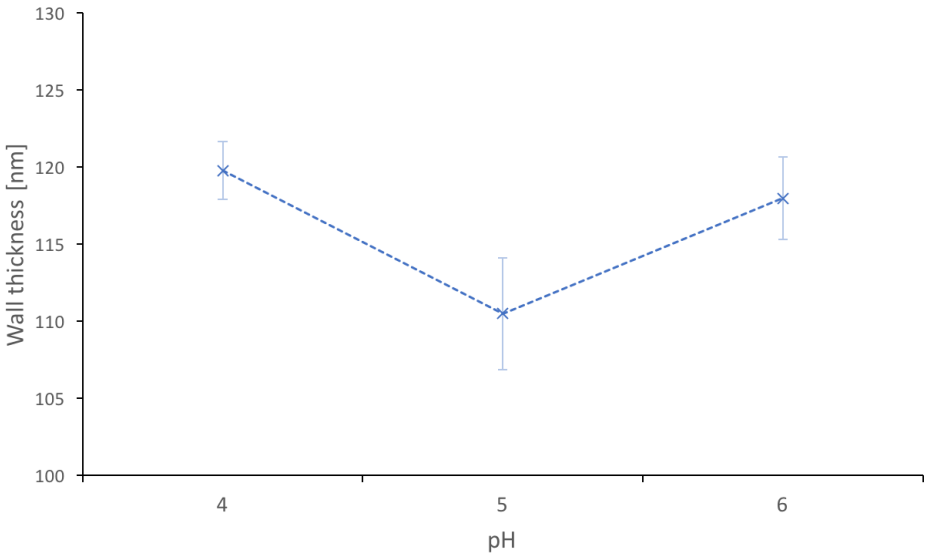

Figure 3.25: Evolution of the wall thickness for $(CHI/HA)_6$ nanotubes assembled with increasing pH at fixed 0.15 M NaCl concentration (based on 3 measurements for each pH value).

From this plot, one can see that the results are no different from those obtained for flat films. Indeed, tubes assembled at pH 4 and pH 6 show thicker layers than tubes built at pH 5, as is suggested by the ionisation curves (Figure 1.10). The difference in average thickness between pH 5 and the other values nearly amounts to ca. 10 nm. However, the error bars, which are nearly touching in the case of pH 5 and 6, suggest that the effect on layer thickness is actually quite small. This again is not surprising since the variations in the degree of ionisation are only small for these pH values.

To analyse the effect of pH on the nanotubes morphology, the PC membranes were dissolved and the tubes were dispersed in dichloromethane and in water. They were then observed using STEM and SEM, respectively. Examples of the obtained images are presented in Figure 3.26 and 3.27. By observing tubes dispersed in CH_2Cl_2, there are no visible differences in the morphology of tubes assembled at different pH. In all three samples, the tubes are prone to bend and have a tendency to stick to each other. On images of the nanotubes after water contact, one can easily observe that the morphology of tubes assembled at pH 6 is quite different from the tubes assembled a lower pH. Indeed, when assembled at pH 6, the nanotubes tend to roll up and for entangled complexes. In the other samples, the tubes also tend to bend, but not as much.

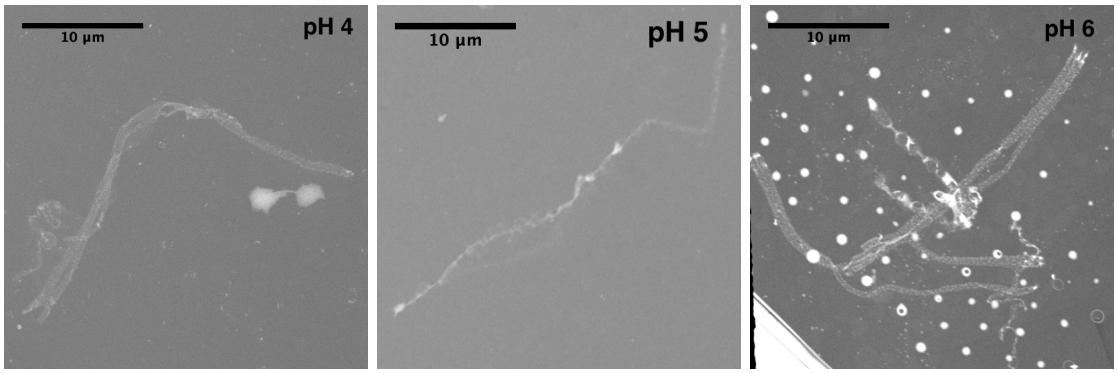

Figure 3.26: STEM images of $(CHI/HA)_6$ nanotubes assembled in NaCl with increasing pH, dispersed in CH_2Cl_2. From left to right: pH 4, pH 5 and pH 6.

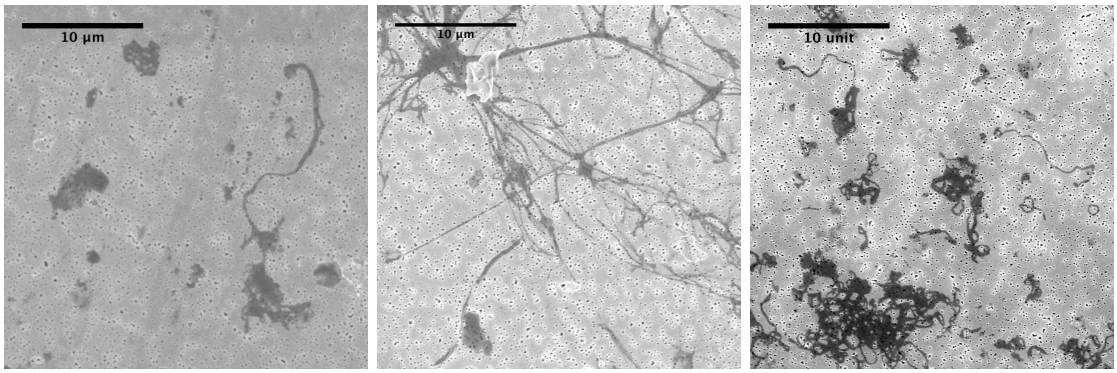

Figure 3.27: SEM images of $(CHI/HA)_6$ nanotubes assembled in NaCl with increasing pH, dispersed in H_2O. From left to right: pH 4, pH 5 and pH 6.

In order to quantify the effect pH has on the nanotubes morphology, the rigidity index was computed for each sample. Results are gathered in Figure 3.28. They are in full agreement with the observations made based on SEM and STEM images: when dispersed in CH_2Cl_2, pH has no significant effect on the rigidity of the tubes. However, when dispersed in water, there is an important loss of rigidity for all samples, and even more for tubes assembled at pH 6.

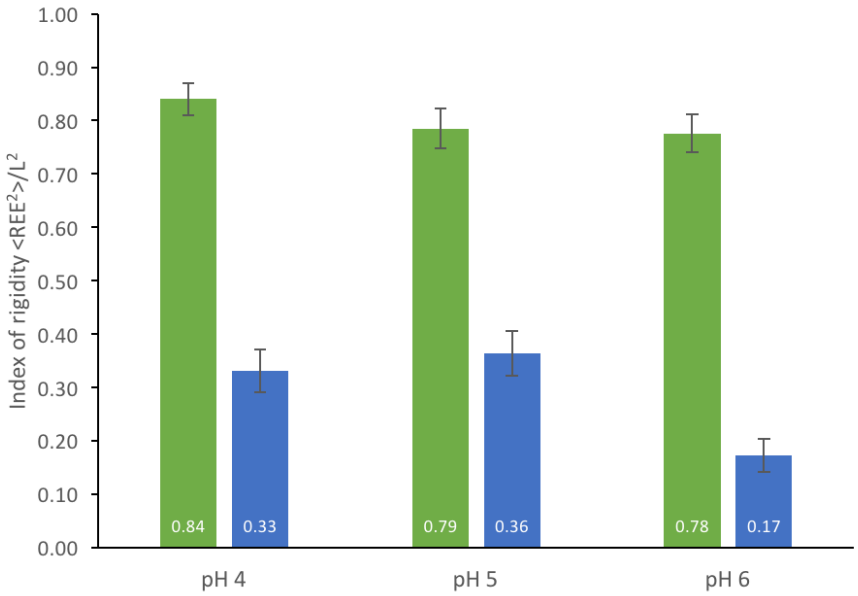

Figure 3.28: Evolution of the rigidity index for $(CHI/HA)_6$ nanotubes assembled with increasing pH at fixed 0.15 M NaCl concentration, dispersed in CH_2Cl_2 and in H_2O (based on the measurements of 25 nanotubes).

In conclusion, pH has no noticeable effect on layer thickness and on rigidity when the tubes are dispersed in an organic media. However, when in contact with water, tubes assembled at pH 6 are much more affected by rigidity loss than tubes build at lower pH. One possible assumption for this would be that layers assembled at pH 6 are only held together by weak electrostatic interactions. Indeed, pH 6 being close to chitosan's pKa, the charge density on CHI chains is quite low. When dispersed in water, some of the interactions break, resulting in the partial disassembly on the multilayers.

3.2.3 Effect of the ionic strength

The second analysed processing condition was the ionic strength. The typical salt concentration used when building CHI/HA multilayers is 0.15 M [14, 19, 22, 26, 27]. With the objective to see what effect the addition of salt has on the multilayers build-up, we compared CHI/HA multilayers built in increasing concentration of NaCl. The pH was fixed at 6.

On flat Si wafers

The effect of ionic strength was first investigated on flat silicon substrates. CHI/HA films with increasing numbers of layers were assembled on 1 cm^2 Si wafer pieces in the presence of 0 M, 0.15 M and 0.5 M NaCl. Once dried, the layer thickness was measured using ellipsometry. The measurements are gathered in Figure 3.29. For 6 bilayers, the final thicknesses of the dried films are gathered in Table 3.2.

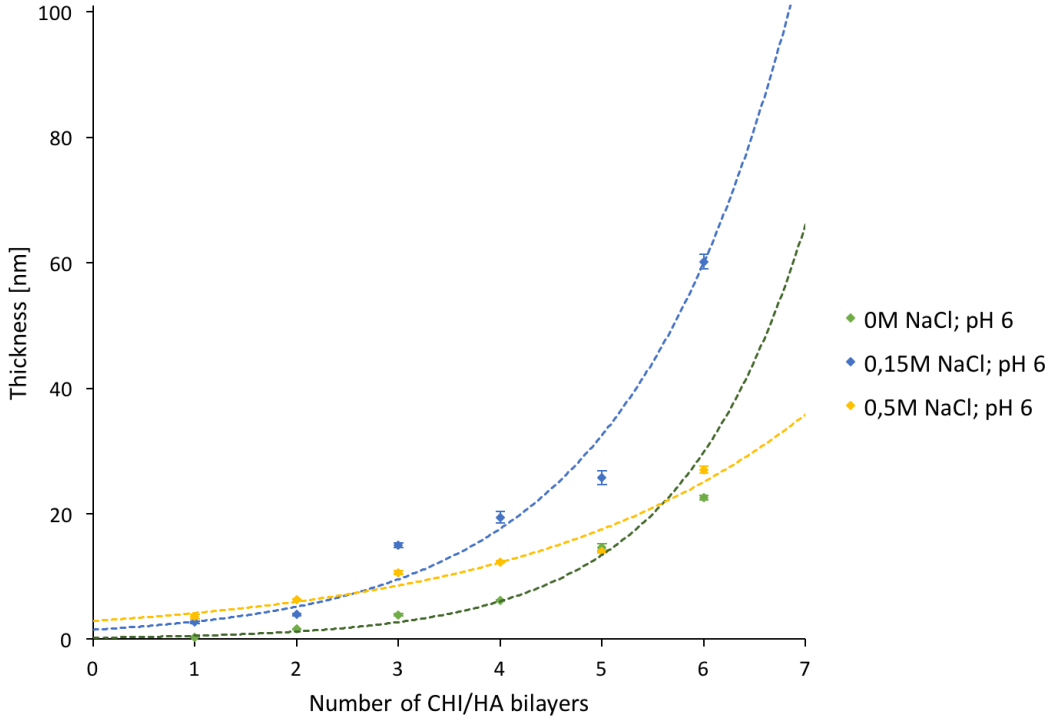

Figure 3.29: Evolution of the film thickness for CHI/HA multilayers on Si substrates built in increasing salt concentrations at pH 6.

Table 3.2: Final dry thickness for $(CHI/HA)_6$ multilayers assembled on Si substrates with increasing NaCl concentration at pH 6.

pH	NaCl [M]	Final thickness [nm]
6	0	22.6±0.4
6	0.15	60.2±4.3
6	0.5	27.0±0.5

The results presented in Table 3.2 show that the addition of 0.15 M NaCl causes the layers to considerably gain in thickness. This observation correlates with the results found by Lundin *et al.* when they analysed the effect of salt concentration on CHI/HEP multilayers. They compared films assembled in the presence of 0.03 M NaCl to layers fabricated in 0.15 M NaCl. They observed that film grew thicker and adsorbed more chains when the assembly was carried out at 0.15 M instead of 0.0 3M NaCl [63].

The pH value of 6 was chosen in order to assess if 0.5 M was below the critical ionic strength or not, the critical ionic strength being defined as the concentration above which salt causes the desorption of the layers. The results above would suggest that 0.5 M is close to the critical ionic strength for LbL assembly.

When analysing the growth regime of each sample, one can see that for the first three bilayers, adding 0.5 M of NaCl does result is thicker layers than when adding 0.15 M. However, while in the other samples the thickness grows exponentially for further layers, the layers assembled in 0.5 M NaCl only grow slightly thicker, bordering on a linear growth. Besides the assumption of desorbing chains, this could also be explained by the "in" and "out" diffusion that characterises the exponential growth of multilayers, which was described in Section 1.1.2. Indeed, one could make the assumption that when in the presence of 0.5 M of NaCl, the PE chains are too bulky to diffuse in and out of the layers. Layers, therefore, grow in a linear manner where chains only interact with the uppermost layer, instead of taking up an exponential growth.

In a nanoporous template

Next, CHI/HA nanotubes were built in nanoporous templates at pH 6 using different salt concentrations (namely 0, 0.15 and 0.5 M). The average diameter of the tubes was measured using gas-flow porometry and the wall thickness was computed from those measurements. The results are gathered in Figure 3.30.

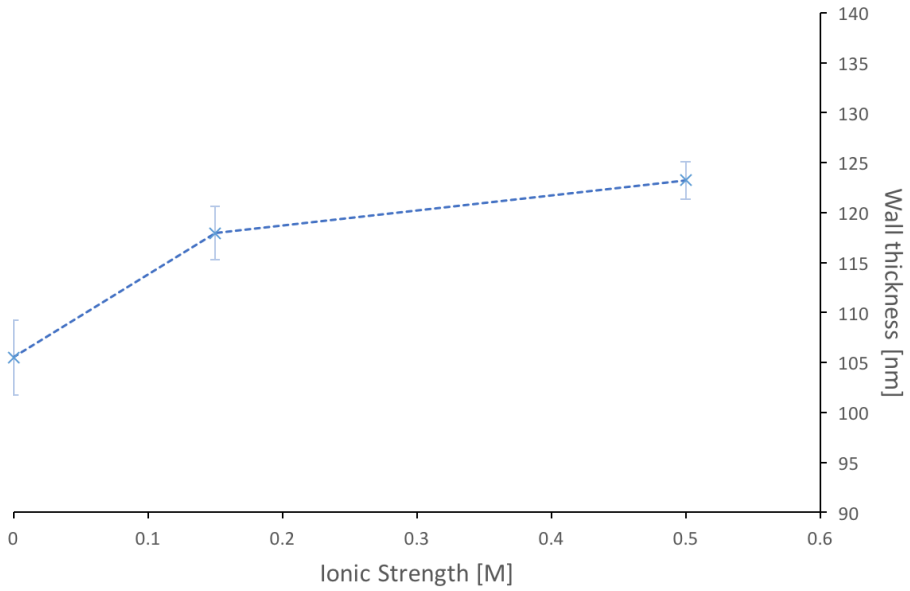

Figure 3.30: Evolution of the wall thickness for $(CHI/HA)_6$ nanotubes built in increasing concentrations of NaCl at pH 6 (based on 3 measurements for each salt concentration).

Contrary to flat films, the nanotubes wall thickness increases with salt concentration. Indeed, when assembled in the presence 0.5 M of NaCl, the tubes did not exhibit the decrease in thickness observed for films built on Si substrates. The trend is thus different than for flat films. One

possible explanation for this could be that chain diffusion inside the pores is improved by adding salt. Even if some chains desorb due to the high ionic strength (which was assumed to be the case for flat films built in 0.5 M of NaCl), this loss could be compensated by the improved diffusion. Moreover, one could also presume that even though part of the chains desorb, they are not able to easily leave the confined environment and are therefore included in the layers upon drying.

The morphology of the tubes dispersed in organic and aqueous solutions was studied using STEM and SEM. Examples of the resulting images are shown in Figures 3.31 and 3.32. For CH_2Cl_2-dispersed tubes, one can see that at 0 M and 0.5 M salt concentration, the multilayers break open at some spots along the tubes. This is not the case when the nanotubes are built in the presence of 0.15 M NaCl. After contact with water, multilayers assembled at 0.5 M salt concentration appear fuzzier than the other samples. Other observations on the morphology when dispersed in water cannot be made: in all three samples, the tubes tend to bend and aggregate.

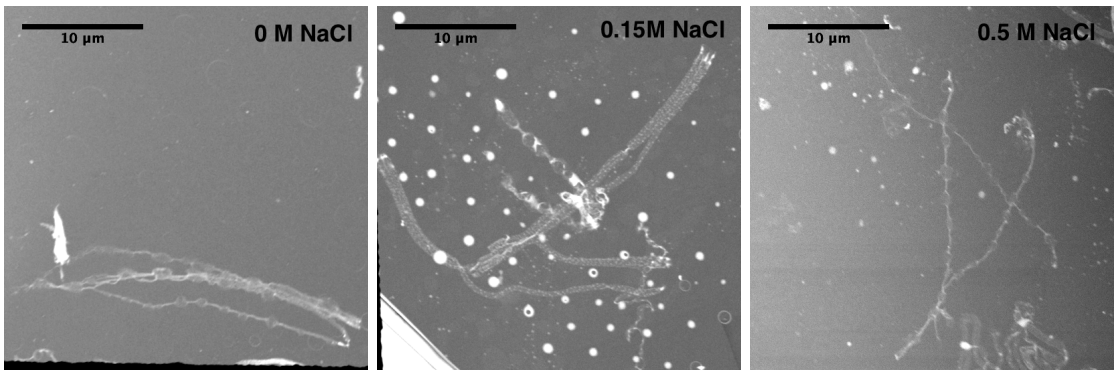

Figure 3.31: STEM images of $(CHI/HA)_6$ nanotubes built with increasing concentration of NaCl at pH 6, dispersed in CH_2Cl_2. From left to right: 0 M, 0.15 M and 0.5 M.

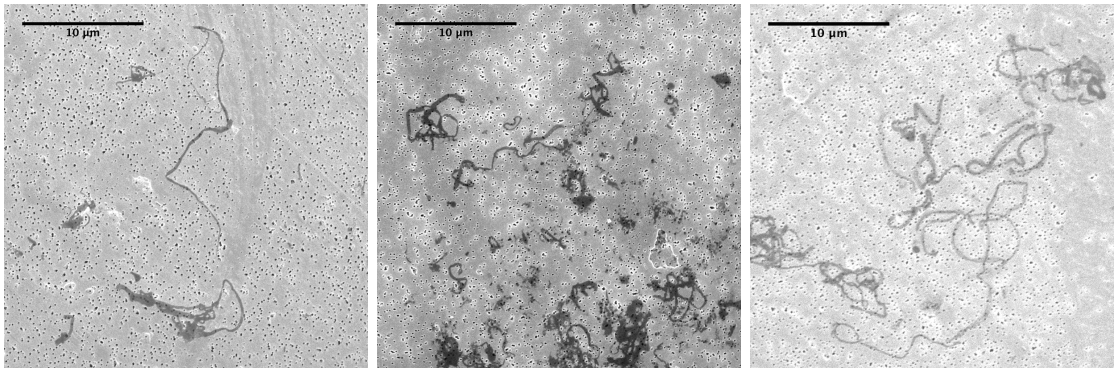

Figure 3.32: SEM images of $(CHI/HA)_6$ nanotubes built with increasing concentration of NaCl at pH 6, dispersed in H_2O. From left to right: 0 M, 0.15 M and 0.5 M.

The final step to assess the effect of ionic strength consisted of computing the rigidity index based on 25 nanotubes for each sample, in both media. The obtained values are represented in Figure 3.33. In this plot, one can see that tubes assembled in 0.5 M NaCl are more rigid, but the errors bars indicate that this increase is not significant. There is also a strong loss of rigidity upon dispersion in water. Once again, in this media, there is no noticeable trend, except for a loss of ca. 75 % of rigidity.

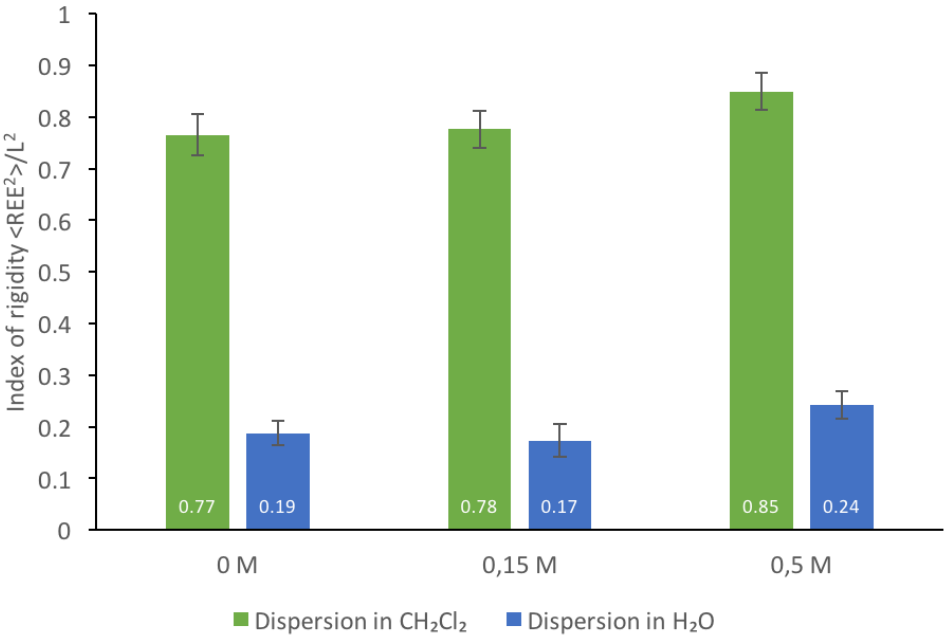

Figure 3.33: Evolution of the rigidity index for $(CHI/HA)_6$ nanotubes assembled with increasing concentrations of NaCl at pH 6, dispersed in CH_2CL_2 and in H_2O (based on the measurements of 25 nanotubes).

The effect of pH seems to dominate the effect of salt, and without further investigations on samples assembled at lower pH values, it is not possible to make any significant conclusions about the effect of ionic strength on the nanotubes morphology.

3.2.4 Cross-linking

For the purpose of increasing the rigidity of CHI/HA nanotubes in water, the cross-linking of the multilayers was investigated. This reaction involves two cross-linkers: EDC and sulfo-NHS. The specifics of the reaction were described in Section 1.3.2.

On flat Si wafers

Flat films of CHI/HA containing 20 bilayers were built in 0.15 M of NaCl and at pH 5 on flat 1 cm^2 squares of silicon. Part of the samples were then cross-linked in 30 mM EDC and 50 mM sulfo-NHS. The pH of this solution was fixed at 5.5. The samples were stored in this solution for 24h at 4°C. Once dried, the layer thickness was measured using ellipsometry. The thickness reached 250.6±3.5 nm for the samples that were not cross-linked and 253.0±10.6 nm for the cross-linked films. This means that layers do not swell or shrink during cross-linking.

Next, to see how the chemical nature of the multilayers evolves during the reaction, FTIR measurements were performed on films with and without cross-linking. Figure 3.34 presents the substraction of the two measured spectra, and could thus be compared to Figure 1.18. As cross-linking with EDC and sulfo-NHS involves the formation of amide bonds, one expects the peaks related to carboxylic groups of HA to decrease, while the bands related to amines I and II should increase. On Figure 3.34, one can see that this is indeed the case: carboxylic bands at ca. 1400 and 1600 cm^{-1} are slightly decreased after cross-linking, and bands related to amide I and amine II (in the 1440-1500 cm^{-1} and 1630-1700 cm^{-1} range respectively) show a small increase.

The drop in the saccharides peaks at ca. 1030 and 1080 cm^{-1} as well as the appearance of an ester band around 1200 cm^{-1} indicate the formation of C−O ester bonds. In the literature, it is suggested that these bonds occur between the carboxylic acid groups of HA and the hydroxyl groups of CHI [16].

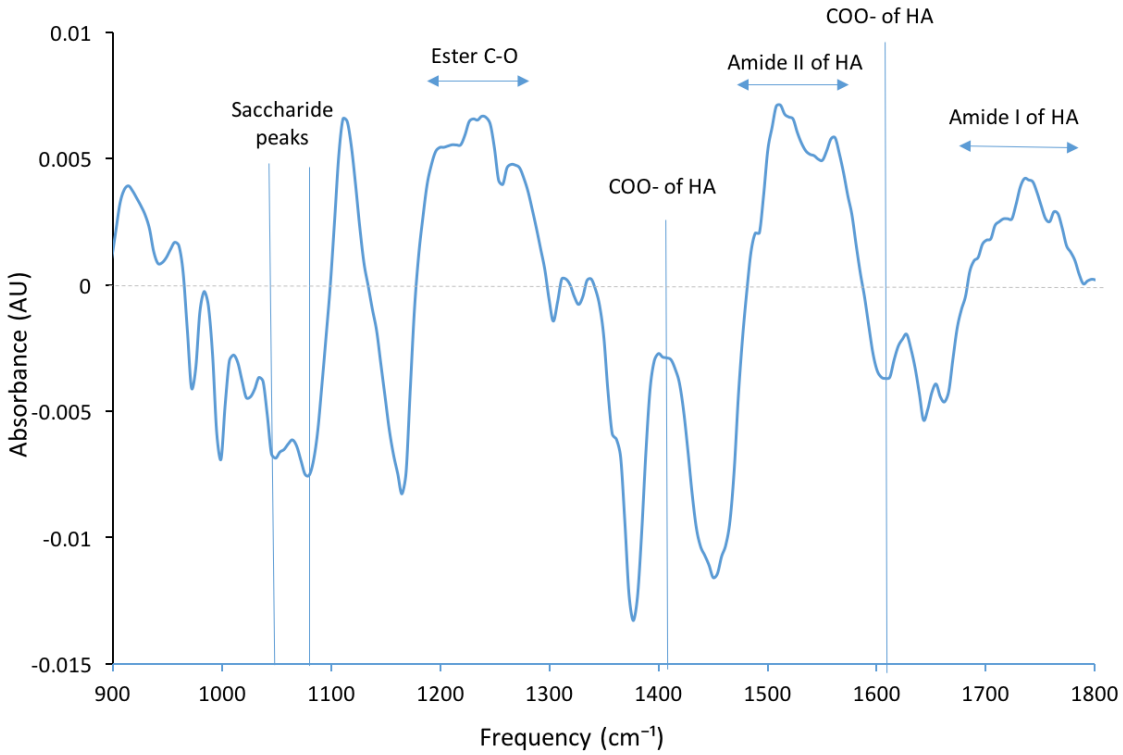

Figure 3.34: Difference between the initial spectrum before cross-linking and the spectrum after 24 hours cross-linking in EDC/sulfo-NHS , for $(CHI/HA)_{20}$ assembled in 0.15 M NaCl at pH 5.

FTIR analysis thus indicates that a cross-linking reaction indeed occurs, but that its extent is limited. Indeed, the values obtained in the Figure 3.34 are much smaller than those obtained by Picart *et al.* (see Figure 1.18). In this paper, cross-linkers were, however, used in much higher concentrations, namely 200 mM of EDC [27]. According to Boudou *et al.*, with 30 mM of EDC, ca. 15 % of the NH_3^+ groups and ca. 25 % of the COO^- groups have reacted. For 200 mM, these degrees of consumption are increased to ca. 45 % and ca. 70 % respectively. The maximum percentages of reacted groups are achieved by using 500 mM of EDC, for which ca. 50 % of the NH_3^+ groups and 80 % of the COO^- groups have been consumed [19].

In a nanoporous template

After assessing the extent of the cross-linking reaction on flat films, the effect of such a reaction in a confined geometry was investigated. For this purpose, nanotubes comprised of 6 CHI/HA bilayers were assembled at pH 4 in the presence of 0.15 M NaCl. Some of the PC templates were then put in a solution containing 30 mM EDC and 50 mM sulfo-NHS, with a pH fixed at 5.5 and with 0.15 M of added salt. They were immersed for 24h at 4°C, before being thoroughly rinsed.

Porometry measurements provided the average nanotubes inner diameter, which were translated into wall thickness. Before cross-linking, the multilayers presented a thickness of 119.7±1.9 nm (based on the measurement of 4 samples). After cross-linking, the sample had an average wall

thickness of 109.2±4.7 nm (based on the measurement of 2 samples). This decrease in thickness could be attributed to the rearrangements of the polysaccharide chains when placed in solution.

To investigate if cross-linking affected the tubes morphology, the multilayers were released from their templates and dispersed in both CH_2Cl_2 and water. These samples were then observed using STEM and SEM, respectively. Instances of the obtained images for nanotubes dispersed in CH_2Cl_2 are represented in Figures 3.35. For nanotubes dispersed in H_2O, one must refer to Figures 3.37 and 3.38 for samples without and with cross-linking, respectively. From the images after PC dissolution, no visible effect of cross-linking on the tubes morphology can be observed.

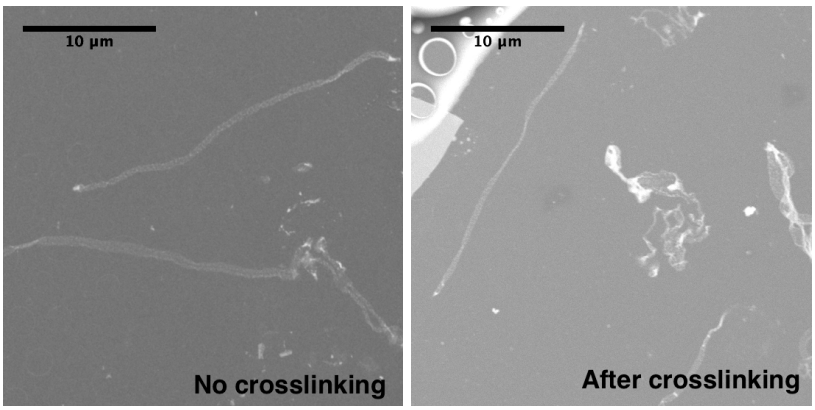

Figure 3.35: STEM images of $(CHI/HA)_6$ nanotubes assembled in 0.15 M NaCl and pH 4, dispersed in CH_2Cl_2. From left to right: before and after cross-linking.

In order to quantify how cross-linking affects the nanotubes morphology, the rigidity index was computed for 25 tubes before and after cross-linking. The average values obtained for these calculations are presented in Figure 3.36.

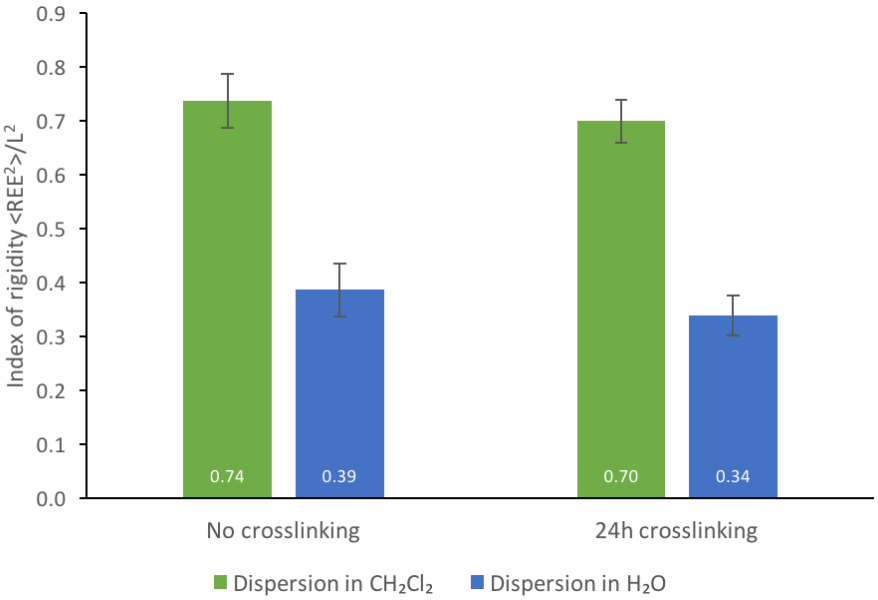

Figure 3.36: Evolution of the rigidity index for $(CHI/HA)_6$ nanotubes assembled at pH 4 with 0.15 M NaCl before and after crosslinking, dispersed in CH_2CL_2 and in H_2O (based on the measurements of 25 nanotubes).

For this graph, one can see that there is no effect of cross-linking on the tubes rigidity. This suggests that the limited extent of the cross-liking reaction was not enough to stiffen the tubes. This could be solved by either using larger concentrations of cross-linkers. Another solution could be to add the cross-linkers to one of the dipping steps during the LbL assembly and therefore perform a cross-linking step every bilayer.

3.2.5 Effect of storage in water

Like for PAH/PSS nanotubes, we investigated how CHI/HA tubes behave when dispersed in water for long periods of time. This experiment was performed in parallel with the previous one, using the same samples. Indeed, both cross-linked and non-crosslinked tubes were left in water for increasing periods of time. At specific intervals (namely less than 1h and after 24 and 72 hours), a few droplets of each solution were placed upon separate gold-coated PET filters and then observed using SEM. Instances of these observations are gathered in Figures 3.37 and 3.38 for samples without and with cross-linking, respectively. From these images, one can observe that tubes tend to entangle, but this was already observed in previous samples. The cross-linked tubes also seem to be more prone to breakage, which is quite surprising as these are supposed to contain stronger covalent bonds.

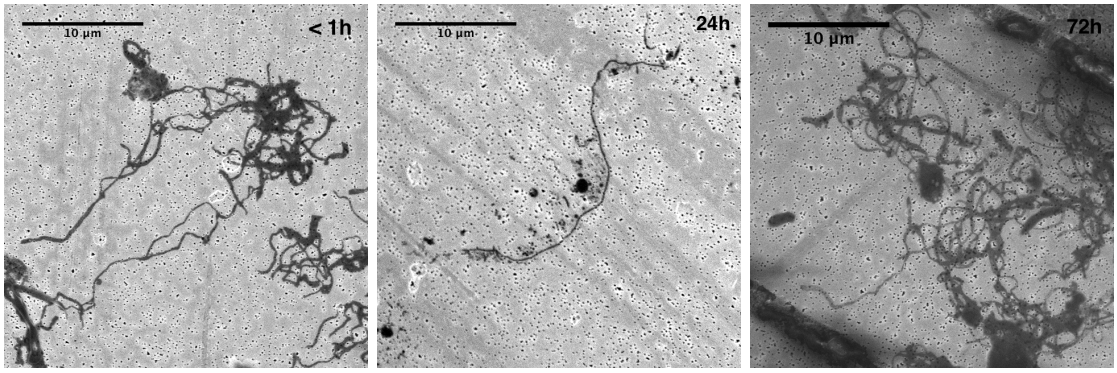

Figure 3.37: SEM images of $(CHI/HA)_6$ nanotubes assembled in 0.15 M NaCl and pH 4, dispersed in H_2O for increasing amounts of time. From left to right: <1h, 24h and 72h.

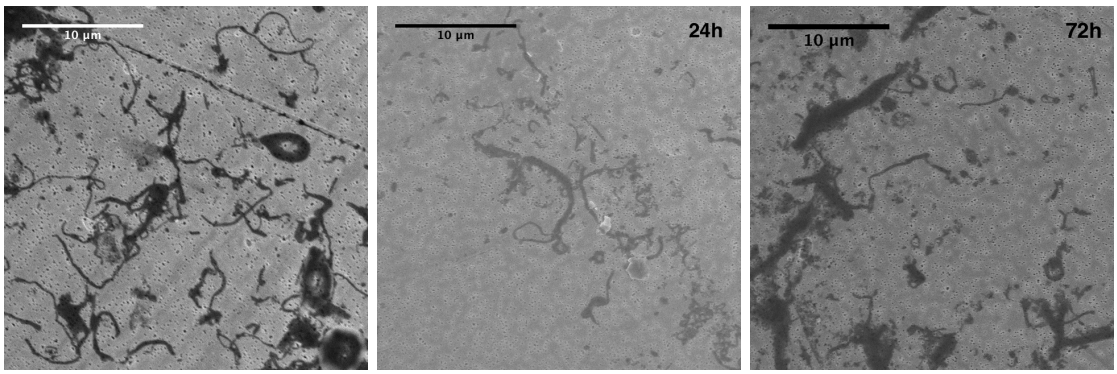

Figure 3.38: SEM images of $(CHI/HA)_6$ nanotubes assembled in 0.15 M NaCl and pH 4, crosslinked for 24h, dispersed in H_2O for increasing amounts of time. From left to right: <1h, 24h and 72h.

Next, the effect of storage in water was quantified with the rigidity index. The results are gathered in Figure 3.39. After 24 hours dispersed in water, the samples become even more flexible but further storage does not seem to affect the tubes rigidity further. One can also observe that there is no effect of cross-linking on the nanotubes rigidity. The index is indeed similar for both samples.

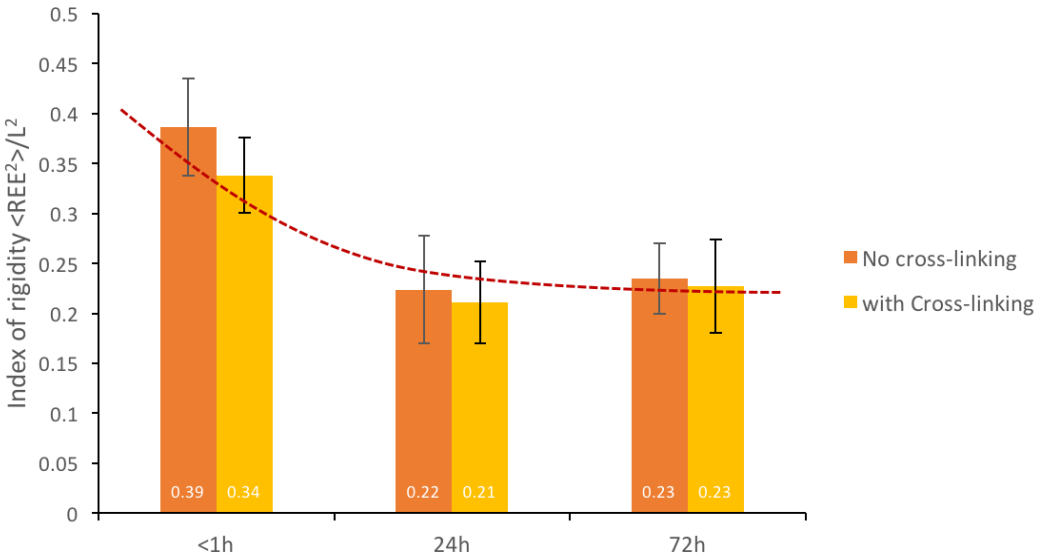

Figure 3.39: Evolution of the rigidity index for $(CHI/HA)_6$ nanotubes assembled at pH 4 with 0.15 M NaCl before and after cross-linking, dispersed H_2O for increasing amounts of time (based on the measurements of 25 nanotubes).

From this experiment, one can thus say that tubes are affected after storage in water, but there is no difference between 24 and 72 hours. This experiment also indicated that the cross-linking did not achieve the hoped-for results, meaning stiffen the tubes. The suggestions made in the previous section to solve this issue are still valid here: either use higher concentrations of EDC and sulfo-NHS, or perform a cross-linking step after each bilayer.

3.3 Summarising table

Table 3.3: Summarising table of the gathered results for LbL nanotubes.

	$(PAH/PSS)_6$	$(CHI/HA)_6$
Effect of ionic strength (NaCl concentration)	Thickness gain upon addition of salt to the PE solution, but no significant effect upon further increase of the salt concentration. Rigidity is decreased for [NaCl]≥0.4 M	Thickness gain upon addition of salt to the PE solution, increasing with NaCl concentration.
Physical cross-linking by $CaCl_2$	Thickness gain upon addition of 5 mM $CaCl_2$ to the PE solution, but no significant effect above 5 mM of $CaCl_2$. Rigidity is slightly improved for 0.15 M $CaCl_2$.	/
Effect of pH	No effect on thickness or morphology when increasing pH 5.5 to pH 6.5.	No noticeable effect on wall thickness or morphology in CH_2Cl_2, but increased rigidity loss in water for pH 6. The effect of pH dominates the effect of ionic strength.
Nanotubes rigidity in CH_2Cl_2	Average rigidity index of ca. 0.85	Average rigidity index of ca. 0.78
Water contact & loss of rigidity	Average rigidity index of ca. 0.71, meaning there is a rigidity loss of ca. 16.5 %. Slight decrease of rigidity upon storage in water for long periods of time.	Average rigidity index of ca. 0.33 for pH 4 and 5 and of ca. 0.18 for pH 6, meaning there is a rigidity loss of ca. 55% and 75% respectively. When stored in water for longer period of time, there is a decrease in rigidity for the first 24 hours.
Chemical cross-linking by EDC/sulfo-NHS	/	No effect on wall thickness and tubes rigidity for the selected concentrations of EDC and sulfo-NHS

Conclusion

The general objective of this study was to understand the effect of processing conditions on the assembly of multilayer nanotubes, in view of building core-shell structures for drug delivery applications. Two polyelectrolyte pairs were surveyed: first PAH and PSS, two synthetic polyelectrolytes, followed by CHI and HA, both polysaccharides. For both systems, we studied the effect of variations in pH and ionic strength during assembly, as well as the impact of cross-linking (ionic cross-linking for PAH/PSS and chemical cross-linking for CHI/HA). The last investigated aspect was the impact of prolonged contact with water on the nanotubes morphology.

In our study, we observed that PAH/PSS multilayers grow in a linear manner. This was expected since a linear growth was reported for these synthetic polyelectrolytes in multiple papers. As many experiments needed to be performed in the scope of this thesis, we explored if it was possible to decrease the dipping time. In our team, the typical dipping time is 30 minutes, but we were able to build PAH/PSS nanotubes using 10 minutes dips, without affecting the tubes properties in water. The multilayers properties were, however, relatively impacted by the ionic strength of the polyelectrolyte solutions. Indeed, we noted that the addition of salt during the assembly caused the layers to grow thicker, whatever the substrate (i.e. flat or nanoporous). Despite that, increasing the ionic strength to higher values (e.g. 0.5 M) did not cause a noteworthy climb in the multilayers thickness. When assembling PAH/PSS multilayers, our group adds both monovalent salt NaCl and multivalent salt $CaCl_2$ to the PE solutions, since the latter may lead to the physical cross-linking of the layers. Nonetheless, during our studies, no such cross-linking was observed. Although the rigidity of the nanotubes was slightly improved for nanotubes assembled in 15 mM $CaCl_2$ and 0.1 M NaCl, the morphology remained overall the same whatever the ionic strength. For the investigations above, the pH was fixed at 5.5. We explored if the nanotubes would be affected by increasing the pH to 6.5 during the assembly but observed no effect, nor on the wall thickness, nor on the morphology of the nanotubes. The lack of impact could be related to the possible saturation of the 300 nm-pores for 6 bilayers, even with the thinnest layers. Finally, we investigated the effect of prolonged water contact on PAH/PSS nanotubes morphology. It was observed that the nanotubes morphology remained overall stable, even for prolonged periods of time. All in all, PAH/PSS nanotubes stayed stiff whatever the assembling conditions and could, therefore, be used as rigid segment when building core-shell structures.

For CHI/HA multilayers, we observed an exponential growth, as is expected for two weak semi-natural polyelectrolytes. This indeed corresponds to the growth regime reported in numerous papers. Independently of the chosen substrate (i.e. Si wafers or PC membrane), the CHI/HA multilayers were fairly affected by the pH chosen during the assembly due to the varying degrees of ionisation of both polysaccharides. Moreover, the morphology of the nanotubes released in water was also dependent on pH: the samples experienced a considerable loss of rigidity, and even more so for tubes assembled at pH 6. On the other hand, the effect of ionic strength was contrasting for CHI/HA. While the highest ionic strength (0.5 M) gave thicker multilayers in porous templates, flat films were rather thin, which might be due to the chains desorption when in the presence of large concentrations of salt. The study of the tubes morphology showed that

overall the effect of pH dominates the effect of ionic strength, since the loss of rigidity upon contact with water was considerable but similar for all samples. To improve the rigidity of the tubes, we studied the chemical cross-linking of the multilayers with EDC and sulfo-NHS and observed that it had no effect on the rigidity of the multilayers nor on the nanotubes morphology and stability when stored in water for prolonged periods of time. On the whole, CHI/HA multilayers are softer and more affected by assembling conditions than PAH/PSS.

The main difference between the studied polyelectrolyte pairs lies in the effect of water contact. Indeed, PAH/PSS nanotubes were only slightly affected when dispersed in water and remained stable after prolonged contact with the aqueous medium. On the other hand, for CHI/HA nanotubes, the loss of rigidity was much higher. For numerical values concerning this aspect, one must refer to Table 3.3. These observations could be explained by the hydrophobic and hydrophilic nature of, respectively, PAH/PSS and CHI/HA, which is linked to the ionisation of the chains (which is itself dependent on pH and ionic strength). As a matter of fact, multilayers composed of weak polyelectrolytes such as CHI and HA tend to have weak and reduced interactions holding them together and can, therefore, be highly hydrated. PAH/PSS multilayers, in contrast, are held together by a greater extent of inter-chain pairings and are, therefore, less prone to swell in water. In terms of rigidity, CHI/HA multilayers would therefore benefit from being paired with PAH/PSS multilayers in core-shell systems. As to layers thickness, both systems had a similar inner pore diameter when assembled in porous templates, but CHI/HA multilayers were twice as thick as PAH/PSS layers on flat substrates. This reflects that LbL growth is different in confined geometries.

This study thus provided a first analysis of how assembling conditions may affect LbL multilayers. Many aspects of this survey, however, need further exploration in order to gain a deeper understanding of the LbL process. For example, our study was limited to the assembly of six bilayers, but further studies may investigate if the parameters have a different impact when more or fewer layers are assembled, as the pores were most probably saturated in water with six bilayers. For some factors also, only the effect of small variations on the multilayers was studied. For example, larger variations of pH could be investigated. How the pore diameter of the PC membrane affects the multilayer growth could also be studied. Moreover, other parameters like for example temperature and molecular weight remain mostly unexplored, especially when considering LbL nanotubes, and are worthy of further investigations. The cross-linking of CHI/HA multilayers especially requires further research, by varying the concentration of crosslinkers or by performing several cross-linking steps during the assembly.

This work is fundamental to gain a better understanding in the build-up of core-shell nanotubes with soft and rigid multilayers, which is ongoing in the group. The properties, morphology and stability in water of CHI/HA multilayers could indeed be affected and even improved by partnering with PAH/PSS multilayers. The effect of the position of each system (i.e. core or shell) on the nanotubes morphology still needs to be explored, as well as the impact of the assembling conditions on this hybrid structure. The fabrication of this type of structure is quite promising for drug delivery applications, as it allows the assembly of multifunctional nanotubes. Core-shell systems are therefore quite interesting and worthy of further investigations.

Template fabricated LbL nanotubes thus have a promising future, especially in the development of new drug delivery systems, but further studies are still required to fully understand and optimise their build up. A lot of research still needs to be dedicated to this subject before all the aspects of LbL drug delivery nanotubes are fully comprehended. Some of the points that need further exploration in the view of drug delivery applications are the surface functionalisation, the drug loading, the cellular uptake and the drug release. The study presented in this report is only one instance of the growing interest in LbL systems and we hope that many more will be performed in the future.

Appendices

Appendix A

Drug delivery

A.1 Drug loading

On requirement for drug delivery systems is the ability to correctly incorporate toxic and fragile therapeutics compounds and shield them from the body. This can be achieved by three methods, which are depicted in Figure 1.24: i) incorporation of the drug into the layers, ii) the preloading of the template with the drug, and iii) trapping of the cargo inside the delivery vehicles [41,48,50,51]. .

Layer incorporation The second approach consists of mixing the drug with one of the building blocks of the LbL-assembled system. This results in a uniform loading of the drug along the system. The quantity of loaded drug is controlled by the number of assembled layers. This method is mostly used on flat films for the delivery of accurate doses of therapeutics [50, 51].

Template incorporation This last approach does not concern nanotubes, as it is more suited for colloidal systems. It consists of preloading the template with therapeutics compounds prior to the Lbl assembly. The drug is thus protected by the template during the assembly process. The template is dissolved once the last layer is deposited, leaving the cargo inside the multilayer capsule [50, 51].

Postloading The first method consists of loading the drug in already formed nanotubes or capsules. The bioactive molecules enter the hollow cavity through diffusion and become trapped. The size of the molecule needs to be considered, as a particle whose diameter is too large cannot enter the pore or the capsule. One must also note that this method is even more successful if there are interactions between the incorporated therapeutic molecules and the inner surface of the LbL system. These interactions may encourage the diffusion and retain the drug particles [41].

A.2 Drug release

Once the carrier has reached its target and has been incorporated into the cells, the drug release can either be "passive", meaning it occurs through drug diffusion, or it can be stimuli-responsive. There are three types of stimuli: biological, physical (light, electric or magnetic field, temperature) or chemical (pH, ionic strength). The release of the drug might also require the degradation of the carrier. Here is a quick review of some release routes [50, 51, 52]:

- Diffusion-based release:

  Functional molecules of lower molecular weight undergo a diffusion-controlled release due to a concentration gradient between the drug-carrier and the environment. The diffusion mechanism depends on the wall porosity, pore size and the rate of diffusion for the loaded molecules. However, such a diffusion-based delivery has the disadvantage of occurring in a short period of time. For many biomedical applications, the needed release time extends over at least several days in order to minimise the toxicity. A possible solution for this problem is the incorporation of low-permeability barrier layers within the multilayers.

- Light-triggered release:

  Near-infrared (NIR) light, which is suitable for biomedical applications, can also be used as a remote trigger for drug delivery. This type of delivery provides spatial and temporal regulation of the drug release. Lbl nano-carrier can be rendered sensitive to by incorporating metal nanoparticles into the multilayers. Such assembled drug vehicles shatter upon NIR irradiation.

- Hydrolytic degradation:

  This method involves polymers that degrade gradually in physiological conditions due to hydrolysis. Indeed, in such conditions, the hydrolic cleavage of the polymer is increased, causing the polymer to fall apart. Some materials may also undergo changes in their net charge in physiological conditions, inducing the multilayers degradation. These are called "charge-shifting" polymers.

- pH-responsive release:

  When the drug carriers include weak polyelectrolytes, the local variations of pH in the targeted tissues can trigger the drug release. pH response may then induce a change in the permeability or even the decomposition of the carrier membrane, thus allowing the release of the included drug. Another effect can be the increase of the drug flux from the LbL membrane when the drug is part of the layers.

- Salt-triggered release:

  Hydrophilic LbL films are known to swell with increasing ionic strength. Indeed, salt ions weaken the electrostatic interactions between PEs and increase the osmotic pressure inside the multilayers. As a result, when adding sufficient salt, a LbL assembled drug delivery platform can become more permeable or even dissolve. Increased ionic strength may also induce the release of molecules for the layers themselves.

- Enzymatic degradation:

  When using polypeptides and polysaccharides as building materials, the presence of specific enzymes may induce the degradation of the Lbl drug carrier. Enzymes like proteases and nucleases are present in specific areas of the body, enabling a localised breakdown of the nano-carrier. Films can however be made resistance to this type of degradation by cross-linking.

Appendix B

Summary of multilayers thickness and rigidity index values

Table B.1: Multilayers thickness for varying build up conditions, for 10 min dippings.

System	pH	[NaCl], M	[$CaCl_2$], mM	Flat thickness, nm	Nanotubes wall thickness, nm
$(PAH/PSS)_6$	5.5	0.1	5	27.6±0.4	120±2.7*
$(PAH/PSS)_6$	5.5	0	0	4.9±0.1	/
$(PAH/PSS)_6$	5.5	0.1	0	23.6±0.3	104**
$(PAH/PSS)_6$	5.5	0.1	15	26.4±0.3	121**
$(PAH/PSS)_6$	5.5	0.1	25	/	117**
$(PAH/PSS)_6$	5.5	0.1	35	/	123**
$(PAH/PSS)_6$	5.5	0	15	26.5±0.2	120**
$(PAH/PSS)_6$	5.5	0.2	15	28.0±0.2	121**
$(PAH/PSS)_6$	5.5	0.3	15	/	124**
$(PAH/PSS)_6$	5.5	0.4	15	/	120**
$(PAH/PSS)_6$	5.5	0.5	15	32.8±0.5	126**
$(PAH/PSS)_6$	6.5	0.1	5	/	126**
$(CHI/HA)_6$	5	0.15	0	46.4±7.7	110.5±3.6*
$(CHI/HA)_6$	4	0.15	0	55.9±1.4	119.7±1.9*
$(CHI/HA)_6$	6	0.15	0	60.2±4.3	117.9±2.7*
$(CHI/HA)_6$	6	0	0	22.6±0.4	105.5±3.7*
$(CHI/HA)_6$	6	0.5	0	27.0±0.5	123.2±1.8*
$(CHI/HA)_6$ crosslinked	4	0.15	0	/	109.2±4.7*

*Error based on (on average) 3 different measurements

**Error based on one single measurement, but one could take ±2.7 nm as indicative error range

Table B.2: Rigidity index for varying build up conditions.

System	pH	[NaCl], M	[$CaCl_2$], mM	For CH_2Cl_2 dispersion	For H_2O dispersion
$(PAH/PSS)_6$	5.5	0.1	5	0.84±0.04	0.66±0.04
$(PAH/PSS)_6$	5.5	0.1	0	0.86±0.04	0.66±0.05
$(PAH/PSS)_6$	5.5	0.1	15	0.91±0.03	0.70±0.04
$(PAH/PSS)_6$	5.5	0.1	25	0.86±0.04	0.61±0.04
$(PAH/PSS)_6$	5.5	0.1	35	0.83±0.04	0.67±0.04
$(PAH/PSS)_6$	5.5	0	15	0.82±0.04	0.77±0.04
$(PAH/PSS)_6$	5.5	0.2	15	0.86±0.03	0.79±0.04
$(PAH/PSS)_6$	5.5	0.3	15	0.87±0.03	0.79±0.04
$(PAH/PSS)_6$	5.5	0.4	15	0.80±0.04	0.71±0.04
$(PAH/PSS)_6$	5.5	0.5	15	0.74±0.04	0.69±0.05
$(PAH/PSS)_6$	6.5	0.1	5	0.87±0.02	0.76±003
$(CHI/HA)_6$	5	0.15	0	0.78±0.04	0.36±0.04
$(CHI/HA)_6$	4	0.15	0	0.84±0.03	0.33±0.04
$(CHI/HA)_6$	6	0.15	0	0.79±0.04	0.17±0.03
$(CHI/HA)_6$	6	0	0	0.77±0.04	0.19±0.02
$(CHI/HA)_6$	6	0.5	0	0.85±0.04	0.24±0.03
$(CHI/HA)_6$ crosslinked	4	0.15	0	0.70±0.04	0.34±0.04

List of Tables

3.1 Final dry thickness for $(CHI/HA)_6$ multilayers assembled on Si substrates with increasing pH at fixed 0.15 M NaCl concentration. 51
3.2 Final dry thickness for $(CHI/HA)_6$ multilayers assembled on Si substrates with increasing NaCl concentration at pH 6. 54
3.3 Summarising table of the gathered results for LbL nanotubes. 62

B.1 Multilayers thickness for varying build up conditions, for 10 min dippings. 69
B.2 Rigidity index for varying build up conditions. 70

List of Figures

1 Illustration of the growing interest in LbL assembly, based on the number of yearly publications with keywords of (a) "layer- by-layer" since 1967 and (b) "layer-by-layer" and "assembly" since 1992 [4]. 1

1.1 Schematic representation of the assembly of a multilayer via electrostatic interactions [3]. 4
1.2 Illustration of various nanostructures that can be achieved through LbL assembly on templates [10]. 5
1.3 Schematic representation of Layer-by-Layer assembly process through the (a) dipping, (b) spin-coating and (c) spraying method for electrostatic interactions [11]. 6
1.4 Schematic illustration of the Lbl assembly techniques [12]. 7
1.5 Model for exponential growth: A) "out" diffusion of polycations, B) "in" diffusion of polyanions, C) negative charge overcompensation, D) "out" diffusion of polyanions, E) "in" diffusion of polycations and F) positive charge inversion [17]. 8
1.6 Film thickness as a function of the number of PAH/PSS layers [18]. 9
1.7 Film thickness as a function of the deposited CHI/HA layers [19]. 9
1.8 Average thickness contributed by a PAA (solid line) and PAH (dashed line) adsorbed layer as a function of solution pH [20]. 10
1.9 Film thickness as a function of PAH/PSS layers deposited on a silicon substrate for different pH values [18]. 11
1.10 Ionisation curves of CHI and HA versus pH [22]. 11
1.11 Thickness profile for CHI/HA multilayers assembled on PEI functionalised Si substrates, at different pH/NaCl concentrations [22]. 12
1.12 Schematic representation of a thinner layer with planar chain conformation and higher charge density on the left and a thicker layer with loopy chain conformation and lower charge density on the right [23]. 12
1.13 Thickness of PAH/PSS bilayers as a function of the ionic strength of the dipping solution [24]. 13
1.14 Quartz crystal microbalance of CHI/HA multilayered films on glass slides for different salt concentrations. The parameter $-\Delta(f/\nu)$ is proportional to the deposited amount of polymer [14]. 14
1.15 Effect of molecular weight on the exponential growth and thickness of CHI/HA multilayers [32]. 15
1.16 Cross-linking reaction scheme for carboxyl-to-amine linking using EDC and sulfo-NHS [37]. 17
1.17 Molar density of covalent amide bonds created during the cross-linking reaction for (PAH/PGA) (o), (CHI/HA) ($\Diamond$) and (PLL/HA) ($\triangle$) films [19]. 17
1.18 Resulting substraction of the spectra before and after cross-linking for three EDC concentration: 25 mM (thin black line), 200 mM (circles), and 750 mM (thick black line) [27]. 18

1.19 Schematic representation of the synthesis of a AAO template: (i) polishing, (ii) first anodisation, (iii) AAO wet etching and (iv) second anodisation [38]. 19
1.20 Schematic representation of the track-etching process of a PC template [40]. . . . 19
1.21 Schematic representation of the Lbl assembly in a nanoporous template [6]. . . . 20
1.22 Schematic representation of the two growth regimes for LbL assembly in nanoporous substrates [43]. 20
1.23 $(PAH/PSS)_{15}$ multilayers assembled on nanoporous AAO-membrane templates as a function of $CaCl_2$ concentration: (a) 1, (b) 5, (c) 50, (d) 100 mM. The inset is (a) shows the AAO membrane before the LbL assembly [47]. 22
1.24 Methods for drug encapsulation within LbL capsules. a) Incorporation of the cargo in the capsule walls b) Preloading the template with the drug before LbL assembly c) Postloading the drug delivery system by changing the wall permeability [50]. . 23
1.25 Drug delivery path: i) nano-carrier internalisation by endocytosis; ii) endosomal or lysosomal vesicle; iii) rupture of the vesicle; iv) release of the nano-carrier in the cytosol; v) drug release from the nano-carrier; vi) further transport into the nucleus or other organelles [50]. 24
1.26 Schematic representation of nanoparticle loading in hollow nanotubes of 200 nm inner diameter [41]. 25

2.1 Chemical structure of PSS and PAH polyelectrolytes. 28
2.2 Chemical structure of CHI and HA polyelectrolytes [55]. 28
2.3 Scheme of one cycle of the assembly of polyelectrolytes multilayers inside nanopores [57]. 31
2.4 Schematic illustration of the nanotubes collection (a) filtration of adjuvant dispersed in CH_2CL_2 through PET filter; (b) formation of the adjuvant pellet on the PET filter; (c) filtration of adjuvant dispersed in the suspension of nanotubes in CH_2CL_2; (d) formation of a powder inside which the nanotubes are trapped; (e) addition of water to dissolve the adjuvant and release the nanotubes [6]. 31
2.5 Schematic illustration of how the tubes are prepared before microscopy observations 33

3.1 Evolution of the film thickness for PAH/PSS multilayers assembled on flat silicon wafers in 0.1 M NaCl and 5 mM $CaCl_2$ at pH 5.5 36
3.2 Evolution of the $(PAH/PSS)_6$ final wall thickness for increasing dipping times (based on one measurement per sample, see Table B.1 for indicative error values). 37
3.3 STEM images of $(PAH/PSS)_6$ nanotubes assembled with increasing dipping time dispersed in CH_2Cl_2 (left to right: 10 minutes, 20 minutes and 30 minutes). . . . 38
3.4 STEM images of $(PAH/PSS)_6$ nanotubes assembled with increasing dipping time dispersed in CH_2Cl_2 (left to right: 10 minutes, 20 minutes and 30 minutes). . . . 38
3.5 SEM images of $(PAH/PSS)_6$ nanotubes assembled with increasing dipping time dispersed in H_2O (left to right: 10 minutes, 20 minutes and 30 minutes). 38
3.6 Evolution of the rigidity index for $(PAH/PSS)_6$ nanotubes assembled with increasing dipping times, dispersed in CH_2CL_2 and in H_2O (based on the measurements of 25 nanotubes). 39
3.7 Evolution of the film thickness for PAH/PSS multilayers on Si substrates built in increasing concentrations of $CaCl_2$ at fixed 0.1 M NaCl concentration. 40
3.8 Evolution of the film thickness for PAH/PSS multilayers on Si substrates built in increasing concentrations of NaCl at fixed 15 mM $CaCl_2$ concentration. 40
3.9 Thickness per bilayer for $(PAH/PSS)_6$ multilayers Si substrates, built in increasing $CaCl_2$ (left) and NaCl concentrations (right). 41
3.10 Evolution of the film thickness for PAH/PSS multilayers on Si substrates with increasing ionic strength. 41

3.11 Evolution of the wall thickness for $(PAH/PSS)_6$ nanotubes for increasing concentrations of $CaCl_2$ at fixed 0.1 M NaCl concentration (1 measurement per sample, see Table B.1 for guide value for the error bars). 42
3.12 STEM images of $(PAH/PSS)_6$ nanotubes assembled in 0.1 M of NaCl and increasing concentration of $CaCl_2$, dispersed in CH_2Cl_2. From left to right: 0 mM, 5 mM, 15 mM and below, 25 mM and 35 mM. 43
3.13 SEM images of $(PAH/PSS)_6$ nanotubes assembled in 0.1 M of NaCl and increasing concentration of $CaCl_2$, dispersed in H_2O. From left to right: 0 mM, 5 mM, 15 mM and 25 mM and 35 mM on the second row. 43
3.14 Evolution of the rigidity index for $(PAH/PSS)_6$ nanotubes assembled in increasing concentrations of $CaCl_2$ at fixed 0.1 M NaCl concentration, dispersed in CH_2CL_2 and in H_2O (based on the measurements of 25 nanotubes). 44
3.15 Evolution of the wall thickness for $(PAH/PSS)_6$ nanotubes built in increasing concentrations of NaCl at fixed 15 mM $CaCl_2$ concentration (1 measurement per sample, see Table B.1 for indicative error values). 44
3.16 STEM images of $(PAH/PSS)_6$ nanotubes assembled in 15 mM of $CaCl_2$ and increasing concentration of NaCl, dispersed in CH_2Cl_2. From left to right: 0 M, 0.1 M and 0.2 M; on the second row: 0.3 M, 0.4 M and 0.5 M. 45
3.17 SEM images of $(PAH/PSS)_6$ nanotubes assembled in 15 mM of $CaCl_2$ and increasing concentration of NaCl, dispersed in H_2O. From left to right: 0 M, 0.1 M and 0.2 M; on the second row: 0.3 M, 0.4 M and 0.5 M. 46
3.18 Evolution of the rigidity index for $(PAH/PSS)_6$ nanotubes assembled in increasing concentrations of NaCl at fixed 15 mM $CaCl_2$ concentration, dispersed in CH_2Cl_2 and in H_2O (based on the measurements of 25 nanotubes). 46
3.19 STEM images of $(PAH/PSS)_6$ nanotubes assembled in 5mM $CaCl_2$ and 0.1 M NaCl at pH 5.5 (left) and at pH 6.5 (right), dispersed in CH_2Cl_2. 47
3.20 SEM images of $(PAH/PSS)_6$ nanotubes assembled in 5mM $CaCl_2$ and 0.1 M NaCl at pH 5.5 (left) and at pH 6.5 (right), dispersed in water. 48
3.21 Evolution of the rigidity index for $(PAH/PSS)_6$ nanotubes assembled for different pH value, at fixed 5 mM $CaCl_2$ and 0.1 M NaCl concentrations, dispersed in CH_2Cl_2 and in H_2O (based on the measurements of 25 nanotubes). 48
3.22 SEM images of $(PAH/PSS)_6$ nanotubes assembled in 5mM $CaCl_2$ and 0.1 M NaCl at pH 5.5, dispersed in water for (from left to right) 6h, 24h, 48h and 72h. 49
3.23 Evolution of the rigidity index for $(PAH/PSS)_6$ nanotubes assembled at fixed 15 mM $CaCl_2$ and 0.1 M NaCl concentrations, dispersed in H_2O for increasing times (based on the measurements of 25 nanotubes for each sample). 49
3.24 Evolution of the film thickness for CHI/HA multilayers assembled on Si substrates at fixed 0.15 M NaCl and pH 5. 50
3.25 Evolution of the wall thickness for $(CHI/HA)_6$ nanotubes assembled with increasing pH at fixed 0.15 M NaCl concentration (based on 3 measurements for each pH value). 52
3.26 STEM images of $(CHI/HA)_6$ nanotubes assembled in NaCl with increasing pH, dispersed in CH_2Cl_2. From left to right: pH 4, pH 5 and pH 6. 52
3.27 SEM images of $(CHI/HA)_6$ nanotubes assembled in NaCl with increasing pH, dispersed in H_2O. From left to right: pH 4, pH 5 and pH 6. 53
3.28 Evolution of the rigidity index for $(CHI/HA)_6$ nanotubes assembled with increasing pH at fixed 0.15 M NaCl concentration, dispersed in CH_2Cl_2 and in H_2O (based on the measurements of 25 nanotubes). 53
3.29 Evolution of the film thickness for CHI/HA multilayers on Si substrates built in increasing salt concentrations at pH 6. 54

3.30 Evolution of the wall thickness for $(CHI/HA)_6$ nanotubes built in increasing concentrations of NaCl at pH 6 (based on 3 measurements for each salt concentration). 55
3.31 STEM images of $(CHI/HA)_6$ nanotubes built with increasing concentration of NaCl at pH 6, dispersed in CH_2Cl_2. From left to right: 0 M, 0.15 M and 0.5 M. . 56
3.32 SEM images of $(CHI/HA)_6$ nanotubes built with increasing concentration of NaCl at pH 6, dispersed in H_2O. From left to right: 0 M, 0.15 M and 0.5 M. 56
3.33 Evolution of the rigidity index for $(CHI/HA)_6$ nanotubes assembled with increasing concentrations of NaCl at pH 6, dispersed in CH_2CL_2 and in H_2O (based on the measurements of 25 nanotubes). 57
3.34 Difference between the initial spectrum before cross-linking and the spectrum after 24 hours cross-linking in EDC/sulfo-NHS , for $(CHI/HA)_{20}$ assembled in 0.15 M NaCl at pH 5. 58
3.35 STEM images of $(CHI/HA)_6$ nanotubes assembled in 0.15 M NaCl and pH 4, dispersed in CH_2Cl_2. From left to right: before and after cross-linking. 59
3.36 Evolution of the rigidity index for $(CHI/HA)_6$ nanotubes assembled at pH 4 with 0.15 M NaCl before and after crosslinking, dispersed in CH_2CL_2 and in H_2O (based on the measurements of 25 nanotubes). 59
3.37 SEM images of $(CHI/HA)_6$ nanotubes assembled in 0.15 M NaCl and pH 4, dispersed in H_2O for increasing amounts of time. From left to right: <1h, 24h and 72h. 60
3.38 SEM images of $(CHI/HA)_6$ nanotubes assembled in 0.15 M NaCl and pH 4, crosslinked for 24h, dispersed in H_2O for increasing amounts of time. From left to right: <1h, 24h and 72h. 60
3.39 Evolution of the rigidity index for $(CHI/HA)_6$ nanotubes assembled at pH 4 with 0.15 M NaCl before and after cross-linking, dispersed H_2O for increasing amounts of time (based on the measurements of 25 nanotubes). 61

Bibliography

[1] Gero Decher and Jong-Dal Hong. Buildup of ultrathin multilayer films by a self-assembly process, 1 consecutive adsorption of anionic and cationic bipolar amphiphiles on charged surfaces. *Makromolekulare Chemie. Macromolecular Symposia*, 46(1):321–327, 1991.

[2] P. Bertrand, A. Jonas, A. Laschewsky, and R. Legras. Ultrathin polymer coatings by complexation of polyelectrolytes at interfaces: suitable materials, structure and properties. *Macromolecular Rapid Communications*, 21(7):319–348, 2000.

[3] João Borges and João F. Mano. Molecular interactions driving the layer-by-layer assembly of multilayers. *Chemical Reviews*, 114(18):8883–8942, 09 2014.

[4] Fang-Xing Xiao, Mario Pagliaro, Yi-Jun Xu, and Bin Liu. Layer-by-layer assembly of versatile nanoarchitectures with diverse dimensionality: a new perspective for rational construction of multilayer assemblies. *Chem. Soc. Rev.*, 45:3088–3121, 2016.

[5] Rui R. Costa and Joao F. Mano. Polyelectrolyte multilayered assemblies in biomedical technologies. *Chem. Soc. Rev.*, 43:3453–3479, 2014.

[6] Saghi Saghazadeh. *Polyelectrolyte multilayer nanotubes for drug delivery applications*. PhD thesis, Université Catholique de Louvain, Institute of Condensed Matter and Nanosciences, Bio and soft matter, Ecole Polytechnique de Louvain, 2015.

[7] Saghi Saghazadeh, Shouwei Zhang, Damien Lefèvre, Aurélie Le Beulze, Alain M. Jonas, and Sophie Demoustier-Champagne. Universal method to transfer membrane-templated nano-objects to aqueous solutions. *Langmuir*, 31(26):7264–7273, 07 2015.

[8] P Gentile, I Carmagnola, T Nardo, and V Chiono. Layer-by-layer assembly for biomedical applications in the last decade. *Nanotechnology*, 26(42):422001, 2015.

[9] Stefaan De Koker, Richard Hoogenboom, and Bruno G. De Geest. Polymeric multilayer capsules for drug delivery. *Chem. Soc. Rev.*, 41:2867–2884, 2012.

[10] Yajun Wang, Alexandra S. Angelatos, and Frank Caruso. Template synthesis of nanostructured materials via layer-by-layer assembly. *Chemistry of Materials*, 20(3):848–858, 02 2008.

[11] Yang Li, Xu Wang, and Junqi Sun. Layer-by-layer assembly for rapid fabrication of thick polymeric films. *Chem. Soc. Rev.*, 41:5998–6009, 2012.

[12] G. Decher J. Rühe. Project B2: Polymer multilayers at solid substrates. `http://www.softmattergraduate.uni-freiburg.de/project/2010-2015/B2/b2`. Accessed: 2016-12-04.

[13] X Arys, AM Jonas, A Laschewsky, R Legras, and F Mallwitz. *Layered Polyelectrolyte Assemblies*, chapter 19. CRC Press, 2017/03/26 2005.

[14] Ludovic Richert, Philippe Lavalle, Elisabeth Payan, Xiao Zheng Shu, Glenn D. Prestwich, Jean-François Stoltz, Pierre Schaaf, Jean-Claude Voegel, and Catherine Picart. Layer by layer buildup of polysaccharide films: Physical chemistry and cellular adhesion aspects. *Langmuir*, 20(2):448–458, 01 2004.

[15] Peter Bieker and Monika Schönhoff. Linear and exponential growth regimes of multilayers of weak polyelectrolytes in dependence on pH. *Macromolecules*, 43(11):5052–5059, 06 2010.

[16] C. Picart, J. Mutterer, L. Richert, Y. Luo, G. D. Prestwich, P. Schaaf, J.-C. Voegel, and P. Lavalle. Molecular basis for the explanation of the exponential growth of polyelectrolyte multilayers. *Proceedings of the National Academy of Sciences*, 99(20):12531–12535, 2002.

[17] Ph. Lavalle, C. Gergely, F. J. G. Cuisinier, G. Decher, P. Schaaf, J. C. Voegel, and C. Picart. Comparison of the structure of polyelectrolyte multilayer films exhibiting a linear and an exponential growth regime: An in situ atomic force microscopy study. *Macromolecules*, 35(11):4458–4465, 05 2002.

[18] Magdalena Elzbieciak, Marta Kolasinska, and Piotr Warszynski. Characteristics of polyelectrolyte multilayers: The effect of polyion charge on thickness and wetting properties. *Colloids and Surfaces A: Physicochemical and Engineering Aspects*, 321(1–3):258–261, 5 2008.

[19] Thomas Boudou, Thomas Crouzier, Rachel Auzély-Velty, Karine Glinel, and Catherine Picart. Internal composition versus the mechanical properties of polyelectrolyte multilayer films: The influence of chemical cross-linking. *Langmuir*, 25(24):13809–13819, 12 2009.

[20] S. S. Shiratori and M. F. Rubner. pH-Dependent Thickness Behavior of Sequentially Adsorbed Layers of Weak Polyelectrolytes. *Macromolecules*, 33(11):4213–4219, 05 2000.

[21] Kölher R. von Klitzing R. and Chenigny C. *Neutro Reflectometry at Polyelectroly Multilayers*, chapter 11. EngineeringPro collection. Wiley, 2012.

[22] Jacobo Hernández-Montelongo, Vicente F. Nascimento, Duber Murillo, Thiago B. Taketa, Prasana Sahoo, Alessandra A. de Souza, Marisa M. Beppu, and Monica A. Cotta. Nanofilms of hyaluronan/chitosan assembled layer-by-layer: An antibacterial surface for Xylella fastidiosa. *Carbohydrate Polymers*, 136:1–11, 1 2016.

[23] Jonas Daniel Mendelsohn. *Polyelectrolyte multilayers : nanofabricated architectures for bio-interface materials*. PhD thesis, Massachusetts Institute of Technology. Dept. of Materials Science and Engineering, 2002.

[24] Ralf Köhler Regine von Klitzing and Chloe Chenigny. *Neutron Reflectometry at Polyelectrolyte Multilayers*, pages 219–268. Wiley-VCH Verlag GmbH & Co. KGaA, 2012.

[25] AppliChem GmbH. Biological buffers.

[26] J. Hernandez-Montelongo, E. G. Lucchesi, I. Gonzalez, W. A. A. Macedo, V. F. Nascimento, A. M. Moraes, M. M. Beppu, and M. A. Cotta. Hyaluronan/chitosan nanofilms assembled layer-by-layer and their antibacterial effect: A study using Staphylococcus aureus and Pseudomonas aeruginosa. *Colloids and Surfaces B: Biointerfaces*, 141:499–506, 5 2016.

[27] C. Picart, A. Schneider, O. Etienne, J. Mutterer, P. Schaaf, C. Egles, N. Jessel, and J.-C. Voegel. Controlled degradability of polysaccharide multilayer films in vitro and in vivo. *Advanced Functional Materials*, 15(11):1771–1780, 2005.

[28] J. K. Sheehan, C. Arundel, and C. F. Phelps. Effect of the cations sodium, potassium and calcium on the interaction of hyaluronate chains: a light scattering and viscometric study. *International Journal of Biological Macromolecules*, 5(4):222–228, 1983.

[29] Huiguang Zhu, Rohit Srivastava, J Quincy Brown, and Michael J McShane. Combined physical and chemical immobilization of glucose oxidase in alginate microspheres improves stability of encapsulation and activity. *Bioconjugate chemistry*, 16(6):1451–1458, Nov-Dec 2005.

[30] Peter Nestler, Malte Paßvogel, and Christiane A. Helm. Influence of polymer molecular weight on the parabolic and linear growth regime of PDADMAC/PSS multilayers. *Macromolecules*, 46(14):5622–5629, 07 2013.

[31] Mathias Lösche, Johannes Schmitt, Gero Decher, Wim G. Bouwman, and Kristian Kjaer. Detailed structure of molecularly thin polyelectrolyte multilayer films on solid substrates as revealed by neutron reflectometry. *Macromolecules*, 31(25):8893–8906, 12 1998.

[32] Piotr Kujawa, Patricia Moraille, Jacqueline Sanchez, Antonella Badia, and Françoise M. Winnik. Effect of molecular weight on the exponential growth and morphology of hyaluronan/chitosan multilayers: A surface plasmon resonance spectroscopy and atomic force microscopy investigation. *Journal of the American Chemical Society*, 127(25):9224–9234, 06 2005.

[33] Koji Itano, Jeeyoung Choi, and Michael F. Rubner. Mechanism of the pH-Induced Discontinuous Swelling/Deswelling Transitions of Poly(allylamine hydrochloride)-Containing Polyelectrolyte Multilayer Films. *Macromolecules*, 38(8):3450–3460, 04 2005.

[34] Piotr Kujawa, Jacqueline Sanchez, Antonella Badia, and Francoise M Winnik. Probing the stability of biocompatible sodium hyaluronate/chitosan nanocoatings against changes in salinity and pH. *J Nanosci Nanotechnol*, 6(6):1565–1574, Jun 2006.

[35] Ludovic Richert, Fouzia Boulmedais, Philippe Lavalle, Jérôme Mutterer, Emmanuelle Ferreux, Gero Decher, Pierre Schaaf, Jean-Claude Voegel, and Catherine Picart. Improvement of stability and cell adhesion properties of polyelectrolyte multilayer films by chemical cross-linking. *Biomacromolecules*, 5(2):284–294, 03 2004.

[36] Thomas Boudou, Thomas Crouzier, Claire Nicolas, Kefeng Ren, and Catherine Picart. Polyelectrolyte multilayer nanofilms used as thin materials for cell mechano-sensitivity studies. *Macromolecular Bioscience*, 11(1):77–89, 2011.

[37] ThermoFisher Scientif. EDC (1-ethyl-3-(3-dimethylaminopropyl)carbodiimide hydrochloride). `https://www.thermofisher.com/order/catalog/product/22980`. Accessed: 2017-04-01.

[38] Zhiyuan Ling and Yi Li. *Mechanisms of Nanoporous Alumina Formation and Self-organized Growth*, pages 1–30. Springer International Publishing, Cham, 2015.

[39] E. Ferain and R. Legras. Track-etch templates designed for micro- and nanofabrication. *Nuclear Instruments and Methods in Physics Research Section B: Beam Interactions with Materials and Atoms*, 208:115–122, 8 2003.

[40] H. Hanot and E. Ferain. Industrial applications of ion track technology. *Nuclear Instruments and Methods in Physics Research Section B: Beam Interactions with Materials and Atoms*, 267(6):1019–1022, 3 2009.

[41] Teruyuki Komatsu. Protein-based nanotubes for biomedical applications. *Nanoscale*, 4(6):1910–1918, 2012.

[42] Halima Alem, Françoise Blondeau, Karine Glinel, Sophie Demoustier-Champagne, and Alain M. Jonas. Layer-by-layer assembly of polyelectrolytes in nanopores. *Macromolecules*, 40(9):3366–3372, 05 2007.

[43] C. J. Roy, C. Dupont-Gillain, S. Demoustier-Champagne, A. M. Jonas, and J. Landoulsi. Growth mechanism of confined polyelectrolyte multilayers in nanoporous templates. *Langmuir*, 26(5):3350–3355, 03 2010.

[44] Diana G. Ramírez-Wong, Cristina Coelho-Diogo, Carole Aimé, Christian Bonhomme, Alain M. Jonas, and Sophie Demoustier-Champagne. Effects of geometrical confinement in membrane pores on enzyme-based layer-by-layer assemblies. *Applied Surface Science*, 338:154–162, 5 2015.

[45] Deepak M. Kalaskar, Claude Poleunis, Christine Dupont-Gillain, and Sophie Demoustier-Champagne. Elaboration of nanostructured biointerfaces with tunable degree of coverage by protein nanotubes using electrophoretic deposition. *Biomacromolecules*, 12(11):4104–4111, 11 2011.

[46] María Alba, Pilar Formentín, Josep Ferré-Borrull, Josep Pallarès, and Lluís F. Marsal. pH-responsive drug delivery system based on hollow silicon dioxide micropillars coated with polyelectrolyte multilayers. *Nanoscale Research Letters*, 9(1):411, 2014.

[47] Younghyun Cho, Woo Lee, Young Kuk Jhon, Jan Genzer, and Kookheon Char. Polymer nanotubules obtained by layer-by-layer deposition within AAO-membrane templates with sub-100-nm pore diameters. *Small*, 6(23):2683–2689, 2010.

[48] R. Sadeghi, A. Kalbasi, Z. Emam-jomeh, S. H. Razavi, J. Kokini, and A. A. Moosavi-Movahedi. Biocompatible nanotubes as potential carrier for curcumin as a model bioactive compound. *Journal of Nanoparticle Research*, 15(11):1931, 2013.

[49] Elvin Blanco, Haifa Shen, and Mauro Ferrari. Principles of nanoparticle design for overcoming biological barriers to drug delivery. *Nat Biotech*, 33(9):941–951, 09 2015.

[50] Alisa L. Becker, Angus P. R. Johnston, and Frank Caruso. Layer-by-layer-assembled capsules and films for therapeutic delivery. *Small*, 6(17):n/a–n/a, 2010.

[51] Svetlana Pavlukhina and Svetlana Sukhishvili. *CHAPTER 17 Smart Layer-by-Layer Assemblies for Drug Delivery*, volume 2, pages 117–152. The Royal Society of Chemistry, 2013.

[52] Michiya Matsusaki and Mitsuru Akashi. Functional multilayered capsules for targeting and local drug delivery. *Expert Opinion on Drug Delivery*, 6(11):1207–1217, 2009. PMID: 19831583.

[53] Xue Qu, Gang Lu, Eishun Tsuchida, and Teruyuki Komatsu. Protein nanotubes comprised of an alternate layer-by-layer assembly using a polycation as an electrostatic glue. *Chemistry – A European Journal*, 14(33):10303–10308, 2008.

[54] Jonathan B. Gilbert, Janice S. O'Brien, Harini S. Suresh, Robert E. Cohen, and Michael F. Rubner. Orientation-specific attachment of polymeric microtubes on cell surfaces. *Advanced Materials*, 25(41):5948–5952, 2013.

[55] Jorge Almodóvar, Laura W. Place, Jarrod Gogolski, Kristin Erickson, and Matt J. Kipper. Layer-by-Layer assembly of polysaccharide-based polyelectrolyte multilayers: A spectroscopic study of hydrophilicity, composition, and ion pairing. *Biomacromolecules*, 12(7):2755–2765, 07 2011.

[56] X. Arys. *Understanding Ordering in Polyelectrolyte Multilayers: Effect of the Chemical Architecture of the Polycation*. PhD thesis, Université Catholique de Louvain, Institute of Condensed Matter and Nanosciences, Bio and soft matter, Ecole Polytechnique de Louvain, 2000.

[57] Sophie Demoustier-Champagne Cécile J. Roy, Cédric C. Buron and Alain M. Jonas. *Nanoconfined Polyelectrolyte Multilayers: From Nanostripes to Multisegmented Functional Nanotubes*, pages 613–636. Wiley-VCH Verlag GmbH & Co. KGaA, 2012.

[58] A. Tronin, Y. Lvov, and C. Nicolini. Ellipsometry and x-ray reflectometry characterization of self-assembly process of polystyrenesulfonate and polyallylamine. *Colloid and Polymer Science*, 272(10):1317–1321, 1994.

[59] Marta Kolasińska, Rumen Krastev, and Piotr Warszyński. Characteristics of polyelectrolyte multilayers: Effect of PEI anchoring layer and posttreatment after deposition. *Journal of Colloid and Interface Science*, 305(1):46–56, 1 2007.

[60] G. Ladam, P. Schaad, J. C. Voegel, P. Schaaf, G. Decher, and F. Cuisinier. In situ determination of the structural properties of initially deposited polyelectrolyte multilayers. *Langmuir*, 16(3):1249–1255, 02 2000.

[61] Stephan T. Dubas and Joseph B. Schlenoff. Swelling and smoothing of polyelectrolyte multilayers by salt. *Langmuir*, 17(25):7725–7727, 12 2001.

[62] Long Liu, Yanfeng Liu, Jianghua Li, Guocheng Du, and Jian Chen. Microbial production of hyaluronic acid: current state, challenges, and perspectives. *Microbial Cell Factories*, 10(1):99, 2011.

[63] Maria Lundin, Faten Solaqa, Esben Thormann, Lubica Macakova, and Eva Blomberg. Layer-by-layer assemblies of chitosan and heparin: Effect of solution ionic strength and pH. *Langmuir*, 27(12):7537–7548, 06 2011.

Rue Archimède, 1 bte L6.11.01, 1348 Louvain-la-Neuve **www.uclouvain.be/epl**